Spring 2014

The structure and properties of ternary zinc phosphate glasses for optical applications

Charmayne Elizabeth Smith

Department: Materials Science and Engineering

THE STRUCTURE AND PROPERTIES OF TERNARY ZINC PHOSPHATE GLASSES FOR OPTICAL APPLICATIONS

by

CHARMAYNE ELIZABETH SMITH

A DISSERTATION

Presented to the Faculty of the Graduate School of the

MISSOURI UNIVERSITY OF SCIENCE AND TECHNOLOGY

In Partial Fulfillment of the Requirements for the Degree

DOCTOR OF PHILOSOPHY

in

MATERIALS SCIENCE AND ENGINEERING

2014

Approved by:

Richard K. Brow, Advisor
Wayne Huebner
Denise Krol
Matthew J. O'Keefe
Jeffrey D. Smith

PUBLICATION DISSERTATION OPTION

The introduction and literature review sections in this document provide pertinent information about the properties and structure of ternary zinc phosphate glasses that are the focus of this work. The body of this dissertation has been compiled in the style for publication in peer reviewed journals. The first paper, entitled "The Structure and Properties of Zinc Aluminophosphate Glasses," was accepted for publication in the *Journal of Non-Crystalline Solids* in November 2013. The second paper, entitled "Phase Relationships in the ZnO-Al_2O_3-P_2O_5 System," will be submitted to the *Journal of the American Ceramic Society* in March 2014. The third paper, "The Properties and Structure of Zinc Magnesium Phosphate Glasses," was submitted for publication in the *Journal of Non-Crystalline Solids* in December 2013. The fourth paper, "Compositional Dependence of Irradiation Induced Defects in Zinc Aluminophosphate Glasses," will be submitted to the *Journal of the American Ceramic Society* in April 2014.

The appendix includes experimental results on the effects of the systematic substitution of CaO for ZnO on the propertis and structures of ternary phosphate glasses with O/P ratios of 3.0. This work is presented in the format of the *Journal of Non-Crystalline Solids* and is entitled "Effects of the Direct Substitution of CaO for ZnO in Zinc Phosphate Glasses." There is also work discussed on the effects of fictive temperature on density and refractive index in a zinc phosphate glass with O/P=3.25.

ABSTRACT

This dissertation focuses on the properties and structures of ternary zinc phosphate glasses that have recently been investigated as substrates for femto-second (fs) laser writing. Although these glasses have potential for use as optical substrates, their poor chemical properties limit their applications. In this work, ternary zinc phosphate glasses were studied to find compositions with enhanced chemical durability and the properties and structures of the investigated glasses are reported.

Paper 1 and Paper 2 include the first systematic studies of the properties, structures of zinc aluminophosphate (ZAP) glasses and phase relationships in the ZnO-Al_2O_3-P_2O_5 system, respectively. Adding alumina to a Zn-metaphosphate glass reduces dissolution rates in water by 4 orders of magnitude and increases the glass transition temperatures. The average Al coordination number can be predicted from a structural model that considers the number of non-bridging oxygens to coordinate metal cations, and this work is the first reported use of this model for a ternary phosphate glass.

Paper 3 is the first systematic study of how the properties and structures of zinc magnesium polyphosphate glasses change when MgO replaces ZnO for compositions with fixed O/P ratios. The Mg^{2+} and Zn^{2+} ions have similar field strengths, but have much different effects on glass properties that are discussed in terms of relative polarizabilities (refractivities) and electron configurations of the Mg^{2+} and Zn^{2+} ions.

In Paper 4, the creation of electronic defects in zinc phosphate glasses by exposure to ultraviolet and x-ray radiation is described. The nature of the defects formed is dependent on the glass composition and similar defects are created when these glasses are exposed to femto-second laser radiation.

ACKNOWLEDGEMENTS

Thank you to the GAANN selection committee (Profs. O'Keefe, Huebner, Hilmas, Brow) for awarding me my fellowship and showing faith in my pursuit of a PhD.

Prof. Brow, thank you for everything. You are a phenomenal advisor. I know if I remember even half of the things you tried to teach me I will one day be the President of ACerS and finally be able to make up my own words in the literature ☺. Thanks to the Brow family for lending us your father/husband; students are needy. Terry, thanks for all the hugs ☺. Thanks to the current and past members of the Brow group, especially Lina Ma for phosphate/HPLC discussions. Ryan Jones you will forever be "my undergrad" ☺. Thanks to Profs. Krol and Tsai and Drs. Troy, Fletcher and Lin for laser use and great discussions. To Profs. Krol, Smith, Huebner and O'Keefe, thank you for your guidance. Each of you has contributed something unique and invaluable to my PhD career.

Thank you Mommy and Daddy for everything, especially your love and support; I love you and you made me the person I am today. "…Though I walk through the valley of the shadow of death, I shall fear no evil…" and we know why :D !! Thank you Grandma and Grandpa; your contributions to a poor student will always be remembered.

Dr. Kelley Wilkerson, I have no words for how grateful I am for all you've helped me through. Thanks to my life coach, Dr. Eric "BoBo" Bohannon and thanks Dr. Jeremy Watts, especially for all the times involving brisket and Animation Domination :)

To Jason Lonergan, my love, I'm so happy that you are in my life. You are my sanity, my calm, my inspiration, my joy, my warmth... My all. I love you.

Thanks to Ron, Brian and the wonderful administrative assistants (angels from heaven) for MRC and MSE. This list is incomplete, but I appreciate everyone in my life!

TABLE OF CONTENTS

LIST OF ILLUSTRATIONS

SECTION Page

PAPER 1

PAPER 4

LIST OF TABLES

SECTION

1. INTRODUCTION

The main goals of this work are to develop glasses with improved chemical durability as compared to binary zinc phosphate glasses, and to understand how changes in composition affect the structures and properties of those glasses. Zinc phosphate glasses are of interest due to their responses to femto-second (fs) laser irradiation and it is desired to develop chemically stable glasses as substrates for waveguide fabrication.

Phosphate glasses are of interest as optical materials due, in part, to their large glass-forming range and their high solubility for rare-earth ions, which makes them useful for laser glasses [1-3]. They are also of interest for optical applications due to their low ultraviolet (UV) cut-off wavelength, which has been shown to be < 400 nm, depending on composition [4, 5]. Binary zinc phosphate glasses, while promising for optical materials, have poor chemical durability, compared to silica based glasses [6]. The addition of certain oxides, such as B_2O_3 and Nb_2O_5, has been shown to facilitates the formation of more hydrolytically stable bonds, which promotes a better resistance to aqueous attack [7-9]. Modifying glass compositions with components like Al_2O_3 results in improved chemical durability through decreased dissolution rates [10], but the effects of added oxides on the structural organization and properties, such as density and refractive index, have not been determined.

To date, the properties and structures of ternary zinc phosphate glass systems containing MgO, CaO and Al_2O_3 have not been fully explored. An immediate goal of this work is to develop glass forming- and phase stability-diagrams, where lacking, while understanding the properties and structures across a wide range of compositions.

The exploration of zinc phosphate glasses as optical substrates is of interest because the use of fs lasers allows the creation of subsurface, structural alterations that can be used to develop precise, three-dimensional structures for integrated optical devices [11]. The interaction of the laser results in variations in structure and properties, the most important of which is the change in the refractive index in the focal volume of the laser relative to the surrounding material. The binary zinc phosphate glass containing 60 mol% ZnO, with a structure defined by an oxygen to phosphorus (O/P) ratio of 3.25, exhibits an increase in refractive index as a result of fs-laser irradiation, which is a desirable response for waveguide fabrication [12, 13].

The refractive index change induced in glasses as a result of fs laser irradiation has been shown to be correlated to electronic defect formation in the laser focal volume [12, 14]. Hole- and electron-centers that form due to high energy radiation result from the excitation of the entire network where ejected electrons deposit on a variety of phosphate-oxygen moieties [15, 16]. Determining the relationships between defect formation and composition gives insight into how the structure responds to optical radiation.

Ultimately, this work should provide new and fully characterized ternary zinc phosphate glass compositions. These compositions should have improved resistance to aqueous attack and be suitable for femtosecond laser processing.

2. LITERATURE REVIEW

Phosphate glasses are of interest for a number of applications, including sealing glasses [17, 18], bioactive materials [19, 20], and laser or optical systems [21-23]. Their desirable properties, such as low glass transition temperatures (T_g) [24] and large glass forming regions, drive investigations into a variety of binary and ternary phosphate families [25-30]. The properties of phosphate glasses are dependent on the structures that make up the glassy network. The structural units should be understood in order to engineer glasses for the applications of interest. The main focus of this review will be phosphate systems whose principal constituents are ZnO, Al_2O_3, and/or MgO.

2.1 PHOSPHATE CHEMISTRY

Phosphate compounds are known to form networks of interconnected tetrahedral structures [31]. Phosphorus-oxygen-phosphorus bonds are spread throughout the structure, forming rings and/or chains which contribute to the prototypical, high connectivity phosphate network. With increasing modifier oxide content, the phosphate units are dispersed throughout the network in shorter chains or single phosphate tetrahedra which terminate due to charge balancing with metal cations in the structure. These phosphate structures are established by the composition which can be described using the Q^i nomenclature, where "i" represents the number of bridging oxygens (i = 0, 1, 2, or 3) associated with a phosphate unit (Figure 2.1).

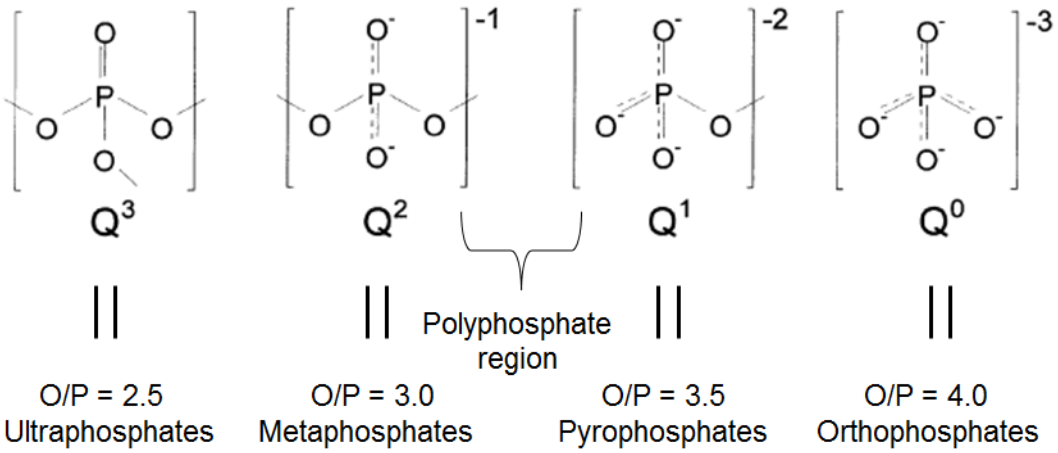

Figure 2.1: Tetrahedral classifications for phosphate compounds/glasses [32]

Figure 2.1 shows the progression of the changes in structural units as modifier oxides are added to the phosphate network. For the Q^3 tetrahedra in P_2O_5, there are three oxygen bonds that bridge to other phosphorus tetrahedra and one phosphorus-oxygen double bond. The introduction of a modifying oxide to P_2O_5 results in the formation of non-bridging oxygens and the depolymerization of the network as described by the reaction:

$$2Q^i + R_2O \rightarrow 2Q^{i-1} \quad (1)$$

The addition of monovalent or divalent oxides to a phosphate glass composition can be represented by the formula $xR_2O(R'O)\cdot(1\text{-}x)P_2O_5$. The compositional range between $0 < x < 0.5$ is classified as the ultraphosphate range, which is characterized by structures with Q^3 and Q^2 units, whose relative amounts depend on the composition. Phosphate compositions are classified into families based on the units present in the structure. The metaphosphate and pyrophosphate compositions are defined as $x = 0.5$ (Q^2) and $x = 0.67$ (Q^1), respectively. The intermediate region between $0.5 < x < 0.67$ is the polyphosphate region and network structures are dominated by a mixture of Q^2 and

Q^1 units. Compositions with $x > 0.67$ transition to mainly Q^0 units and are classified as orthophosphates. The use of composition to predict changes in structural moieties in the phosphate network allows connections to be drawn between analyzed compositional data and the expected configuration of the phosphate network.

2.2 GLASS STRUCTURE AND PROPERTIES OF BINARY PHOSPHATE GLASSES

Vitreous P_2O_5 is known to be highly susceptible to hydrolysis [31]. Ultraphosphate glasses are hygroscopic and must be prepared in a controlled environment [3]. Glasses in the metaphosphate and polyphosphate ranges are more chemically stable than the ultraphosphate compositions and, as a result, are more extensively discussed in the literature. Although different metal oxides affect the glass properties and structures in different ways, it has been reported that the addition of metal oxides can improve resistance of a glass to aqueous attack [24, 33-35]. The effects of individual oxides can be understood by different characteristics of cations, including the cationic field strength or the cation coordination number.

Hoppe developed a model to explain how the number of non-bridging oxygens present in the structure can determine the coordination configuration of the metal cation(s) [36]. Hoppe noted that all modifying cations that are added to the phosphate network require non-bridging (terminal) oxygen atoms to bond with, and he recognized that there must be a correlation between the coordination configuration of the metal cations and the available number of terminal oxygen (TO). For binary phosphate glasses with the molar composition $xMe_{2/\nu}O\ (1\text{-}x)P_2O_5$, where ν is the valence of the metal cation (Me), the number of terminal oxygens per Me is given by:

$$N_{TO} = \frac{v(x+1)}{x} \tag{2}$$

Compositional regions occur, with distinct structural configurations predicted by this model, that are related to the coordination number of the Me cations (CN_{Me}): $N_{TO} > CN_{Me}$, $N_{TO} = CN_{Me}$, and $N_{TO} < CN_{Me}$. Figure 2.2 provides a visual representation of each.

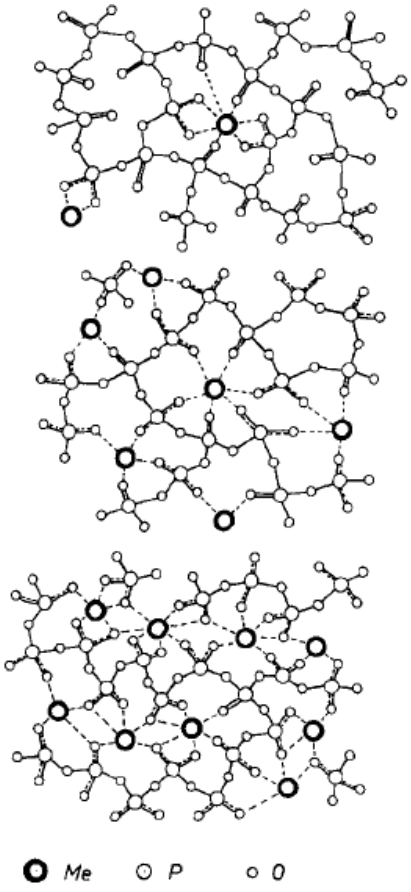

Figure 2.2: Schematic of network structures for binary phosphate glasses corresponding to the three characteristic regions defined by N_{TO}; from Hoppe [36]

Region I (Figure 2.2, top) is defined by $N_{TO} > CN_{Me}$ and involves compositions where an excess number of terminal oxygens are available to coordinate the Me cations.

This excess of terminal oxygens means that higher coordination numbers are possible for Me cations without the need to share common terminal oxygens. Thus, the Me cations are isolated from one another in the phosphate network. Region II (Figure 2.2, middle) is defined by $N_{TO} = CN_{Me}$ and indicates the compositions where every terminal oxygen is involved in the coordination sphere of every metal cation, but these metal cations do not share common terminal oxygens. The average CN_{Me} can decrease with increasing TO in this compositional range. However, there is a minimum CN_{Me} that is possible and Region III (Figure 2.2, bottom) encompasses the compositions where $N_{TO} < CN_{Me}$. For these compositions, metal polyhedra must share common terminal oxygens to form a subnetwork of metal polyhedral (MeO_n) unit linkages because there are insufficient numbers of terminal oxygen to isolate these polyhedra. This compositional range allows for the possibility of corner- and edge-sharing between MeO_n units [36]. Studies on the relationships between modifier coordination, composition, and properties have been conducted and it is generally found that the metal coordination number decreases with increasing metal oxide content [37, 38].

2.2.1 Zinc Phosphate Glasses. Understanding the properties and structures of binary glasses can give insight into the ternary systems. Brow et al. [3] prepared glasses in the compositional range of $0.5 \leq x \leq 0.71$ for the $xZnO\cdot(1\text{-}x)P_2O_5$ system and found that glass formation occurred in the explored area with no phase separation or crystallization. Tischendorf et al. extended the glass forming range by preparing compositions using the roller-quenching technique, by melting glasses with ZnO concentrations as high as 80 mol%, although evidence is shown for phase separation at ~75mol% ZnO [39]. This tendency was found in the present work as well. Tischendorf

[39] and Sales [40] experimentally confirmed the systematic increase in the network depolymerization (following Equation 1), with increasing amounts of ZnO, as described by Van Wazer [31].

Meyer conducted a study on the density and structure of $xZnO \cdot (1-x)P_2O_5$ glasses with $0 \leq x \leq 0.5$ [41] and found that the density increases monotonically with added ZnO, up to x~0.33. The trend in density was supported by the structural changes that occur in the network, as reflected by a shift of features in Raman spectra and FTIR data at $x \geq 0.33$. Kordes et al. also contributed some of the early work on binary metal oxide (MeO) ultraphosphate glasses, from pure P_2O_5 to near the metaphosphate composition [42-44]; one such investigation found discontinuities in properties such as refractive index and density at the metaphosphate composition. Due to these discontinuities, Kordes classified the binary Zn- and Mg- phosphates as "abnormal" systems [44]. More recently, research surrounding the compositions beyond the metaphosphate region was completed and the results of the packing density can be seen in Figure 2.3 [45].

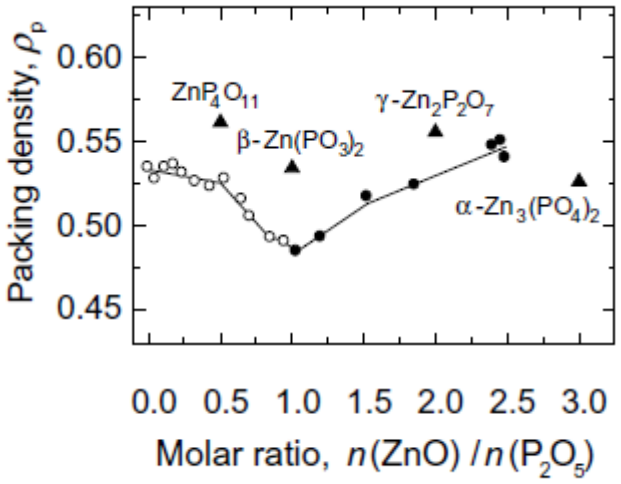

Figure 2.3: Packing densities (open circles [46] and closed circles [45]) of the zinc phosphate binary glasses (line is drawn to guide the eye). For comparison, packing densities for crystalline zinc phosphate compounds are shown as triangles; from Walter et al., [45].

The explanation for the discontinuity in properties was a change in the coordination number of the metal cations (CN), from six to four. X-ray diffraction studies have been used to investigate metal cation coordination numbers and bond lengths for compositions of MgO and ZnO phosphate systems near the metaphosphate region [47, 48]. The overall CN of zinc and magnesium did not vary significantly about the metaphosphate composition and into the polyphosphate regime. The data for CN_{Me} for ZnO, MgO and CaO phosphate glasses are shown in Table 2.1 [47]. While Matsubara et al. disproved the notion of attributing a large CN change to the "abnormal" status of Zn- and Mg- phosphates, an alternate explanation was not provided [47].

Table 2.1: Bond distances (r) and coordination numbers (N) for P-O, O-O, and Me-O (Me = Mg, Zn, or Ca) pairs, from the diffraction studies of Matsubara, et al [47].

x	0.45		0.50		0.55	
	r_{ij}	N_{ij}	r_{ij}	N_{ij}	r_{ij}	N_{ij}
$(MgO)_x(P_2O_5)_{1-x}$ glass						
P–O	0.154	3.95 ± 0.23	0.153	3.70 ± 0.23	0.153	4.00 ± 0.23
Mg–O	0.203	4.90 ± 0.23	0.203	4.30 ± 0.21	0.203	4.50 ± 0.18
O–O	0.250	5.00 ± 0.20	0.250	4.35 ± 0.17	0.252	4.80 ± 0.15
$(ZnO)_x(P_2O_5)_{1-x}$ glass						
P–O	0.153	4.10 ± 0.27	0.153	4.10 ± 0.23	0.153	4.10 ± 0.23
Zn–O	0.198	3.90 ± 0.20	0.195	4.00 ± 0.18	0.197	3.70 ± 0.16
O–O	0.251	5.00 ± 0.20	0.252	5.00 ± 0.17	0.250	5.50 ± 0.18
$(CaO)_x(P_2O_5)_{1-x}$ glass						
P–O	0.155	4.20 ± 0.23	0.154	4.10 ± 0.21	0.154	4.20 ± 0.18
Ca–O	0.238	5.40 ± 0.20	0.237	5.40 ± 0.18	0.238	5.20 ± 0.15
O–O	0.256	4.20 ± 0.15	0.256	4.50 ± 0.14	0.257	4.20 ± 0.11

In the $xZnO\cdot(1\text{-}x)P_2O_5$ glass system, the increase of x from 0.35 to 0.80 results in an increase in refractive index and a minimum in the glass transition temperature (T_g) near x = 0.6 (Figure 2.4) [3, 39, 49].

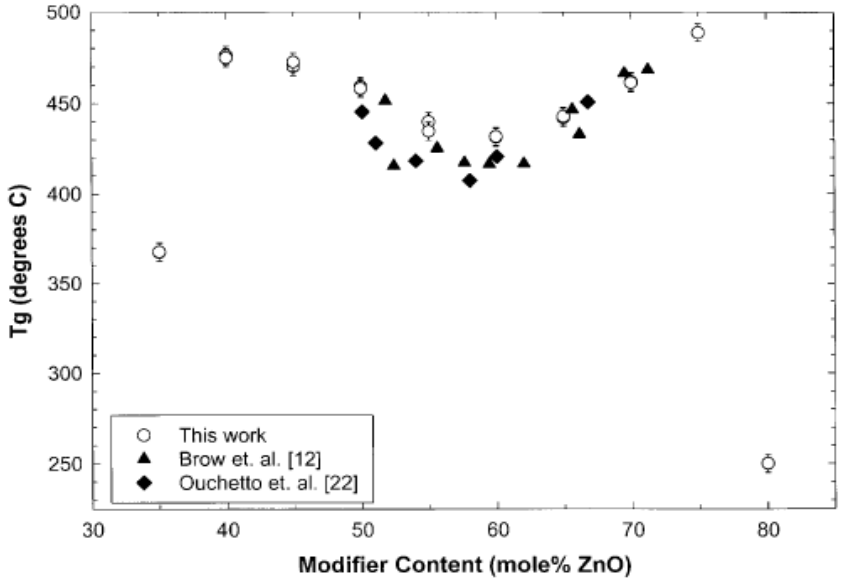

Figure 2.4: DSC measurements of the T_g in x $ZnO\cdot(1\text{-}x)$ P_2O_5 glasses taken directly from Tischendorf, et al. [39].

Kubo et al. also used Raman and infrared (IR) spectroscopy to analyze the change in structural units with ZnO addition while discussing the minimum in T_g and a minimum in the coefficient of thermal expansion (CTE) data at 55-60 mol% ZnO [50]. X-ray diffraction allowed for the confirmation that the minima in these thermal properties for this compositional range were not due to a change in Zn-coordination number. The coordination number of zinc was found to be relatively constant (~4.1) between 50-71 mol% ZnO [38, 45]. The discontinuity in properties such as T_g and CTE near x = 0.6 was speculated to be due to a maximum in "real-space distances" between atoms or the switch from isolated ZnO_n and MgO_n polyhedra to face and corner-sharing polyhedra [45, 50].

In addition to changes in structures and properties, the chemical durability of glasses, and how it changes with composition, needs to be understood. Zinc phosphate glasses have been reported to exhibit two different dissolution behaviors in water, either by progressive dissolution and the precipitation of material in solution (Type I) or by dissolution and the formation of a precipitation layer on the reacting glass surface (Type II) [35]. A transition from Type I to Type II behavior occurs for binary zinc phosphate compositions near 60-65 mol% ZnO. Takebe et al. showed that the weight loss rate decreases with increasing ZnO content, although this trend is partially due to the formation of a precipitation layer on the glass surface [35].

When phosphate glasses react in water, the bonds between metal cations and non-bridging oxygens (P-O-Me) are attacked first while the phosphate chains are unbroken. The hydration of the metal-nonbridging oxygen bonds allow phosphate anions to be released, intact, into the solution where they might then hydrolyze after some time (> ~72

hours) [31, 40, 51]. This dissolution behavior allows phosphate glass structures to be investigated with high pressure liquid chromatography (HPLC).

Distributions of phosphate anions are best characterized by liquid chromatography. Phosphate glasses are dissolved into solutions and the units present in solution can be identified and related to the units originally present in the glass structure. The phosphate units are described using P_n terminology, where n = the number of phosphorus tetrahedra in the anion. Examples of zinc phosphate spectra obtained from chromatography measurements are shown in Figure 2.5, and it can be seen that n increases from left to right with the presence of longer chains represented by peaks at greater retention times.

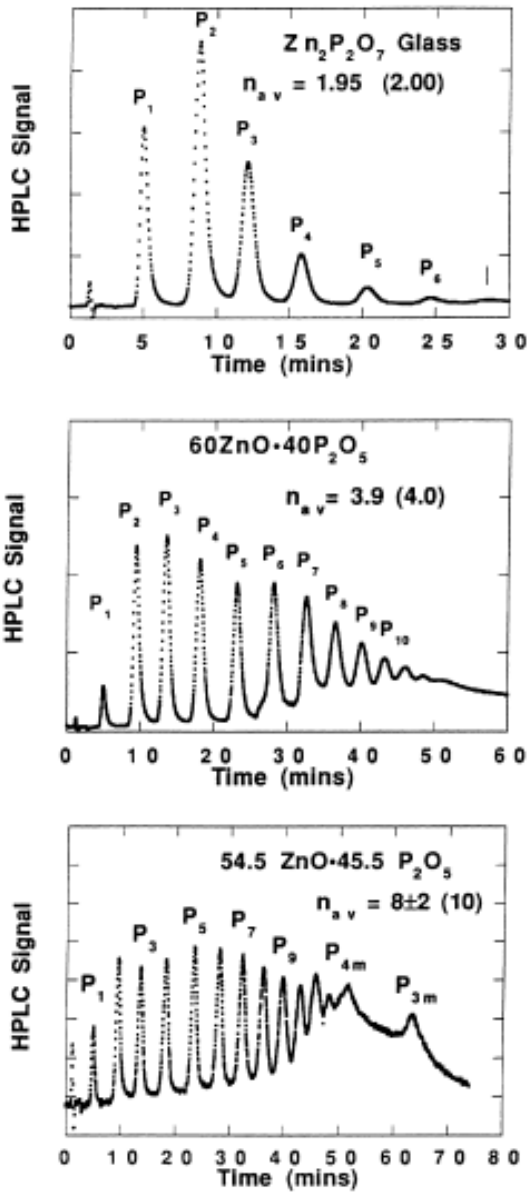

Figure 2.5: Chromatography measurements of binary zinc phosphate glasses with 55 - 67 mol% ZnO. The average chain length calculated for each glass is shown as n_{av}; from Sales [40].

The HPLC technique is only quantitatively useful for compositions in the polyphosphate and pyrophosphate regimes. For a glass with the nominal composition $xM_{2/v}O$ $(1-x)P_2O_5$, the average phosphate anion chain-length, $\bar{n}$, will be given by:

$$\bar{n} = \frac{2}{\sum_j \frac{[M_j][v_j]}{[P]} - 1} \quad (3)$$

where v is the valence of the metal oxide and $[M_j]$ and [P] are the relative atomic fractions of the metal ions and phosphorus, respectively [40].

The metaphosphate structure is comprised of Q^2 units, which form long chains and rings that are not resolved by the chromatography system. An example of the peak overlapping that occurs at longer retention times can be seen for retention times longer than about five minutes in the chromatograph for the 54.5ZnO 45.5P_2O_5 glass in Figure 2.5.

The distribution of phosphate anions in a glass structure can deviate from the predictions of the simple depolymerization reactions, like that shown in Equation (1). For glasses in the xZnO·(1-x)P_2O_5 system, Brow et al. [3] proposed that site disproportionation reactions occurred in the melt, described by:

$$2Q^1 \leftrightarrow Q^2 + Q^0 \quad (4)$$

Disproportionation is likely to occur in melts with larger O/P ratios, such as those near O/P = 3.5, and results in more complex glass structures which lends to increases the glass forming region. The same type of reaction has not been found at lower O/P ratios due to the instability of Q^3 units. HPLC measurements, in addition to liquid or solid state nuclear magnetic resonance (NMR) spectroscopies can be used to characterize disproportionation in the phosphate network.

The degree of disproportionation can be quantified using the HPLC chromatograms by the calculation of k_n, which is the rate constant of reactions such as

Equation 4. The reaction constant for any disproportionation reaction can be calculated by the following equation:

$$k_n = \frac{[(P_{n+1}O_{3n+4})^{-(n+3)}][(P_{n-1}O_{3n-2})^{-(n+1)}]}{[[(P_nO_{3n+1})^{-(n+2)}]]^2} \quad (5)$$

k_n values typically range from 0 to 1, with no detectable disproportionation occurring when $k_n = 0$ [52]. Sales [52] showed that the extent of phosphate anion disproportionation depends on the metal oxide that modifies a glass (Figure 2.6). Increasing the metal cation field strength increases the tendency for disproportionation to occur.

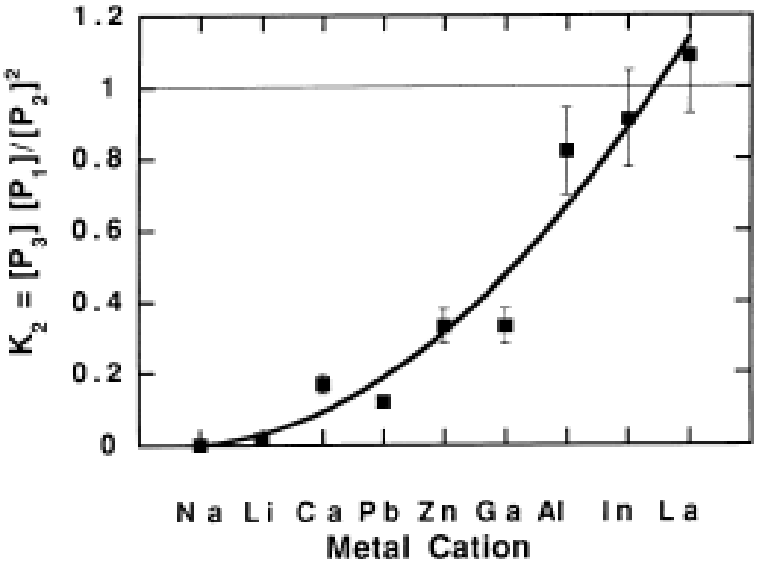

Figure 2.6: Equilibrium constants for disproportionation reactions in melts of binary phosphate glasses, determined using chromatograms and by using Equation 4; from Sales [52].

2.2.2 Magnesium Phosphate Glasses. Studies have been conducted on glasses in the binary magnesium phosphate system as well. Meyer completed an

investigation of magnesium ultraphosphate glasses using vibrational spectroscopy and found that, although the phosphate networks that formed were similar to the Zn-phosphate system, the properties in the two binary systems are different due to a different metal cation present in the structure [53].

Walter et al. not only showed that the coordination numbers of Zn [45] were fairly invariant over the polyphosphate region, but found the same for Mg in phosphate glasses [54]. Interestingly enough, while the Zn-phosphate system exhibits a minimum in the glass transition temperature near 60 mol% ZnO, no such discontinuity occurs in the Mg-phosphate data. These data sets are shown in Figure 2.7.

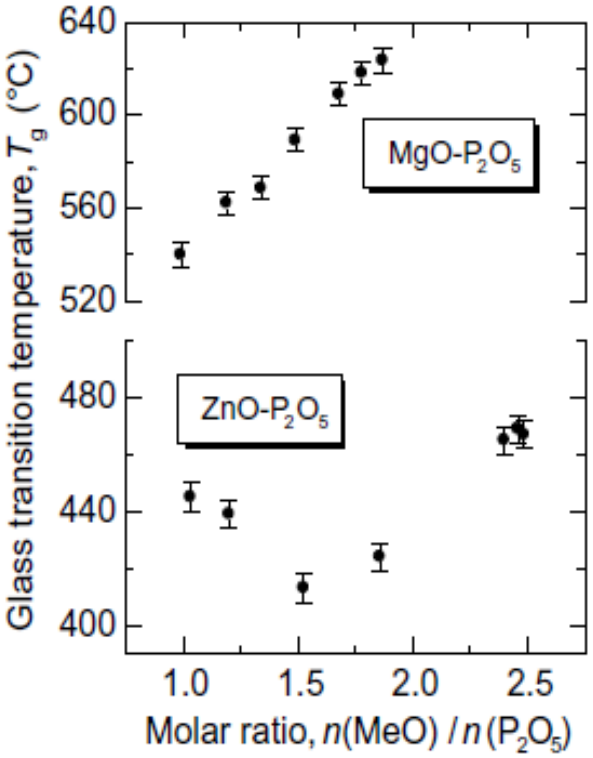

Figure 2.7: The glass transition temperatures of ZnO-P_2O_5 [45] and MgO-P_2O_5 glasses determined by DTA; from Walter et al. [54]

^{31}P NMR spectra have been collected on the binary magnesium phosphate glasses over the compositional range 44 mol% to 59 mol% MgO [55]. As was found in an NMR study of zinc phosphate glasses [3], the addition of MgO depolymerizes the phosphate network.

2.2.3 Aluminum Phosphate Glasses. Alumina additions to binary phosphate glass systems increase structural cross-linking and improve chemical durability. Research on the binary aluminum phosphate glass system has not been as extensive as that on the binary zinc and magnesium phosphate systems. This can be partially attributed to the volatility of P_2O_5 at the high temperatures required to make the aluminum phosphate glasses [31]. The aluminophosphate system tends to have a limited glass forming range (maximum concentration = ~35 mol% Al_2O_3) [37, 56].

Brow et al. used nuclear magnetic resonance (NMR) to understand the effect of alumina on the structure of binary aluminophosphate glasses [37]. The increase in alumina results in a decrease in the average CN_{Al} from ~5.3 to ~4.8 over a range of Al_2O_3 concentrations (31.9 – 34.5 mol%). This trend was confirmed by the structural model developed by Hoppe [36], indicating that the CN_{Al} is determined by the number of terminal oxygens available.

2.3 GLASS STRUCTURE AND PROPERTIES OF TERNARY PHOSPHATE GLASSES

A few studies have been completed on ternary zinc phosphate systems, where the third oxide is magnesia, alumina or calcia, but there is a lack of systematic investigations over a range of compositions and there are no complete studies on their respective glass forming regions.

In 1960, an initial study on glass forming tendencies in the ZnO-Al_2O_3-P_2O_5 system was published, using the binary glass forming limits from that time to make a ternary diagram [57]. The aluminophosphate binary limit was claimed as 30 mol% and the zinc phosphate was projected to be between 70-80 mol%. Fu et al. more recently conducted a study of a few compositions in the zinc aluminophosphate system, with varying O/P ratios and doped with 1% terbium [26]. As the concentration of ZnO increased, while maintaining a constant Al_2O_3 concentration, there was a decrease in molar volume and an increase in density and refractive index due to changing structural units occurred.

A few studies have been conducted on ternary metal oxide aluminophosphate glasses. Metwalli et al. showed that changes in the aluminum CN are dependent on the type and concentration of modifier added [58]. An increase in the ionic character of the modifying cation increses the average aluminum CN (Figure 2.8).

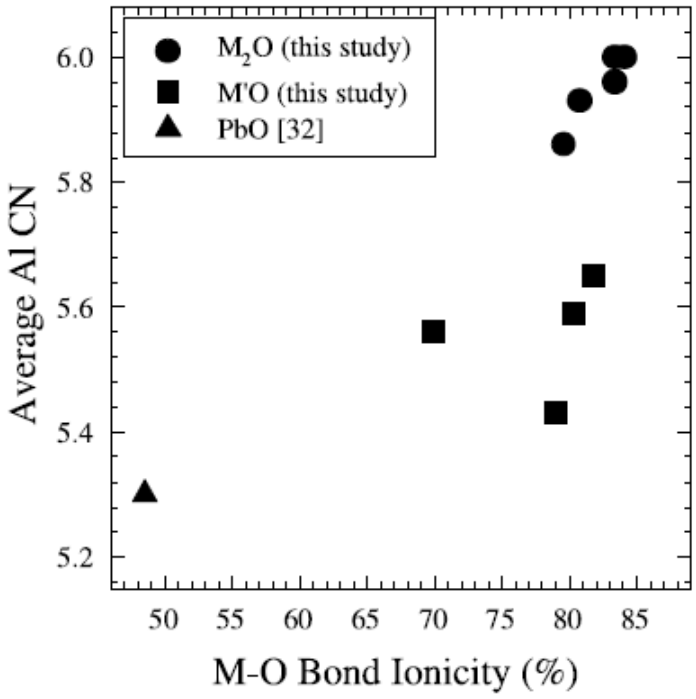

Figure 2.8: The average Al CN versus modifier-oxygen bond ionicity for various 30MO $10Al_2O_3$ $60P_2O_5$ glasses (taken from [58])

Metwalli et al. state that the more covalent an M-O bond is, the more its charge will be depleted from a phosphate tetrahedron. The charge depletion results in a larger donation of electrons from Al^{3+} sites that are also bonded to that tetrahedron. As an aluminum tetrahedron donates more charge than an Al-octahedron to an Al-O-P bond, four coordinated aluminum ions should be preferred with greater covalent bonding [58]. The coordination of alumina impacts the properties of aluminophosphate glasses, as reported by Minami et al.; a decrease in CTE, and increase in T_g, with the addition of alumina is due to an increase the degree of the network cross-links through Al-O-P bonds [34].

A few studies have been completed on glasses in the ZnO-MgO-P_2O_5 (ZMP) system as well. Khor et al. showed replacing P_2O_5 with MgO improves the chemical durability of zinc phosphate glasses, which is to be expected as the addition of modifiers stabilizes the network to offer more resistance to atmospheric attack and hydrolysis [33].

2.4 FEMTO-SECOND LASER IRRADIATION OF PHOSPHATE GLASSES

The impetus for this work was the discovery of the promising response of zinc phosphate glasses to femto-second (fs) laser irradiation. A particular glass, with the nominal composition 60 mol% ZnO 40 mol% P_2O_5, characterized by an O/P ratio of 3.25, was found to have a positive change in refractive index (RI) when fs laser pulses are tightly focused into a small (focal) volume below the glass surface [59]. Interestingly, this change in refractive index occurs at compositions which exhibit minima in thermal properties, i.e. the glass transition temperature, Figure 2.4.

The use of fs laser irradiation allows for nonlinear laser-material interactions which induce permanent structural changes [60]. A Ti:sapphire laser system with a 1 kHz repetition rate was used to irradiate glasses from the zinc phosphate system. The increase in RI in the focal volume relative to the bulk is promising for the use of these glasses as substrates for waveguide fabrication.

Glasses in the zinc phosphate binary system, that are not ideal for waveguide formation, demonstration one or more of the following responses: 1. they do not exhibit a positive change in RI under laser irradiation, 2. they do not have smooth structures under laser writing conditions or 3. their refractive indices in the focal region do not experience a change large enough to produce a viable waveguide (i.e., glasses containing 60+ mol%

ZnO) [59]. The response of certain compositions in the xZnO (1-x)P_2O_5 system to fs laser irradiation can be seen in Figure 2.9.

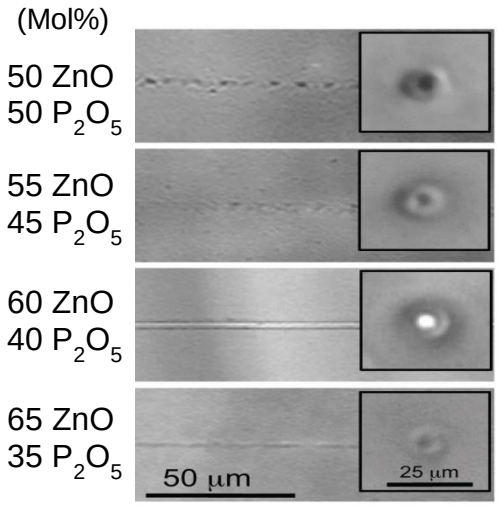

Figure 2.9: White light microscope images of fs-modified zinc phosphate glass, along the waveguide direction (left) and the cross section (right); from Fletcher et al. [59].

Light guiding properties were characterized and changes in refractive index in the irradiated areas were calculated using the numerical aperture of the waveguide [59]. A positive refractive index change was noted in the glass sample with 60 mol% ZnO which is demonstrated by the transmission of white light through the irradiated structure (Figure 2.9).

In addition to microscope images, Raman and fluorescence spectroscopies, can be used to probe the laser-modified volumes and characterize structural changes induced by laser irradiation [59, 61]. Fletcher et al. found that glasses where a negative change in refractive index was created by laser irradiation exhibited a shift to lower wavenumbers

in the main Raman peak attributed to P-O vibrations in Q^2 units (~1200 cm^{-1}), as shown in Figure 2.10.

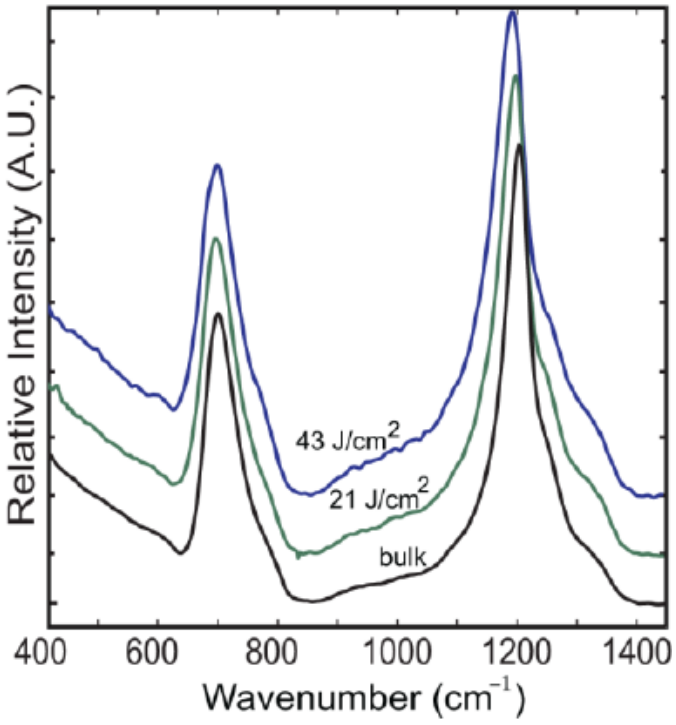

Figure 2.10: Raman spectra of $30ZnO\text{-}10Al_2O_3\text{-}60P_2O_5$ before (bulk) and after modification at fs laser fluences of 21 J/cm^2 (middle) and 43 J/cm^2 (top); from Fletcher et al. [59].

A comprehensive study was completed on crystalline phosphates and Raman peak positions and was referenced to explain the shifts seen in peak position for modified glass volumes. Popovic et al. showed that an increase in wavenumber for the position of Raman peaks assigned to P-O stretching modes are attributed to shorter P-O bond lengths [62]. Assuming this correlation is valid for zinc phosphate glasses, Fletcher et al. showed that glasses with negative Raman shifts exhibited an expansion of the network in the

focal volume, consistent with a decrease in refractive index and a lack of waveguiding. Other work has been conducted with fs laser irradiation of phosphate glasses and it was suggested that the breaking of P-O-P bonds under ionizing irradiation explains the network densification that accompanies a positive refractive index change [63], as determined by variations in the Raman spectra.

A broad peak spanning from 540-740 nm was present in the fluorescence spectra from zinc phosphate glasses irradiated by the fs laser, and the intensity of this peak decreased with increasing ZnO content with focal volumes that did not produce a waveguiding structure, as can be seen in Figure 2.11 [59].

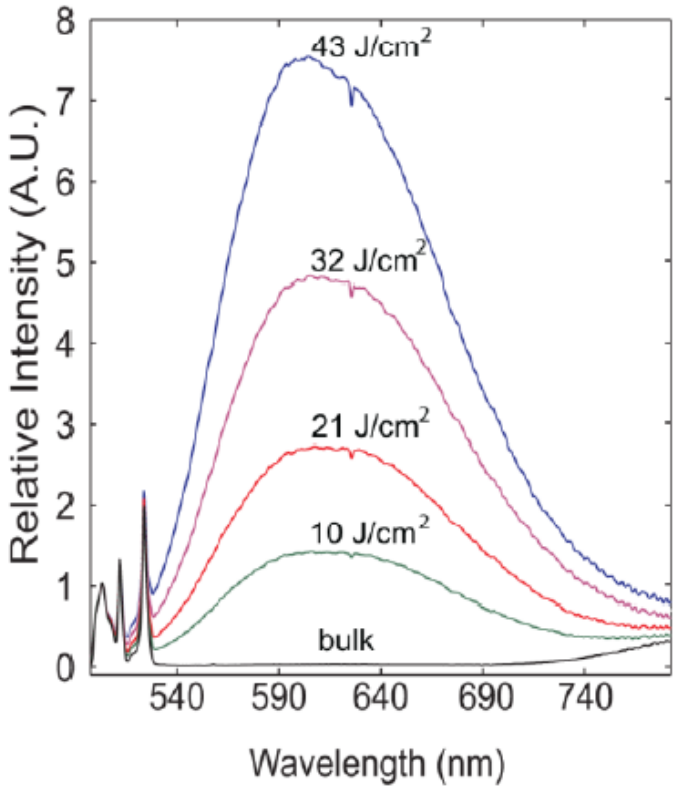

Figure 2.11: Fluorescence spectra of modified and unmodified $30ZnO\text{-}10Al_2O_3\text{-}60P_2O_5$ for laser fluences from 10-43 J/cm^3 [59].

This fluorescence was attributed to the formation of phosphorus oxygen hole centers (POHCs) in the irradiated volume. Glasses with greater negative Raman shifts had larger fluorescence peaks. The 60 mol% ZnO 40 mol% P_2O_5 had no evidence of a significant Raman shift or fluorescence peaks, which has been correlated with the formation of a waveguiding structure in the fs laser focal volume [58].

Work has been conducted on zinc phosphate glasses possessing an O/P ratio = 3.25, with rare earth doping using erbium and ytterbium oxides [61] or up to 10 mol% Al_2O_3 [64]. Although other oxides were added to the binary zinc phosphates, as long as the initial glass structure was defined by an O/P ratio of 3.25 viable waveguiding structures could be produced.

Phosphorus based electronic defects, specifically the phosphorus-oxygen hole center (POHC), have been identified in fs laser irradiated volumes by fluorescence measurements [61, 65]. Understanding the formation of electronic defects, particularly ones that absorb color, can help to elucidate possible mechanisms behind the fs laser induced structural changes. Many studies have been completed involving defect formation under ionizing conditions such as gamma, x-ray and neutron exposure in various types of glasses [66]. It is known that different energy exposures will affect the glass network in varying ways. Higher energy radiation, such as x-rays and gamma rays, will rupture bonds, leading to discoloration in the visible spectrum and partial destruction of the network [16, 67]. UV exposure, or less energetic radiation, induces defects that mainly fluoresce under UV light and only excite the most stable defects [68].

Studies of irradiated phosphate containing glasses established the existence of several electronic defects associated with the phosphorus nuclei [15, 16, 69-74].

Evidence has been given for aluminum-oriented defects in silicate glasses although none have been identified in phosphate glasses. These changes in the electronic structure of the network are commonly characterized using electron spin resonance (ESR) and ultraviolet-visible spectroscopy (UV/Vis). The species shown in Figure 2.12 are the main electron and hole centers found in phosphate, or phosphorus-containing, glasses after ionizing irradiation [16].

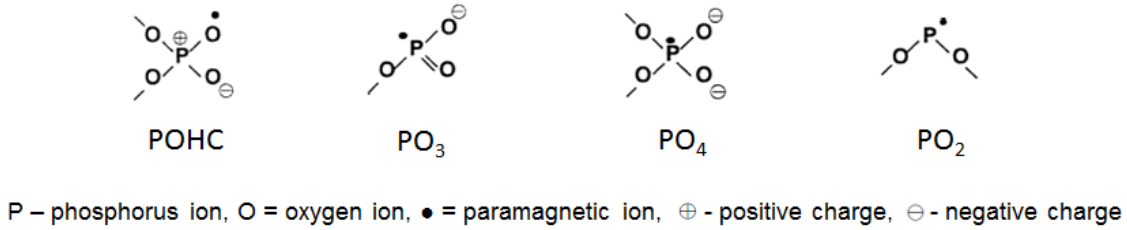

Figure 2.12: The types of electronic defects identified in phosphate glasses; from Ehrt et al. [16]

Ebeling et al. found that the field strength of the modifiers added to phosphates will affect the type of defects that form and the symmetry of their signals in ESR data [69]. This supports the notion that the glass composition has a significant effect on responses to optical stimuli. The compositional changes, and their resulting effect on high intensity responses, should be understood for further development of glasses for optical applications.

2.5 CONCLUSIONS

Additions of metal oxides have been shown to improve the resistance of phosphate glasses to aqueous attack. Although the improvement of chemical durability is a necessity, the addition of oxide compounds to glass formers will result in structural and property changes. Increased atmospheric resistance allows for the characterization of properties and structures, in addition to facilitating the ability to process and alter structures using femto-second laser writing, and developing glasses for more widespread use.

The positive change in refractive index as a response to the fs laser radiation is dependent on the initial structure of the glass substrate, as indicated by the restriction of the waveguiding structures to glasses with an O/P ratio of 3.25. Therefore, to eventually understand this composition-related phenomenon, the structures and properties of the glasses of interest should be thoroughly studied and fully characterized.

Research completed to date has shown that there are viable options for metal oxides to add in order to improve chemical durability. It has been noted that the addition of oxides will change the structure and properties of the base glasses, there for systematic studies should be done to understand the new structures that develop. This is accomplished by the work presented in this dissertation.

REFERENCES

1. Auzel, F. and P. Goldner, *Towards rare-earth clustering control in doped glasses.* Optical Materials, 2001. 16: p. 11.

2. Brow, R.K., *Review: the structure of simple phosphate glasses.* Journal of Non-Crystalline Solids, 2000. 263&264: p. 1-28.

3. Brow, R.K., et al., *The short-range structure of zinc polyphosphate glass.* Journal of Non-Crystalline Solids, 1995. 191: p. 45-55.

4. Khor, S.F., et al., *Optical properties of ultraphosphate glasses containing mixed divalent zinc and magnesium ions.* Optical Materials, 2013. 35: p. 5.

5. Khor, S.F., Z.A. Talib, and W.M. Mat Yunus, *Optical properties of ternary zinc magnesium phosphate glasses.* Ceramics International, 2012. 38: p. 6.

6. Takebe, H., Y. Baba, and M. Kuwabara, *Dissolution behavior of ZnO-P_2O_5 glasses in water.* Journal of Non-Crystalline Solids, 2006. 352: p. 3088-3094.

7. Chenu, S., et al., *Structure and properties of $NaPO_3$-ZnO-Nb_2O_5-Al_2O_3 glasses.* Journal of Non-Crystalline Solids, 2012. 358: p. 11.

8. Koudelka, L. and P. Mosner, *Study of the structure and properties of Pb-Zn borophosphate glasses.* Journal of Non-Crystalline Solids, 2001. 293-295: p. 7.

9. Li, S., P. Chen, and Y. Li, *Structural and physical properties in the system ZnO-B_2O_3-P_2O_5-R_nO_m.* Physica B, 2010. 405: p. 6.

10. Kreidl, N.J. and W.A. Weyl, Journal of American Ceramic Society, 1941. 11.

11. Krol, D.M., et al. *Fs-laser fabrication of photonic structures in glass: the role of glass composition*. in *Fifth International Symposium on Laser Precision Microfabrication*. 2004. Bellingham, WA: SPIE.

12. Fletcher, L.B., et al., *Direct femtosecond laser waveguide writing inside zinc phosphate glass.* Optics Express, 2011. 19: p. 7929-7936.

13. Fletcher, L.B., et al., *Femtosecond laser writing of waveguides in zinc phosphate glasses.* Optical Materials Express, 2011. 1: p. 845-855.

14. Dekker, P., et al., *Annealing dynamics of waveguide Bragg gratings: evidence of femtosecond laser induced colour centres.* Optics Express, 2010. 18(4): p. 10.

15. Ebeling, P., D. Ehrt, and M. Friedrich, *X-ray induced effects in phosphate glasses.* Optical Materials, 2002. 20: p. 11.

16. Ehrt, D., P. Ebeling, and U. Natura, *UV Transmission and radiation-induced defects in phosphate and fluoride-phosphate glasses.* Journal of Non-Crystalline Solids, 2000. 263&264: p. 11.

17. Aitken, B.G., et al., *Non-lead sealing glasses (US patent #5246890),* 1993, Corning Incorportated: United States.

18. Morena, R.M., *Phosphate glasses as alternatives to Pb-based sealing frits.* Journal of Non-Crystalline Solids, 2000. 263&264: p. 6.

19. Knowles, J.C., *Phosphate based glasses for biomedical applications.* Journal of Materials Chemistry, 2003. 13: p. 7.

20. Vitale-Brovarone, C., et al., *Novel phosphate glasses with different amounts of TiO_2 for biomedical applications: Dissolution tests and proof of concept of fibre drawing.* Materials Science and Engineering C, 2011. C31: p. 9.

21. Kodama, H., *Phosphate Optical Glass (US patent 4476233),* S.a. Shapiro, Editor 1984, Nippon Kogaku K. K.

22. Martinez-Martinez, R., et al., *White light generation through the zinc metaphosphate glass activated by Ce^{3+}, Tb^{3+} and Mn^{2+} ions.* Journal of Luminescence, 2009. 129: p. 5.

23. Klein, R.M., et al., *Aluminophosphate Luminescent Glass (US Patent 4134851),* 1979, GTE Laboratories Incorporated. p. 3.

24. Marino, A.E., et al., *Durable phosphate glasses with lower transition temperatures.* Journal of Non-Crystalline Solids, 2001. 298: p. 5.

25. Chen, P., et al., *Sturcture and Crystallization of ZnO-B_2O_3-P_2O_5 Glasses.* Glass Physics and Chemistry, 2011. 37(1): p. 29-33.

26. Fu, C., et al., *Structure and property of ZnO content with Tb^{3+} doped zinc aluminum phosphate glass.* Applied Mechanics and Materials, 2012. 117-119: p. 4.

27. Karabulut, M., E. Metwalli, and R.K. Brow, *Structure and properties of lanthanum-aluminum-phosphate glasses.* Journal of Non-Crystalline Solids, 2001. 283: p. 9.

28. Massera, J., et al., *Effect of the glass composition on the chemical durability of zinc-phosphate-based glasses in aqueous solutions.* Journal of Physics and Chemistry of Solids, 2013. 74: p. 7.

29. Lucacel, R.C., O. Ponta, and V. Simon, *Short-range structure and in vitro behavior of ZnO-CaO-P_2O_5 bioglasses.* Journal of Non-Crystalline Solids, 2012. 358: p. 7.

30. Canioni, L., et al., *Three-dimensional optical data storage using third-harmonic generation in silver zinc phosphate glass.* Optics Letters, 2008. 33(4): p. 3.

31. Van Wazer, J.R., *Phosphorus and its Compounds Volume I: Chemistry*. Vol. 1. 1958, New York: Interscience Publishers, Inc. 954.

32. Brow, R.K., *Review: the structure of simple phosphate glasses.* Journal of Non-Crystalline Solids, 2000. 263&264: p. 28.

33. Khor, S.F., et al., *Degradation study on ternary zinc magnesium phosphate glasses.* Journal of Materials Science, 2011. 46: p. 6.

34. Minami, T. and J.D. Mackenzie, *Thermal expansion and chemical durability of phosphate glasses.* Journal of American Ceramic Society, 1977. 60: p. 4.

35. Takebe, H., Y. Baba, and M. Kuwabara, *Dissolution behavior of ZnO-P_2O_5 glasses in water.* Journal of Non-Crystalline Solids, 2006. 352: p. 7.

36. Hoppe, U., *A structural model for phosphate glasses.* Journal of Non-Crystalline Solids, 1996. 195: p. 10.

37. Brow, R.K., C.A. Click, and T.M. Alam, *Modifier coordination and phosphate glass networks.* Journal of Non-Crystalline Solids, 2000. 274: p. 9-16.

38. Hoppe, U., et al., *Structure of zinc phosphate glasses probed by neutron and X-ray diffraction of high resolving power and by reverse Monte Carlo simulations.* Journal of Non-Crystalline Solids, 2005. 351: p. 12.

39. Tischendorf, B., et al., *A study of short and intermediate range order in zinc phosphate glasses.* Journal of Non-Crystalline Solids, 2001. 282: p. 147-158.

40. Sales, B.C., et al., *Structure of zinc polyphosphate glasses.* Journal of Non-Crystalline Solids, 1998. 226: p. 287-293.

41. Meyer, K., *Characterization of the structure of binary zinc ultraphosphate glasses by infrared and Raman spectroscopy.* Journal of Non-Crystalline Solids, 1997. 209: p. 227-239.

42. Kordes, E., Z. Phys. Chem., 1941. 50B: p. 194.

43. Kordes, E. and R. Nieder, Glastechn. Ber., 1968. 41.

44. Kordes, E., W. Vogel, and R. Feterowsky, Z. Elektrochem, 1953. 57: p. 282.

45. Walter, G., et al., *The structure of zinc polyphosphate glass studied by diffraction methods and ^{31}P NMR.* Journal of Non-Crystalline Solids, 2004. 333: p. 11.

46. Walter, G., et al., *Intermediate range order in MeO-P_2O_5 glasses.* Journal of Non-Crystalline Solids, 1997. 217: p. 299-307.

47. Matsubara, E., et al., *Structural study of binary phosphate glasses with MgO, ZnO, and CaO by X-ray diffraction.* Journal of Non-Crystalline Solids, 1988. 103: p. 8.

48. Hoppe, U., G. Walter, and D. Stachel, *The short range order of metaphosphate glasses investigated by x-ray diffraction.* Physics and Chemistry of Glasses, 1991. 33(6): p. 6.

49. Ouchetto, M., B. Elouadi, and S. Parke, *Study of lanthanide zinc phosphate glasses by differential thermal analysis.* Physics and Chemistry of Glasses, 1991. 32(1): p. 7.

50. Kubo, T., et al., *Thermal properties and structure of zinc phosphate glasses.* Physics and Chemistry of Glasses - European Journal of Glass Science and Technology Part B, 2009. 50(1): p. 4.

51. Sales, B.C., L.A. Boatner, and J.O. Ramey, *Chromatographic studies of the structure of amorphous phosphates: a review.* Journal of Non-Crystalline Solids, 2000. 263&264: p. 12.

52. Sales, B.C., L.A. Boatner, and J.O. Ramey, *Intermediate-range order in simple metal-phosphate glasses: The effect of metal cations on the phosphate-anion distribution.* Journal of Non-Crystalline Solids, 1998. 232-234: p. 6.

53. Meyer, K., A. Barz, and D. Stachel, *Study of the structure of binary magnesium ultraphosphate glasses by vibrational spectroscopy.* Ceramics - Silikaty, 1999. 43(4): p. 6.

54. Walter, G., et al., *Structural study of magnesium polyphosphate glasses.* Journal of Non-Crystalline Solids, 2003. 320: p. 13.

55. Fayon, F., et al., *^{31}P NMR study of magnesium phosphate glasses.* Journal of Non-Crystalline Solids, 2001. 283: p. 7.

56. Rygel, J.L. and C.G. Pantano, *Synthesis and properties of cerium aluminosilicophosphate glasses.* Journal of Non-Crystalline Solids, 2009. 355: p. 8.

57. Syritskaya, Z.M. and V.V. Yakubik, *Toward the study of the glass region in the system P_2O_5-Al_2O_3-ZnO.* Steklo i Keramika (translated), 1960. 17(2): p. 3.

58. Metwalli, E. and R.K. Brow, *Modifier effects on the properties and structures of aluminophosphate glasses.* Journal of Non-Crystalline Solids, 2001. 289: p. 10.

59. Fletcher, L.B., et al., *Direct femtosecond laser waveguide writing inside zinc phosphate glass.* Optics Express, 2011. 19(9): p. 7.

60. Krol, D.M., *Femtosecond laser modification of glass.* Journal of Non-Crystalline Solids, 2008. 354: p. 9.

61. Fletcher, L.B., et al., *Femtosecond laser writing of waveguides in zinc phosphate glasses.* Optical Materials Express, 2011. 1: p. 11.

62. Popovic, L., D. de Waal, and J.C.A. Boeyens, *Correlation between Raman wavenumbers and P-O bond lengths in crystalline inorganic phosphates.* Journal of Raman spectroscopy, 2005. 36: p. 10.

63. Little, D.J., et al., *Mechanism of femtosecond-laser induced refractive index change in phosphate glass under low repetition-rate regime.* Journal of Applied Physics, 2010. 108: p. 5.

64. Troy, N., *Materials and Techniques for the Femtosecond Laser Fabrication of Optical Devices in Glass*, in *Applied Science*2012, University of California, Davis: Davis. p. 67.

65. Ams, M., et al., *Investigation of Ultrafast Laser-Photonic Material Interactions: Challenges for Directly Written Glass Photonics.* IEEE Journal of Selected Topics in Quantum Electronics, 2008. 14(5): p. 12.

66. Griscom, D.L., *Defects in Amorphous Insulators.* Journal of Non-Crystalline Solids, 1978. 31: p. 26.

67. Ehrt, D. and W. Vogel, *Radiation effects in glasses.* Nuclear Instruments and Methods in Physics Research B, 1992. B65: p. 9.

68. Moncke, D. and D. Ehrt, *Photoionization of polyvalent ions*, in *Materials Science Research Horizons*, H.P. Glick, Editor 2007, Nova Science Publishers, Inc. p. 56.

69. Ebeling, P., D. Ehrt, and M. Friedrich, *Influence of modifier cations on the radiation-induced effects of metaphosphate glasses.* Glass Science and Technology, 2003. 76(2): p. 6.

70. Friebele, E.J. and D.L. Griscom, *Radiation Effects in Glass*. Treatise on Materials Science and Technology, ed. M. Tomozawa, R.H. Doremus, and H. Herman. Vol. 17, Glass II. 1979, Troy, New York: Academic Press. 362.

71. Griscom, D.L., *Electron Spin Resonance in Glasses.* Journal of Non-Crystalline Solids, 1980. 40: p. 62.

72. Griscom, D.L., et al., *Fundamental defect centers in glass: Electron spin resonance and optical absorption studies of irradiated phosphorus doped silica glass and optical fibers.* Journal of Applied Physics, 1983. 54: p. 21.

73. Moncke, D. and D. Ehrt, *Irradiation induced defects in glasses resulting in the photoionization of polyvalent dopants.* Optical Materials, 2004. 25: p. 13.

74. Natura, U., T. Feurer, and D. Ehrt, *Kinetics of UV laser radiation defects in high performance glasses.* Nuclear Instruments and Methods in Physics Research B, 2000. 166-167: p. 6.

PAPER

1. THE STRUCTURE AND PROPERTIES OF ZINC ALUMINOPHOSPHATE GLASSES

Charmayne E. Smith and Richard K. Brow
Missouri University of Science and Technology
Rolla, MO 65409, US
Lionel Montagne and Bertrand Revel
Université de Lille 1, Sciences et Technologies
Unité de Catalyse et de Chimie du Solide – UMR CNRS 8181
59655 Villeneuve d'Ascq, France

ABSTRACT

The glass forming region of the ZnO-Al_2O_3-P_2O_5 (ZAP) system was determined and the structures and properties of the glasses were characterized. For glasses with a constant O/P ratio, i.e., with similar average phosphate anion distributions, and with increasing alumina content, there is an increase in molar volume and glass transition temperature and a decrease in density and refractive index. The structures of the ZAP glasses were characterized by Raman spectroscopy, ^{31}P and ^{27}Al magic angle spinning (MAS) nuclear magnetic resonance (NMR) spectroscopy, and high pressure liquid chromatography (HPLC). Systematically shorter phosphate anions constitute the structures of glasses with greater O/P ratios. The average aluminum coordination number (CN_{Al}) changes systematically with composition, from ~4.0 to ~5.6, depending on the numbers of terminal oxygens available to coordinate each Al-cation. Glass properties are sensitive to both the types and concentrations of the P-anions as well as the CN_{Al}.

1.1 INTRODUCTION

Zinc phosphate glasses have been developed for a variety of applications, including low temperature seals [1-3] and as hosts for luminescent ions [4-6]. More recently, it has been shown that the optical properties of zinc phosphate glasses can be modified with a femto-second laser [7-12], making these glasses candidates for a variety of optical devices.

There have been many studies of the structures and properties of binary Zn-phosphate glasses [13-27]; glasses with the nominal molar composition $xZnO\cdot(1\text{-}x)P_2O_5$ have been made with up to 80 mole% ZnO [26]. Kordes classified the $xZnO\cdot(1\text{-}x)P_2O_5$ system as anomalous because of discontinuities in the composition-property relationships near x = 0.5, the metaphosphate composition [13]. It has been argued that such breaks indicate changes in the Zn coordination environment; e.g., the Zn coordination number decreases from 6 to 4 with an increase of the ZnO content to 50 mol% [14, 15]. However, diffraction studies completed more recently indicate a preference for tetrahedral Zn coordination for glasses with ZnO contents from 45-65 mol% [21] and for glasses with ZnO concentrations greater than 50 mol% [23, 28].

Phosphate anionic structures can be described using the Q^n-terminology, where 'n' represents the number of bridging oxygens on a phosphate tetrahedron [19]. For example, changes in the types of phosphate tetrahedra with the addition of ZnO can be represented by the reaction:

$$2Q^n + ZnO \rightarrow 2Q^{n-1} \qquad (1)$$

Here, the oxygen ions accompanying the ZnO added to phosphate glasses replace bridging oxygens (P-O-P) with nonbridging oxygens (P-O-Zn) on the phosphate tetrahedra.

The structures of binary Zn-phosphate (ZP) glasses have been studied by infrared [17, 18] and Raman [17, 18, 20, 26] spectroscopies, ^{31}P NMR [20, 25, 26], X-ray photoelectron spectroscopy (XPS) [16, 27], and high pressure liquid chromatography (HPLC) [24, 26]. For glasses with increasing ZnO-content (increasing O/P ratio), the average phosphate anion becomes shorter as described by Equation 1. For compositions with higher O/P ratios, especially near the pyrophosphate stoichiometry (x=0.67, O/P=3.5), the glasses possess a broader range of P-tetrahedra than are expected from Equation 1. Disproportionation reactions like the one shown here occur in these melts to produce glasses with more complex structures:

$$2Q^1 \rightarrow Q^0 + Q^2 \qquad (2)$$

The broader distribution of phosphate anions that results from such disproportionation reactions may contribute to the larger glass forming range typical of the binary zinc phosphate system.

A disadvantage of the binary zinc phosphate glasses is their relatively poor chemical durability. The bonds between Zn polyhedra and P-anions are readily hydrolyzed, leading to the rapid degradation of the glass surface [29]. Koudelka and others have shown that with the addition of certain oxides, for example B_2O_3 and Nb_2O_5 [30-32], more hydrolytically stable linkages form between the phosphate anions, improving chemical durability.

It has long been known that the addition of alumina to a phosphate glass improves its chemical durability [33]. Brow et al. showed that the coordination environments of Al-cations, and so the properties, of sodium aluminophosphate glasses depend on the O/P ratio [34, 35]. More recent structural studies of Ca- [36] and other ternary aluminophosphate glasses [37] show similar compositional dependences of the Al coordination environments.

Fu, et al. recently reported the density, molar volume, refractive index and Raman spectra for three glasses in the zinc aluminophosphate (ZAP) system, doped with small amounts of terbium oxide [38], while others have studied the luminescence properties of ZAP glasses co-doped with Tm_2O_3 and Dy_2O_3 [5]. Interestingly, there does not appear to be any systematic study of the properties and structures of glasses from the ternary ZnO-Al_2O_3-P_2O_5 system. The purpose of this paper then is to report the glass-forming range for ZAP compositions with O/P > 3, to describe useful properties, and to provide information about their compositionally-dependent structures.

1.2 EXPERIMENTAL PROCEDURES

Zinc aluminophosphate (ZAP) glasses were prepared by batching appropriate mixtures of $NH_4H_2PO_4$ (ACS, 98.0% - Alfa Aesar), ZnO (reagent grade, ≥ 99.0% - Sigma Aldrich), Al_2O_3 (99.5% metals basis – Alfa Aesar) and/or aluminum metaphosphate (Alfa Aesar) to produce 15-25 grams of glass. The batches were thoroughly mixed, calcined in high purity alumina crucibles (AdValue Technology, 99.9%) for 15-18 hours at 500 °C to evolve water and NH_3, then melted at temperatures between 1000-1500 °C for 1-3 hours, depending on the composition. For glasses melted above 1275 °C, the crucibles were covered with alumina discs to minimize P_2O_5 loss.

Melts were quenched by pouring into cylindrical steel molds (10 mm in diameter and 25 mm tall) when possible, or by quenching between two copper plates. Samples were annealed near their glass transition temperatures (T_g) for two hours. The glass-forming region described in this work is defined as those compositions which form x-ray amorphous glasses from melts with a maximum melting temperature of 1500 °C.

Annealed samples, 10 mm in diameter and ~1 mm thick, were polished to a 1200 grit (~5 μm) finish for optical measurements. Refractive index at 632.8 nm was measured using a prism coupler (Metricon model 2010/M); the uncertainty of these measurements is ±0.0004.

The density of annealed glass samples was measured by Archimedes' method using distilled water as the immersion liquid. Three samples of each glass were measured and the standard deviation was recorded (typically ±0.008 g/cm^3). The molar volume was calculated by dividing the density of each glass by the molecular mass, calculated from the analyzed glass compositions, of polished samples, as determined by a Helios NanoLab 600 FIB/FESEM equipped with an energy dispersive spectrometer. The intensities of the Zn-Kα, Al- Kα, and P- Kα lines were determined from at least three different areas on each sample, converted to the relative concentration of each respective oxide using the system sensitivity factors, and the average compositions are reported. Three different pieces of several samples were analyzed in a similar manner, and from these analyses, the overall estimated relative uncertainty of the reported compositions is ±2.5 %.

Glass transition temperatures (T_g) were determined by differential thermal analysis (DTA, Perkin-Elmer DTA-7) by heating 35-40 mg of glass powders (< 75 μm)

at 10 °C/min in high purity, open alumina crucibles under a nitrogen flow. The onset method was used to determine T_g and the estimated uncertainty is ±5 °C.

The coefficient of thermal expansion (CTE) was measured on glass cylinders using an Orton dilatometer, model 1600D, with a heating rate of 10 °C/min. The CTE values were determined as the slope of the linear fit of the dilatometry data between 200 and 400 °C and were reproducible to ±0.2 ppm/°C.

Weight loss measurements were made on bulk glasses to determine relative chemical durability in deionized (DI) water at room temperature (~20 ˚C) for up to 170 hours. Polished samples (~5 μm) were rinsed with acetone and dried before testing. A constant sample surface area (SA) to solution volume ratio of 0.035 cm^{-1} was used for each experiment. Samples were removed from the water periodically, dried and weighed, and then returned to the solution. Three samples were tested for each condition and the average weight loss is reported.

Raman spectra were collected with a Horiba-Jobin Yvon LabRam spectrometer between 100-1500 cm^{-1} using a HeNe laser (632.8 nm) as the excitation source.

Magic Angle Spinning (MAS) Nuclear Magnetic Resonance (NMR) spectroscopy was performed with a Bruker spectrometer with magnetic field strengths of 9.4 T and 18.8 T for ^{31}P and ^{27}Al spectra, respectively. The ^{31}P spectra were collected in 8 scans with a spinning rate of 12,500 Hz, a relaxation delay equal to 120 s and a pulse length of 2.38 μs. The ^{27}Al spectra were collected in 512 scans, 2 s relaxation delay, pulse length of 1 μs and a spinning rate of 20,000 Hz. ^{31}P and ^{27}Al chemical shifts were referenced to 85% H_3PO_4 and 0.1M $AlCl_3$ solutions, respectively. The decomposition of the NMR spectra was carried out using the DM-FIT software [39]. The distribution of quadrupolar

parameters of the ^{27}Al nucleus induces an asymmetric line shape of the resonances, which has been fitted with the Czjzek distribution model of the DMFit software [40].

High pressure liquid chromatography was done to characterize phosphate anion distributions using a Dionex GP50-2 pump, an AD25 absorbance detector and an Ionpack AS7 4 x 250 mm Analytical Ion exchange column. Samples were ground to <53 μm particle size and dissolved in a solution of 5 mM EDTA and 0.22 M NaCl (pH = 10) for 1-3 hrs. and analyzed within 24 hours. Chromatographs were collected with a linear solution gradient from 0.053M NaCl to 0.5 M NaCl, both with 5 mM EDTA. Further information about these types of HPLC measurements can be obtained elsewhere [24, 41].

1.3 RESULTS

Table 1 lists the processing temperatures and times, as well as the as-batched and analyzed (EDS) compositions of the ZAP glasses prepared for this study. Due to the loss of P_2O_5 and the transfer of Al_2O_3 from the alumina crucibles, especially at the higher processing temperatures, the analyzed compositions deviate from the batched compositions.

Figure 1 shows the glass forming range based on the analyzed compositions. Batches that were un-melted at 1500 °C, or that crystallized on cooling, are shown as squares (red) in Figure 1. (These symbols represent nominal compositions, not analyzed.). No alumina-free glasses were prepared because of alumina-transfer from the crucible, and no ultraphosphate compositions were synthesized with O/P ratios less than 3.0 (blue line in Figure 1) because of alumina transfer and the loss of P_2O_5 from the melts. The maximum concentrations of ZnO and Al_2O_3 were about 70 mole% and 34

mole%, respectively. These values are similar to the glass forming limits that were previously established in studies of the binary zinc phosphate [26] and aluminophosphate [42-44] systems. The reported glass forming ranges for these binary systems are also indicated in Figure 1.

1.3.1 Glass Properties. Weight loss data for a series of ZAP glasses with similar O/P ratios of 3.32 ± 0.02, are shown in Figure 2a. Dissolution rates were determined from the slope of the normalized weight loss versus time plot over the course of the experiment, and these rates decreased by several orders of magnitude with increasing alumina content. For example, the dissolution rates for the glasses shown in Figure 2a decreased from $2.5x10^{-5}$ g/cm^2-min for the 50.9ZnO-6.1Al_2O_3-43.0P_2O_5 glass (O/P = 3.30) to $<3x10^{-8}$ g/cm^2-min for the 28.3ZnO-19.9Al_2O_3-51.8P_2O_5 glass (O/P = 3.35), as shown in Figure 2b. Similar decreases in dissolution rates were noted for alumina additions in other series of glasses with similar O/P ratios. For example, the dissolution rates for ZAP glasses with average O/P ratio of 3.06 ± 0.03 are also shown in Figure 2b.

Table 2 gives the properties of the ZAP glasses. For glasses with similar O/P ratios, the densities decrease systematically with greater Al_2O_3, as shown for two series in Figure 3a. The densities of glasses with low alumina contents (< 2.5 mol %) are similar to the densities of binary Zn-phosphate glasses reported in the literature [20, 45, 46]. The overall effects of composition on density are summarized in the contour plot in Figure 3b. In addition to the systematic decrease in density with increasing alumina content, there is a significant increase in density with increasing ZnO content, particularly for glasses with low alumina-contents. Figure 4 shows that the molar volume of ZAP glasses with low (<

2.5 mol%) Al_2O_3-contents decreases systematically with increasing ZnO content, again in agreement with an earlier study of binary Zn-phosphate glasses [20]. The ZAP glasses have slightly greater molar volumes than the binary ZP glasses because the small amounts of alumina in the former reduce density relative to the latter (Figure 3b). The overall relationship between molar volume and ZAP glass composition is shown in the contour plot in Figure 4b.

Figure 5a shows the effect of alumina content on the glass transition temperature (T_g) for two series of ZAP glasses with O/P ratios of 3.10 and 3.24. The inset shows T_g for glasses with similar Al_2O_3 contents (~2.7 mol% and ~10 mol%) as a function of Zn/P ratio. There is a minimum in T_g for a Zn/P ratio close to 0.75. The overall compositional trends can be more easily seen in the contour plot shown in Figure 5b.

The coefficient of thermal expansion (CTE) of the ZAP glasses is in the range 5-7x10^{-6}/°C, and decreases with increasing alumina contents (Table 2).

The effects of the ZnO content on the refractive index (at 632.8 nm) for glasses with low (~2.4 mole%) alumina contents is shown in Figure 6a, and the overall effects of composition are shown in the contour plot in Figure 6b. It is clear that the ZnO content has the most significant effect on refractive index; viz., Figure 6a.

1.3.2 Structural Characterization. Figure 7 shows the Raman spectra of glasses with similar O/P ratios (3.23 ± 0.02) and increasing Al_2O_3 contents. The spectra from glasses with ~2 mole% Al_2O_3 in this work are similar to spectra reported elsewhere for binary Zn-phosphate glasses [20, 26, 47], and peak assignments from those studies are used here (Table 3). For the spectra in Figure 7, the peaks near 700 cm^{-1} are assigned to the symmetric stretch of bridging oxygens in Q^2 units and there is a shoulder near 750

cm^{-1} in some of these spectra that is assigned to P-O-P stretching modes associated with chain terminating (Q^1) tetrahedra. The intense peak near 1200 cm^{-1} and the shoulder near 1250 cm^{-1} are assigned, respectively, to the PO_2 symmetric and asymmetric stretching modes of non-bridging oxygens associated with Q^2 units. Peaks associated with both the P-O-P and PO_2 stretching modes become broader and shift to greater frequencies with increasing alumina contents. In addition, a shoulder to the PO_2 peak near 1100 cm^{-1} develops with increasing alumina and this may be related to the presence of chain terminating Q^1 sites, the PO_3 stretching mode listed in Table 3.

^{31}P MAS NMR spectra are shown in Figure 8a and Figure 8b for select glasses with similar O/P ratios (3.09 ± 0.05) and with similar alumina contents (2-3 mole%) but varying O/P ratios, respectively. The peaks near -31 ppm in Figure 8a are associated with Q^2 units and the small peak near -10 ppm is due to Q^1 tetrahedra [20]. The Q^2 peak systematically broadens and shifts to more negative ppm for glasses with increasing alumina content; similar behavior has been reported for Q^2 ^{31}P peaks from other aluminophosphate glasses with similar O/P ratios [35, 37, 48]. The shift and broadening of this ^{31}P resonance is due to the formation of P-O-Al bonds, which modify the chemical shielding of the Q^2 sites. Figure 8b shows how changing the O/P ratio affects the principal peaks and their associated spinning sidebands. As the O/P ratio increases, peaks due to Q^2 tetrahedra (near -31 ppm) are replaced by those due to Q^1 tetrahedra (-13 ppm) and Q^0 tetrahedra (+3 ppm), in agreement with previous studies [20].

Figure 9a shows the ^{27}Al NMR spectra for glasses with similar O/P ratios (3.09 ± 0.04) and with increasing alumina content. There are three distinct peaks in these spectra, each indicating a different coordination environment for aluminum. The peaks are

centered near 36 ppm, 7 ppm and -17ppm and are attributed to 4-, 5-, and 6-coordinated aluminum, respectively [35, 49, 50]. As more alumina is added to the glasses with similar O/P ratios, the average aluminum coordination number, calculated from the respective areas of each peak, increases as shown in Figure 9b.

Figure 10a shows the HPLC chromatographs of glasses with similar Al_2O_3 contents (2-3 mole%) and different O/P ratios, whereas Figure 10b shows chromatographs of glasses with similar O/P ratios (3.33 ±0.02) and increasing alumina contents. Each peak represents a P-anion with increasing numbers of tetrahedra (left-to-right). These phosphate anions are described using the P_n terminology where n is the number of P-tetrahedra in a chain. Glasses with low O/P ratios (close to 3.0) possess longer chains, which are unresolved by the HPLC method and these longer chains form the large hump at longer retention times, as seen in Figure 10a. The chromatograph from the glass with the largest O/P ratio in Figure 10a (O/P = 3.56) is dominated by peaks associated with P_1 (29% relative area), P_2 (52%) and P_3 (15%) anions. The chromatographs for the glasses with similar O/P ratios and increasing alumina contents (Figure 10b) are similar, but possess slightly broader anion distributions for glasses with greater alumina contents.

1.4 DISCUSSION

The addition of alumina to zinc phosphate glass significantly improves the chemical durability (Figure 2); making it possible to design more chemically stable optical substrates for writing optical elements with femto-sec lasers. Recent research at UC-Davis [51] has shown that optical waveguides can be written into the more durable

ZAP glasses with O/P ratios near 3.25 and that the characteristics of these waveguides are as good, or better, as those written into less durable, alumina-free glasses [7, 52].

The density and refractive index of the ZAP glasses are most dependent on the ZnO-content. Glasses with greater ZnO-contents have greater densities (Figure 3) due in part to the greater relative mass of Zn, compared to Al and P, and to the lower molar volumes of the ZnO-rich glasses (Figure 4). The refractive indices of the ZnO-rich glasses are also greater. This is consistent with both the greater ionic refractivity of Zn^{2+} (0.7), compared to Al^{3+} (0.14) and P^{5+} (0.05) [53], and the expected greater refractivity of oxygens associated with the P-O-Zn bonds as compared with oxygens in P-O-P and P-O-Al bonds [54]. For glasses with similar ZnO-contents, the replacement of P_2O_5 by Al_2O_3 has little effect on either density or refractive index.

1.4.1 Phosphate Anion Distributions. When less-acidic metal oxides are combined with P_2O_5 in a melt, the metal oxide polyhedra are incorporated into the phosphate network by sharing oxygens with the phosphate anions. For the ZAP glasses, these structural changes can be summarized by the following reactions:

$$\text{P-O-P} + \text{ZnO} \rightarrow \text{P-O-Zn-O-P} \quad (3)$$

$$\text{P-O-P} + \text{Al}_{2/3}\text{O} \rightarrow \text{P-O-Al}_{2/3}\text{-O-P} \quad (4)$$

The net effect of reactions that reduce the relative numbers of bridging oxygens (P-O-P), like those shown above, is a reduction in the average size of the polyphosphate anions. If one considers a metaphosphate glass (O/P = 3) as consisting of Q^2 tetrahedra that form long chain, or ring, anions then the addition of ZnO and/or Al_2O_3 will shorten those chains (or replace the rings) by incorporating the additional oxygen into chain-terminating (Q^1) sites. Evidence for such structural modifications of glasses with

increasing O/P ratios can be readily seen in the Raman and ^{31}P NMR spectra, and in the chromatographic data. For example, the Q^2 peak near -31 ppm in the ^{31}P NMR spectra in Figure 8b is dominant for the glass with O/P = 3.05, but becomes a shoulder on the dominant Q^1 peak at -13 ppm for the glass with O/P = 3.44. The further incorporation of ZnO to increase O/P to 3.56 results in the creation of Q^0 sites (+3 ppm) to accommodate the added oxygen.

The chromatographic data shown in Figure 10a indicates that the phosphate anions become progressively shorter with increasing O/P ratio. The large hump at longer retention times, due to unresolvable anions with more than about 13 P-tetrahedra, for the glass with an O/P = 3.05 is replaced by single peaks due to anions with four or fewer P-tetrahedra for the glass with an O/P = 3.56. The relationship between the incorporation of oxygen (increasing O/P ratio) into the phosphate network with the addition of metal oxide (whether ZnO or Al_2O_3) and the average phosphate anion can be quantitatively described [44]. For a glass with the nominal composition $xM_{2/v}O$ $(1-x)P_2O_5$, the average phosphate anion chain-length, $\bar{n}$, will be given by

$$\bar{n} = \frac{2}{\sum_j \frac{[M_j][v_j]}{[P]} - 1} \tag{5}$$

where v is the valence of the metal oxide and $[M_j]$ and [P] are the relative atomic fractions of the metal ions and phosphorus, respectively [24]. Using the compositions of the ZAP glasses (Table 1), the predicted $\bar{n}$ from Equation (5) can be compared with that obtained from their respective chromatographs; that comparison is shown in Figure 11. The average chain lengths can also be obtained from the ^{31}P NMR spectra through peak fitting and using the relative percentages of the Q^n units with the following equation:

$$\bar{n} = \left(\frac{100}{\left[\%Q^1/_2 \right] + \%Q^0} \right) \tag{6}$$

The close agreement between the predicted and measured average chain lengths (Figure 11) across the entire range of compositions (O/P ratios) indicates that both ZnO and Al_2O_3 have similar effects on the development of the phosphate network and that reactions (3) and (4) adequately summarize those effects.

For samples with a fixed O/P ratio, the average chain length should be constant. For example, the glasses in Figure 10b each have an O/P ratio of about 3.33 and, by using Equation 5, have an average chain length of 3.0 (±0.2) tetrahedra. However, the chromatographs indicate that the chain length distribution becomes slightly broader with increasing alumina content. Al_2O_3 has also been noted to promote the disproportionation of pyrophosphate anions in the glass melt, as described by [44]

$$2P^2 \rightarrow P^1 + P^3 \tag{7}$$

If this reaction can be described in terms of a chemical equilibrium, then the reaction constant (k_2) will be determined from [44]:

$$k2 = \frac{[P3] \times [P1]}{[P2]2} \tag{8}$$

where $[P_n]$ is the area under the n^{th} peak from the HPLC chromatograms.

Figure 12 shows that k_2 increases with increasing alumina-content for two series of glasses with similar O/P ratios. Thus, the replacement of ZnO by Al_2O_3 broadens the distribution of P-anions that constitute the glass structure.

The replacement of ZnO by Al_2O_3 also affects the average properties of the P-O bonds associated with the different metal polyhedra. For example, Figure 13a shows the effect of the relative concentration of Al_2O_3 on the Raman peak position of the PO_2

stretching mode for a series of ZAP glasses with similar O/P ratios, and Figure 13b shows the position of the ^{31}P NMR peak for the Q^2 tetrahedra for the same glasses. In both cases, there are systematic changes in the peak positions as Al replaces Zn: the PO_2 Raman peak increases in frequency and the ^{31}P NMR Q^2 peak shifts to more negative ppm. Both of these spectral trends indicate a general strengthening, or shortening, of the average P-O bonds associated with the different metal polyhedra. For example, Nelson et al. [55] showed that as the bond force of the metal cation on the PO_2 vibrational unit increases there is a shift to greater frequency of the associated peaks. Popovic et al. have also shown that positive shifts in Raman frequencies result from the systematic shortening of P-O bonds [56]. Similar explanations have been offered for the compositional effects on the positions of ^{31}P NMR peaks in aluminophosphate glasses. For example, it has been shown that the ^{31}P peak for a Q^2 unit connected to an alkali or alkaline earth ion will occur at a more positive chemical shift than the ^{31}P peak for a Q^2 unit connected to aluminum [35]. The chemical shifts of phosphorus become more negative, representing a less shielded P nucleus, with the increase in the cationic potential (charge/radius) for the metal oxides. This is due to the increased MO covalency depleting electron density on the phosphorus, leading to decreased shielding.

The replacement of ZnO by Al_2O_3 substantially increases the glass transition temperature (Figure 5a and 5b) and decreases the coefficient of thermal expansion (Table 2). Similar property trends are noted for other phosphate glasses (i.e., Na-aluminophosphate glasses [35]) and can be related to the replacement of Zn-O-P bonds by stronger Al-O-P bonds to link neighboring phosphate anions. These stronger bonds

are associated with both a greater field strength metal cation ($FS_{Al3+} > FS_{Zn2+}$) and the stronger, shorter P-O bonds implied by shifts in the Raman and ^{31}P NMR peaks.

1.4.2 Al-Coordination Environments. The nature of the coordination polyhedra of the Zn^{2+} and Al^{3+} ions is expected to influence the glass properties. For example, breaks in the compositional trends of properties like T_g, density and refractive index for Na-aluminophosphate (NAP) glasses were related to changes in the average Al coordination number [35]. Although CN_{Al} changes systematically with composition for the ZAP glasses (i.e., Figure 9), the compositional dependence of CN_{Al} for these glasses differs from what is seen with the NAP glasses. For NAP glasses with O/P ratios near 3.0, octahedral Al dominates the aluminophosphate structures. In contrast, the average coordination number of Al in the ZAP glasses with O/P ≈ 3.08 is under 5, and it increases as Al_2O_3 replaces ZnO (Figure 9b). For the NAP glasses, the average CN_{Al} depends on the charge associated with the P-anion [35]. A different relationship exists between CN_{Al} and the compositions of the ZAP glasses.

Hoppe has shown that the coordination environment of a metal cation incorporated in a phosphate glass is influenced by the number of terminal (nonbridging) oxygens (TO) available to coordinate that metal cation[57]. For binary phosphate glasses with the molar composition $xM_{2/v}O\ (1\text{-}x)P_2O_5$, where ν is the valence on the metal cation (M), the number of terminal oxygens per M is given by

$$N_{TO} = \frac{v(x+1)}{x} \tag{9}$$

Hoppe noted that when N_{TO} was greater than the coordination number of the M^{v+} cation (CN_M), then those cation polyhedra could be incorporated into a phosphate structure without needing to share terminal oxygens with other metal cation polyhedra.

When N_{TO} was less than CN_M, then some of the cation polyhedra must share TO. The compositional dependence of the properties of many binary phosphate glasses changes at compositions where $N_{TO}=CN_M$ [57], and in other systems [28], CN_M decreases with increasing $R_{2/v}O$ content so that the cation polyhedra avoid sharing common terminal oxygens. Indeed, Brow et al.[42] have shown that the average coordination number of Al-polyhedra in binary aluminophosphate glasses follows Equation (9), decreasing with increasing O/P ratio to prevent Al-polyhedra from sharing common TO.

Hoppe's model can be extended to ternary glasses to explain the effects of composition on the CN_{Al} in the ZAP glasses. Consider first the coordination number of the Zn-ions. It has been shown in x-ray and neutron diffraction studies of binary zinc phosphate glasses [21, 23, 58] that the preferred coordination number for Zn is four. If one assumes that $CN_{Zn}=4$ for the ZAP glasses and that these Zn tetrahedra do not share terminal oxygens with each other or with any Al-polyhedra, then the number of terminal oxygens remaining, per Al, can be calculated from the molar fractions of the glass constituents according to:

$$\frac{TO}{Al} = \frac{(6[Al_2O_3] + 2[P_2O_5] - 2[ZnO])}{2[Al_2O_3]} \quad (10)$$

Following Hoppe, the ratio TO/Al should then be the minimum CN_{Al} to prevent Zn-tetrahedra and/or Al-polyhedra from sharing common terminal oxygens on any phosphate anions, and for every terminal oxygen to link to one ZnO_4 or one AlO_x polyhedron, where x=4, 5, or 6. If TO/Al<4.0, then some metal cation polyhedra must share common terminal oxygens.

Figure 14 compares the TO/Al ratio from Equation (10) with the average CN_{Al} determined from the ^{27}Al NMR spectra for the ZAP glasses, as well as for several Mg-

aluminophosphate (MAP) glasses described in the literature [59]. The ion sizes of Mg^{2+} and Zn^{2+} are similar so it is likely that Mg-tetrahedra are present in the structures of the MAP glasses and a similar analysis of CN_{Al} can then be made for those compositions. Also shown in Figure 14 are the CN_{Al} reported in an NMR study of binary aluminophosphate (AP) glasses [42] and calculated from Equation 10. There is good agreement between CN_{Al} determined from the ^{27}Al NMR spectra of the ZAP, MAP, and AP glasses for TO/Al>4 and the CN_{Al} calculated from Equation (10). This agreement indicates that the coordination environment of the Al-polyhedra is determined by the number of available terminal oxygens and adjusts to avoid sharing common TOs with the Zn- (or Mg-) tetrahedra that also link different phosphate anions. When TO/Al<4, then some terminal oxygens must be shared by neighboring Al- and/or Zn-polyhedra, and Equation (10) can no longer be used to predict CN_{Al}.

1.5 CONCLUSIONS

An investigation of the properties and structures of zinc aluminophosphate glasses has been completed. The corrosion rate in water has been found to decrease by orders of magnitude with the addition of alumina. For glasses with a constant O/P ratio, increasing amounts of alumina increases the T_g, molar volume and refractive index, while decreasing the density and coefficient of thermal expansion. Spectroscopic and chromatographic measurements reveal that the addition of both zinc and aluminum oxide disrupts the phosphate network, creating smaller phosphorus-oxygen anions. Increasing the alumina content results in shorter, stronger P-O bonds in the network and enhances the disproportionation of phosphate anions at higher O/P ratios.

The coordination number of aluminum depends on the number of terminal oxygens available in the network and the avoidance of metal polyhedra that share common oxygens on a P-tetrahedron. The compositional dependence of CN_{Al} is consistent with Hoppe's model of modifier coordination in phosphate glasses.

1.6 ACKNOWLEDGEMENTS

The authors acknowledge the Department of Education for the Graduate Assistance in Areas of National Need (GAANN) fellowship and the National Science Foundation (DMR 1207520) for funding this work. The authors are also grateful to the FEDER, Region Nord Pas-de-Calais, Ministère de l'Education Nationale de l'Enseignement Superieur et de la Recherche, CNRS, and USTL for funding of NMR spectrometers. The contributions of Missouri S&T colleagues: Dr. Jen-Hsien Hsu for the EDS compositional analysis, Lina Ma for helpful discussions, and Ryan Jones for assistance with the synthesis and characterization of the ZAP glasses are greatly appreciated, as are the discussions on femto-second laser processing with Prof. Denise Krol and her colleagues at UC-Davis.

Tables

Table 1: Compositions, melting time and melting temperature of the ZnO-Al_2O_3-P_2O_5 glasses

Sample ID	Batched Values [mol%]			Analyzed Values [mol%]				Melting Conditions
Glass Designation*	ZnO	Al_2O_3	P_2O_5	ZnO	Al_2O_3	P_2O_5	O/P ratio	Temp [°C] / Time [hr]
46-2-52_2.99	30.0	0.0	70.0	46.4	1.5	52.1	2.99	1000 / 1
49-2-49_3.05	50.0	0.0	50.0	48.5	2.1	49.4	3.05	1200 / 3
47-3-50_3.08	20.0	0.0	80.0	46.9	3.4	49.7	3.07	1200 / 2
38-7-55_3.04	40.0	5.0	55.0	38.2	7.1	54.7	3.04	1280 / 3
33-11-56_3.10	30.0	10.0	60.0	33.2	11.1	55.7	3.10	1250 / 3
27-16-57_3.15	20.0	13.0	67.0	26.9	15.7	57.4	3.15	1350 / 3
22-18-60_3.14	10.0	10.0	80.0	21.7	18.4	59.9	3.14	1400 / 3
0-29-71_3.12	0.0	25.0	75.0	0.0	29.4	70.6	3.12	1500 / 1
55-3-43_3.23	55.0	0.0	45.0	54.6	2.6	42.8	3.23	1100 / 3
52-4-43_3.26	50.0	3.0	47.0	52.4	4.4	43.2	3.26	1100 / 3
40-11-49_3.24	39.0	10.0	51.0	40.5	10.6	48.8	3.24	1250 / 3
25-19-57_3.26	25.0	15.0	60.0	24.8	18.7	56.5	3.22	1350 / 3
26-19-55_3.26	20.0	15.0	65.0	26.1	19.1	54.8	3.26	1400 / 3
13-25-62_3.22	10.0	20.0	70.0	13.4	25.0	61.6	3.22	1450 / 3
0-34-66_3.27	0.0	27.0	73.0	0.0	34.0	66.0	3.27	1500 / 1
51-6-43_3.30	51.0	5.0	44.0	50.9	6.1	43.0	3.30	1250 / 3
44-11-45_3.34	42.0	10.0	48.0	44.1	10.7	45.2	3.34	1250 / 3
36-15-49_3.32	33.0	15.0	52.0	36.1	14.9	49.0	3.32	1350 / 3
28-20-52_3.35	24.0	20.0	56.0	28.3	19.9	51.8	3.35	1450 / 3
61-3-37_3.44	60.0	0.0	40.0	60.5	2.8	36.7	3.44	1150 / 3
58-5-37_3.50	58.3	5.0	36.7	58.2	5.1	36.7	3.50	1175 / 3
55-6-39_3.45	55.0	5.0	40.0	55.0	6.3	38.7	3.45	1300 / 3
64-3-34_3.56	66.7	0.0	33.3	63.5	2.7	33.8	3.56	1100 / 1
64-3-33_3.63	65.0	0.0	35.0	64.1	3.3	32.6	3.63	1250 / 2
70-2-29_3.81	70.0	0.0	30.0	70.0	1.6	28.5	3.81	1075 / 2

*In mole %, ZnO-Al_2O_3-P_2O_5_O/P ratio

Table 2: Properties of the ZnO-Al_2O_3-P_2O_5 glasses

Glass Designation*	Density [g/cm^3]	T_g [$^\circ C$]	CTE [$^\circ C^{-1}$] ($x10^{-6}$)	Refractive Index
46-2-52_2.99	2.759	nm	nm	nm
49-2-49_3.05	2.899	450	6.5	1.5268
47-3-50_3.08	2.779	436	nm	1.5238
38-7-55_3.04	2.778	515	6.2	1.5219
33-11-56_3.10	2.736	525	6.3	1.5226
27-16-57_3.15	2.691	606	nm	1.5238
22-18-60_3.14	2.649	611	nm	1.5218
0-29-71_3.12	2.578	753	5.6	1.5284
55-3-43_3.23	3.033	433	6.2	1.5450
52-4-43_3.26	2.919	437	6.1	1.5325
40-11-49_3.24	2.855	449	5.3	1.5250
25-19-57_3.22	2.631	560	nm	1.5133
26-19-55_3.26	2.666	582	5.9	1.5184
13-25-62_3.22	2.571	633	5.6	1.5134
0-34-66_3.27	2.489	795	nm	1.5105
51-6-43_3.30	2.996	442	5.8	1.5446
44-11-45_3.34	2.811	452	5.3	1.5213
36-15-49_3.32	2.667	492	5.1	1.5086
28-20-52_3.35	2.573	533	nm	1.5033
61-3-37_3.44	3.321	441	6.8	1.5729
58-5-37_3.50	3.291	445	6.4	1.5767
55-6-39_3.45	2.995	465	nm	1.5426
63-3-34_3.56	3.552	453	6.6	1.6115
64-4-33_3.63	3.418	nm	nm	1.5946
70-2-29_3.81	3.736	462	nm	1.6323

*In mole %, ZnO- Al_2O_3-P_2O_5_O/P ratio

Table 3: Raman peak assignments from the literature

Wave-number (cm^{-1})	Structural Units	Ref.		Wave-number (cm^{-1})	Structural Units	Ref.
~350	Bending mode of phosphate polyhedral with zinc modifier	[20]		950-970	$(PO_4)_{symm}$ stretch (NBO), Q^0s	[18, 20]
~575	Bend mode related to zinc phosphate network or ZnO_4	[18, 20]		1010	P-O stretch, Q^1 chain terminator	[20, 47]
680	Symm vibrations of P-O-P bonds	[18, 60]		1048	$(PO_3)_{symm}$ stretch (NBO), Q^1s	[20, 47]
702	POP_{symm} stretch (BO), Q^2s	[18, 20, 47]		1138-1140	P-O stretch, Q^1 chain terminator	[18, 20, 47]
750	Symm vibrations of P-O-P BO atoms	[61]		1170-1180	Stretching vibrations of O-P-O/Symm vibrations of middle chain units (PO2)-	[60, 61]
758	POP_{symm} stretch (BO), Q^1s	[20, 47]		1150-1210	$(PO_2)_{symm}$ stretch (NBO), Q^2s	[18, 20, 47]
790	$(P\text{-}O\text{-}P)_s$ stretch in very short phosphate chains or in rings	[18]		1210-1260	$(PO_2)_{asymm}$ stretch (NBO), Q^2s	[18, 20, 47]
930	Asymmetric vibrations of P-O-P	[61]				

Figures

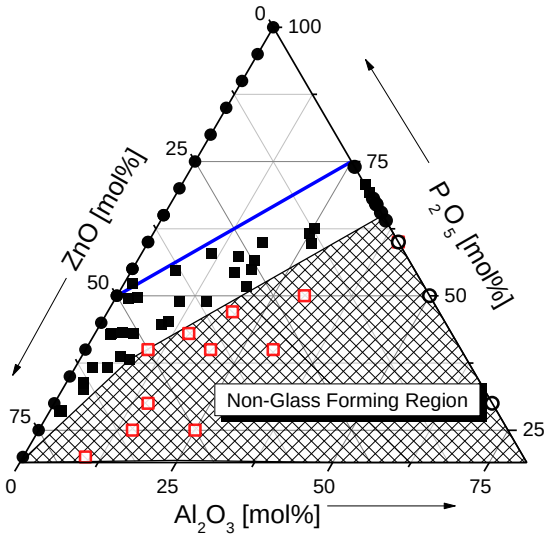

Figure 1: ZAP compositional diagram. Compositions of melt-quenched glasses are shown as black squares and compositions that were un-melted (1500 °C) or crystallized on quenching are indicated by open squares. The cross-hatched area represents the non-glass forming range. The compositions of melt quenched glasses reported in the literature[17],[20],[26],[41],[43] are shown as black circles and those reported to be non-glassforming compositions are shown as open circles The blue line indicates where: O/P=3 with increasing alumina from left to right.

a.

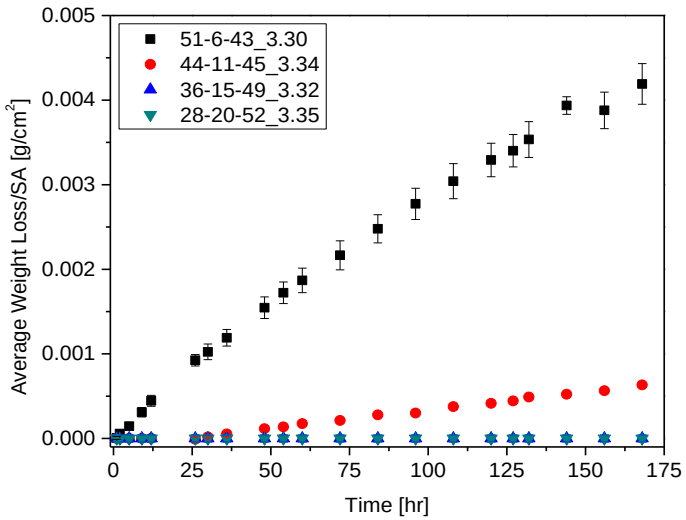

b.

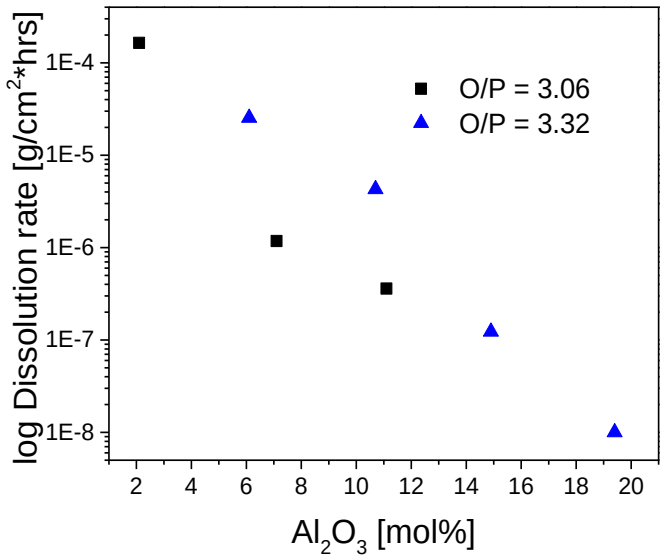

Figure 2: a. Weight loss data and b. log dissolution rates for ZAP glasses with O/P ratio = 3.06 ± 0.03 and 3.32 ± 0.02, in deionized water at room temperature.

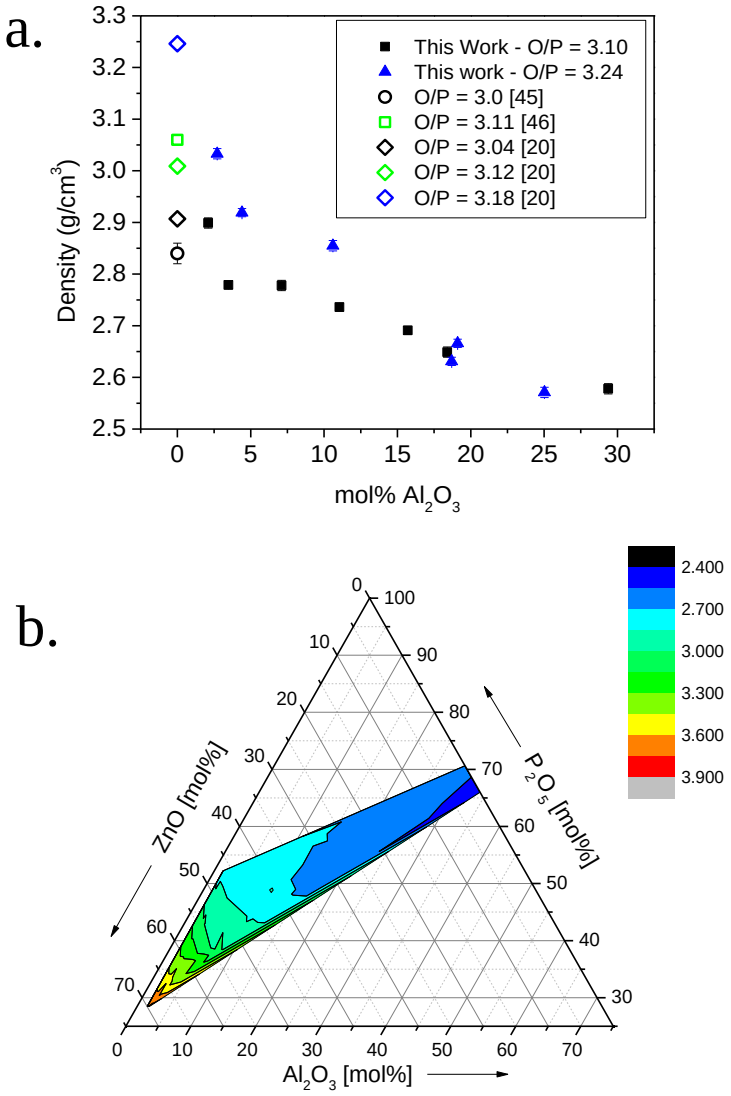

Figure 3: Density for glasses in the ZAP system a. with varying alumina content and the indicated O/P ratios, with representative densities from the literature (open symbols); b. as a contour plot for all compositions.

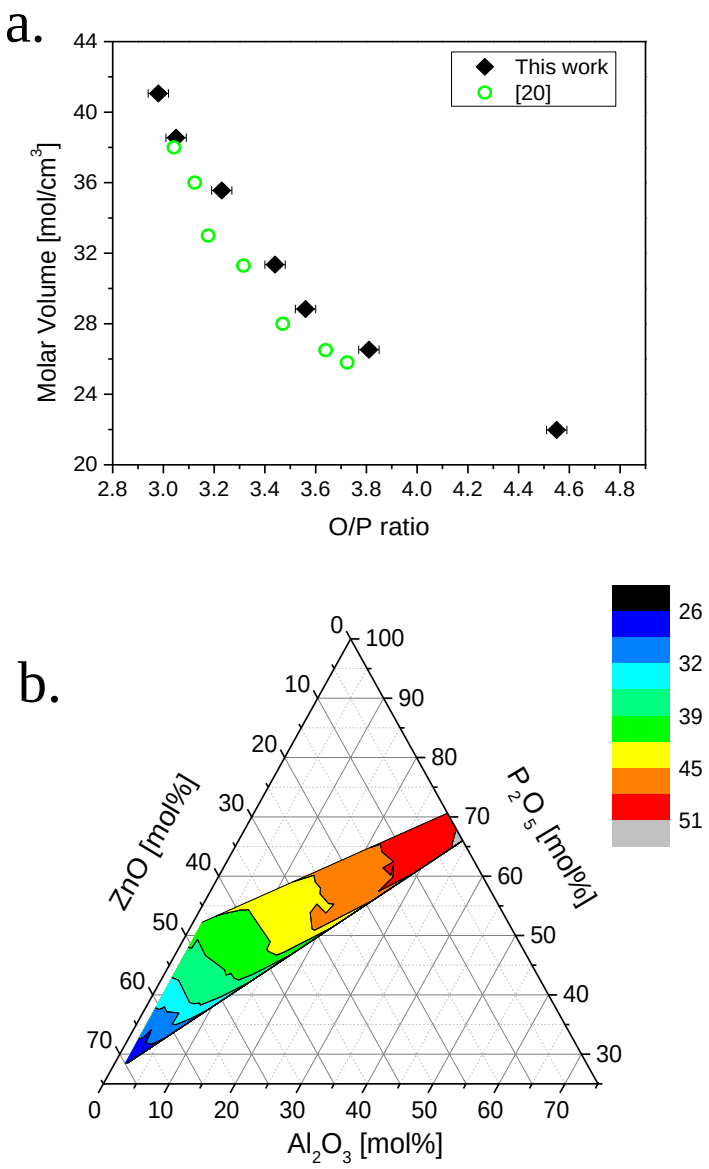

Figure 4: Molar volume for glasses in the ZAP system a. with constant Al_2O_3 content (2.1 ±0.7 mol%) and varying O/P ratio from this work [black] and from Brow et al.[20] [open green circles] and b. as a contour plot for all compositions.

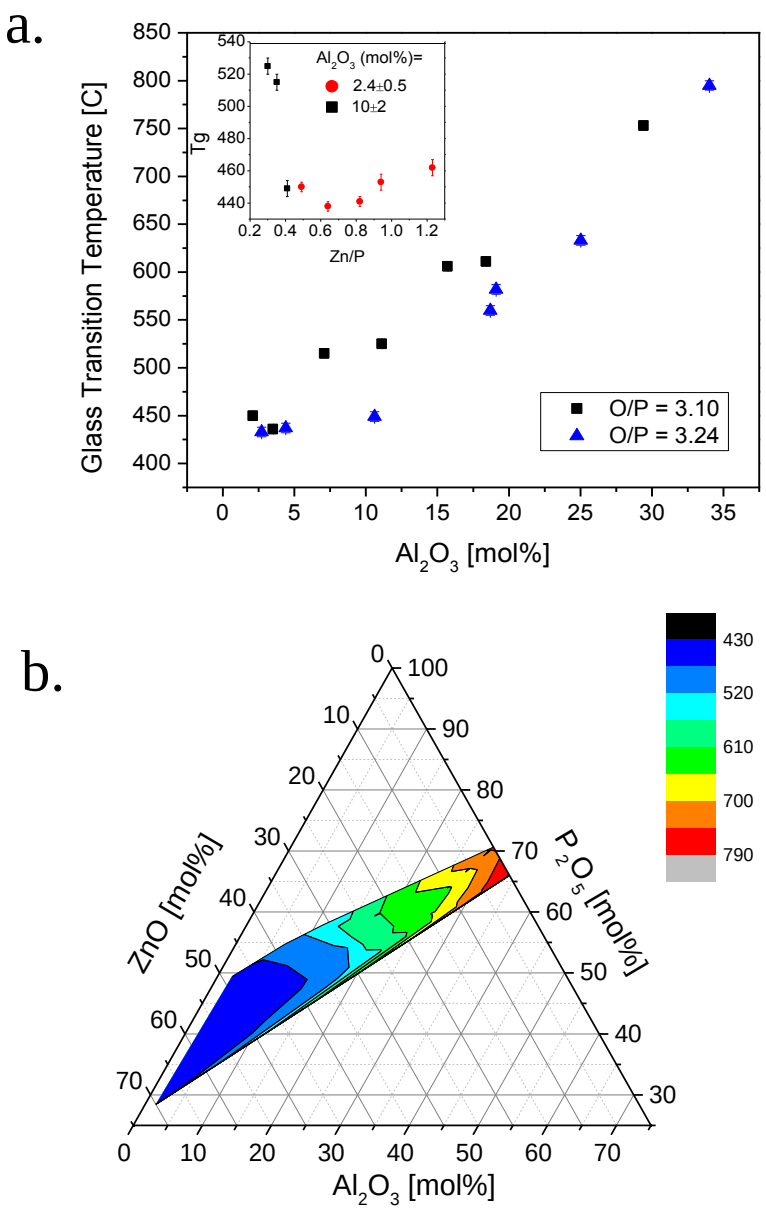

Figure 5: Glass transition temperature for glasses in the ZAP system as a function of Al_2O_3 content for the indicated O/P ratio (Inset: Tg vs. Zn/P ratios for the indicated alumina contents) and b. as a contour plot for all compositions.

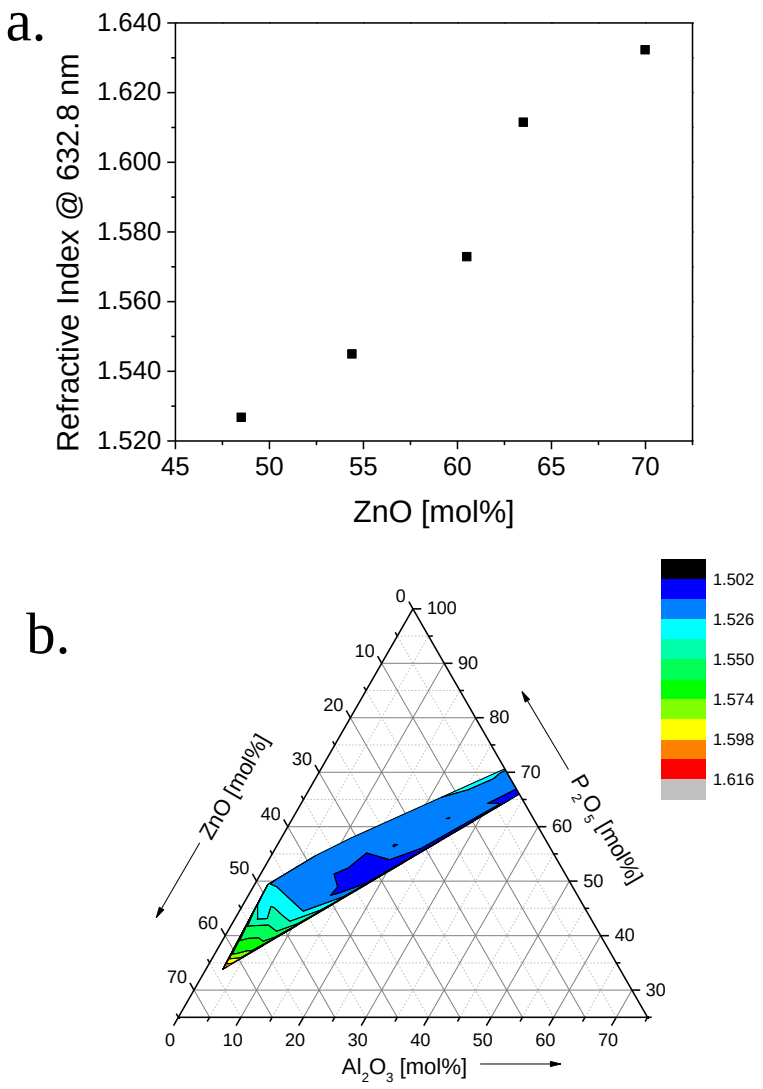

Figure 6: Refractive index for glasses in the ZAP system a. for a constant Al_2O_3 content (2.4 ±0.5 mol%) and increasing ZnO content; and b. as a contour plot for all compositions.

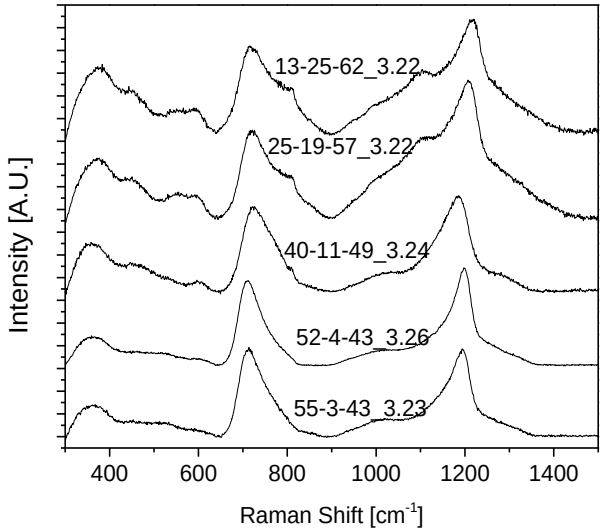

Figure 7: Raman spectra of ZAP glasses with similar O/P ratios (3.23 ± 0.02) and increasing Al_2O_3 contents.

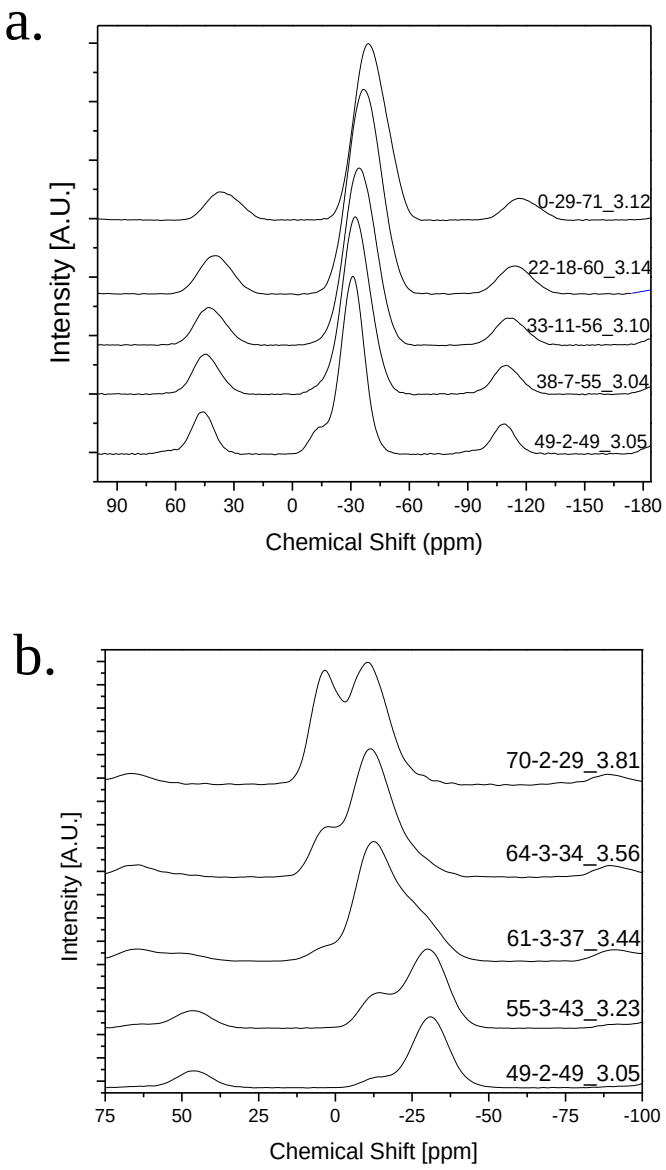

Figure 8: ^{31}P NMR spectra of ZAP glasses with a. similar O/P ratios (3.09 ±0.04) and increasing Al_2O_3 contents; and b. similar Al_2O_3 contents (2.4 ±0.5 mol%) and increasing O/P ratios.

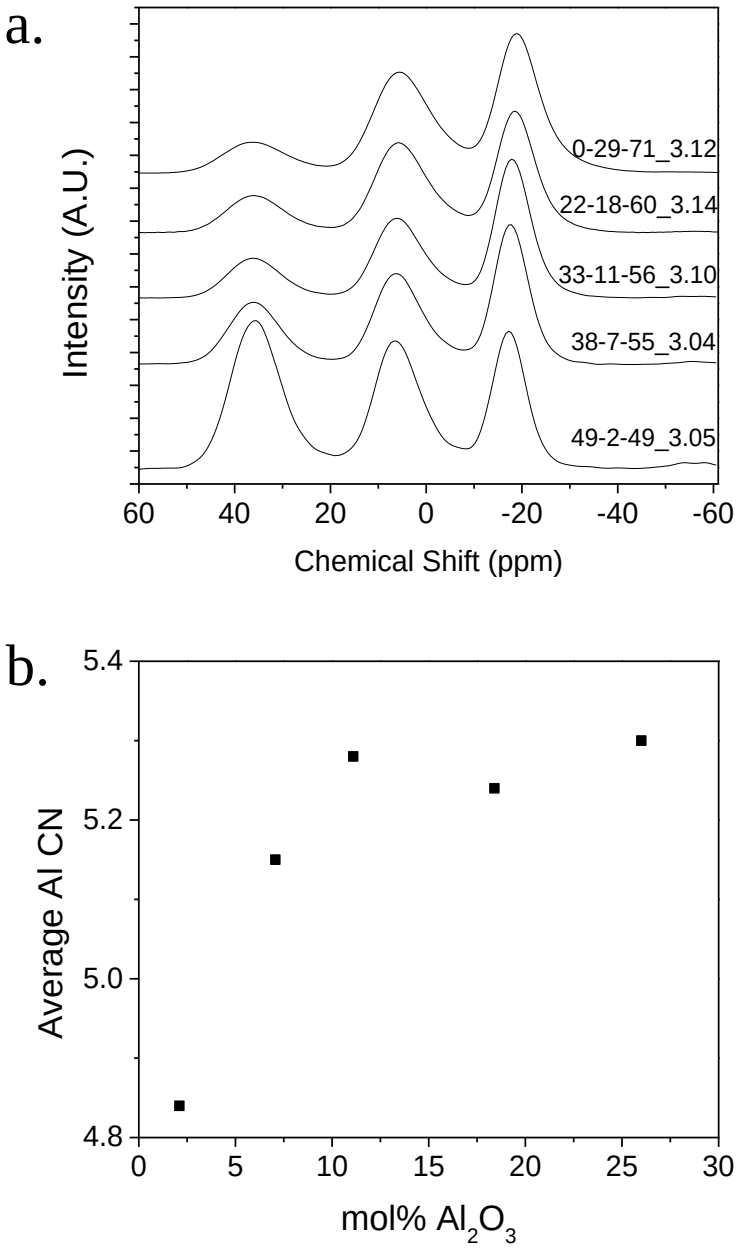

Figure 9: a. ^{27}Al MAS NMR spectra from ZAP glasses with similar O/P ratios (3.09 ±0.04) and b. a plot of the average Al CN as obtained from the ^{27}Al MAS NMR spectra.

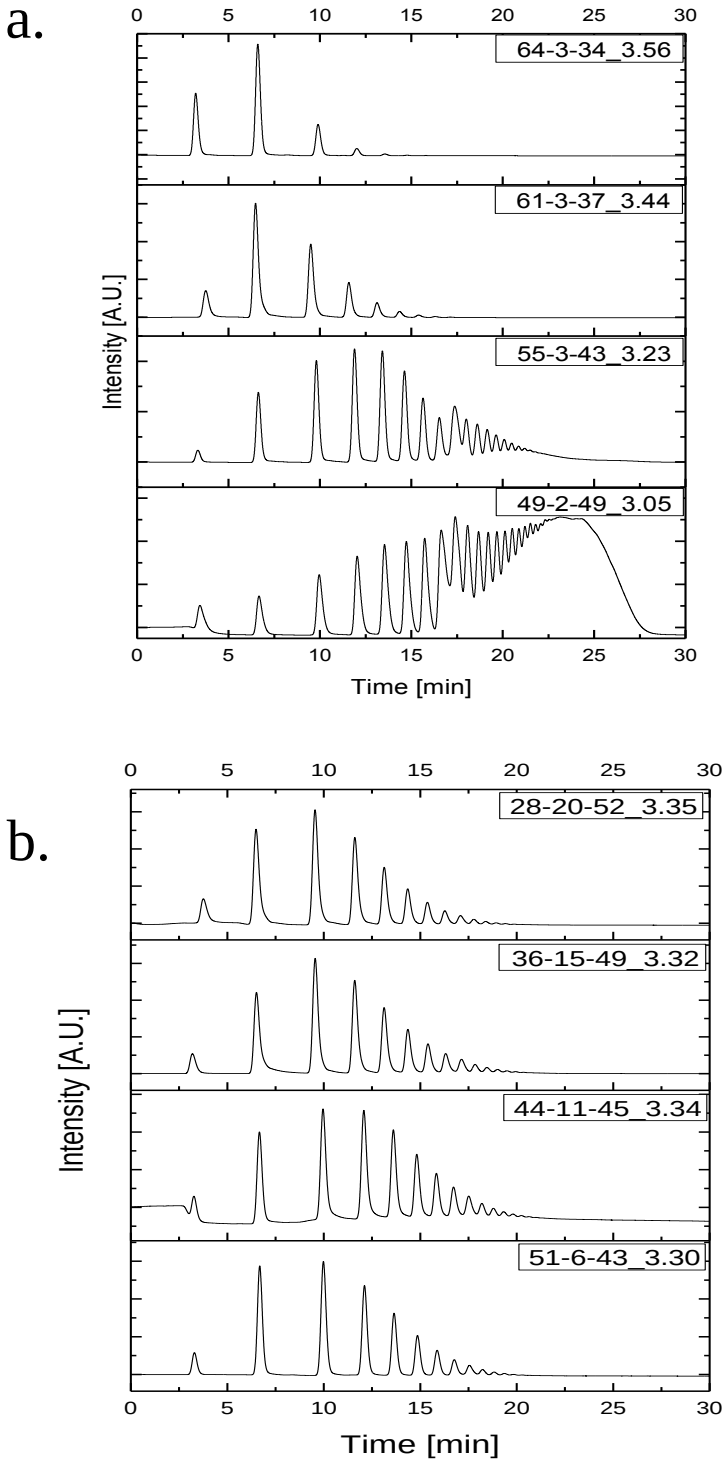

Figure 10: HPLC spectra of ZAP glasses with a. constant Al_2O_3 (2.6 ±0.3 mol%) and different O/P ratios; and b. glasses with similar O/P ratios (3.33 ±0.2) and different Al_2O_3 contents.

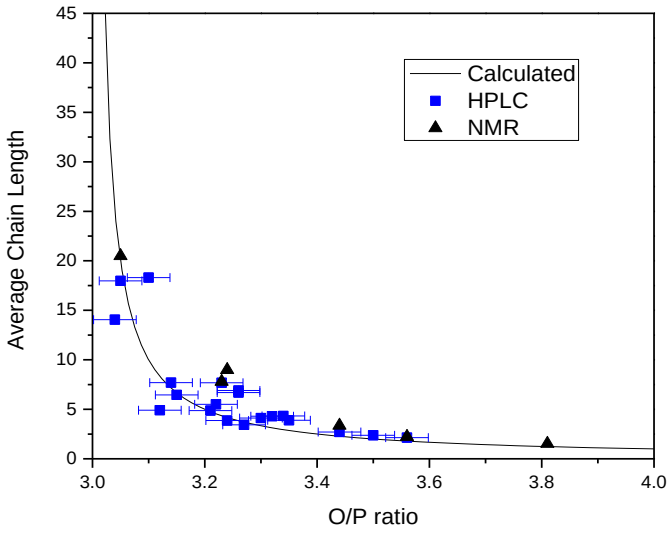

Figure 11: Plot of the average chain length measured from the HPLC chromatographs [blue] and NMR spectra [black] against the O/P ratios from analyzed compositions of the ZAP glasses. The solid line is the expected relationship, based on Equation (5).

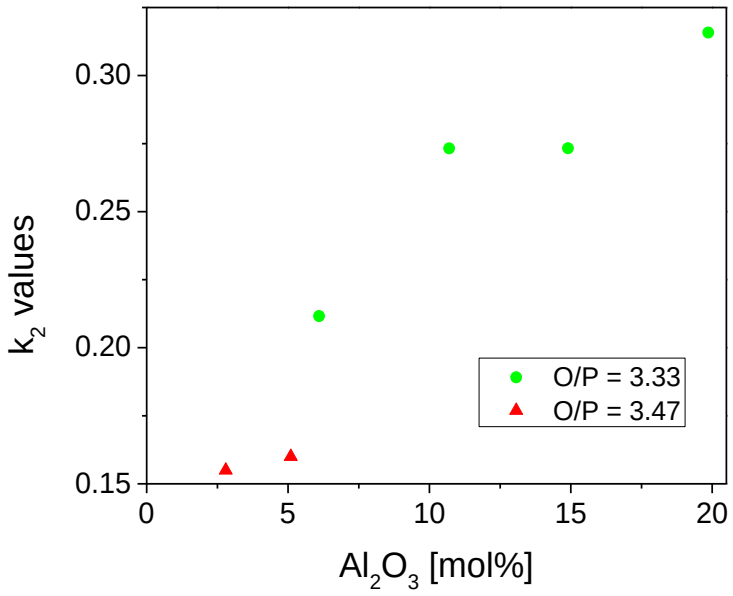

Figure 12: k_2 values calculated from HPLC chromatographs for ZAP glasses with O/P ratios = 3.33 (±0.02) and 3.47 (±0.04).

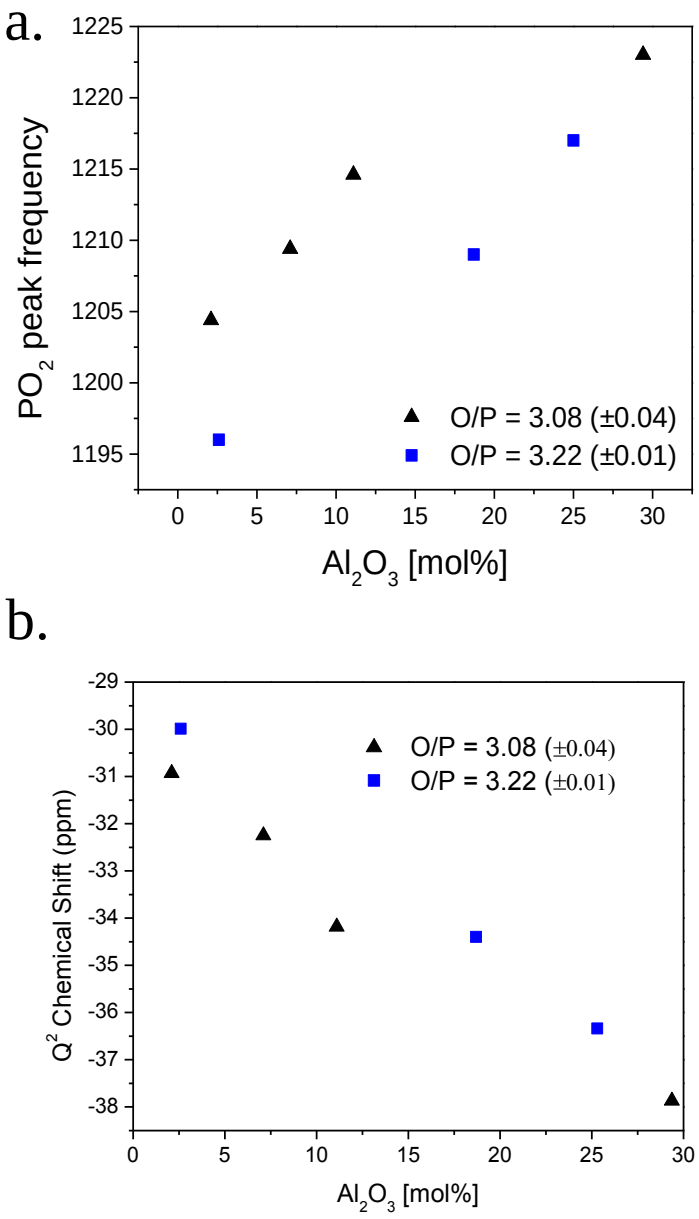

Figure 13: a PO_2 Raman frequency change and b. Q^2 Chemical shift as a function of alumina content for select glasses.

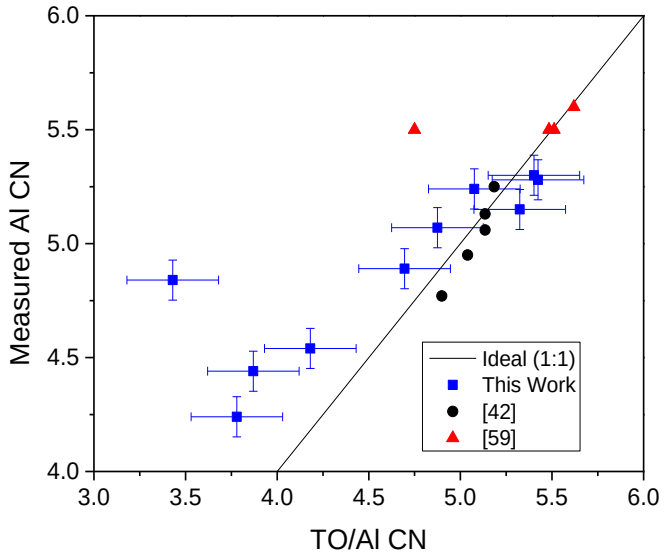

Figure 14: Average Al-coordination number plotted against the TO/Al ratio for ZAP glasses from this work (blue), and for MAP glasses [59] and binary aluminophosphate glasses [42] reported in the literature. The expected relationship for TO/Al>4 (from Equation (10)) is given as the solid line.

REFERENCES

1. Aitken, B.G., et al., *Non-lead sealing glasses*, 1993, Corning Incorportated: United States.

2. Morena, R.M., *Phosphate glasses as alternatives to Pb-based sealing frits.* Journal of Non-Crystalline Solids, 2000. 263&264: p. 6.

3. Wilder Jr., J.A., *Glasses and glass ceramics for sealing to aluminum alloys.* Journal of Non-Crystalline Solids, 1980. 38&39: p. 6.

4. Martinez-Martinez, R., et al., *White light generation through the zinc metaphosphate glass activated by Ce^{3+}, Tb^{3+} and Mn^{2+} ions.* Journal of Luminescence, 2009. 129: p. 5.

5. Lin, C.T., et al., *Luminescence properties of Tm^{3+}/Dy^{3+} co-doped zinc-aluminum phosphate glasses for white LED.* Advanced Materials Research, 2013. 602-604: p. 9.

6. Eriah, A. and S.G. Bhat, *Optical properties of samarium doped zinc-phosphate glasses.* Journal of Physics and Chemistry of Solids, 2007. 68: p. 5.

7. Fletcher, L.B., et al., *Femtosecond laser writing of waveguides in zinc phosphate glasses.* Optical Materials Express, 2011. 1: p. 845-855.

8. Fletcher, L.B., et al., *Single-pass waveguide amplifiers in Er-Yb doped zinc polyphosphate glass fabricated with femtosecond laser pulses.* Optics Letters, 2012. 37(7): p. 3.

9. Troy, N., et al., *Structural modification in Er-Yb doped zinc phosphate glasses with megahertz repetition rate femtosecond pulses*, in *Frontiers in Ultrafast Optics: Biomedical, Scientific, and Industrial Applications XII*, T.I.S.f.O. Engineering, Editor 2012, The International Society for Optical Engineering: San Francisco, CA.

10. Fletcher, L.B., et al., *Effects of rare-earth doping on femtosecond laser waveguide writing in zinc polyphosphate glass.* Journal of Applied Physics, 2012. 112.

11. Fletcher, L.B., et al., *Direct femtosecond laser waveguide writing inside zinc phosphate glass.* Optics Express, 2011. 19(9).

12. Canioni, L., et al., *Three-dimensional optical data storage using third-harmonic generation in silver zinc phosphate glass.* Optics Letters, 2008. 33(4): p. 3.

13. Kordes, E., Z. Phys. Chem., 1941. 50B: p. 194.

14. Kordes, E. and R. Nieder, Glastechn. Ber., 1968. 41.

15. Kordes, E., W. Vogel, and R. Feterowsky, Z. Elektrochem, 1953. 57: p. 282.

16. Crobu, M., et al., *Chain-length-identification strategy in zinc polyphosphate glasses by means of XPS and ToF-SIMS.* Anal Bioanal Chem, 2012. 403: p. 8.

17. Meyer, K., *Characterization of the structure of binary zinc ultraphosphate glasses by infrared and Raman spectroscopy.* Journal of Non-Crystalline Solids, 1997. 209: p. 227-239.

18. Schwarz, J., et al., *Physical properties of PbO-ZnO-P_2O_5 glasses. I.Infrared and Raman Spectra.* Journal of Optoelectronics and Advanced Materials, 2004. 6(3): p. 737-746.

19. Brow, R.K., *Review: the structure of simple phosphate glasses.* Journal of Non-Crystalline Solids, 2000. 263&264: p. 1-28.

20. Brow, R.K., et al., *The short-range structure of zinc polyphosphate glass.* Journal of Non-Crystalline Solids, 1995. 191: p. 45-55.

21. Matsubara, E., et al., *Structural study of binary phosphate glasses with MgO, ZnO, and CaO by X-ray diffraction.* Journal of Non-Crystalline Solids, 1988. 103: p. 8.

22. Suzuya, K., et al., *The structure of binary zinc phosphate glasses.* Journal of Non-Crystalline Solids, 2004. 345&346: p. 80-87.

23. Walter, G., et al., *The structure of zinc polyphosphate glass studied by diffraction methods and ^{31}P NMR.* Journal of Non-Crystalline Solids, 2004. 333: p. 11.

24. Sales, B.C., et al., *Structure of zinc polyphosphate glasses.* Journal of Non-Crystalline Solids, 1998. 226: p. 287-293.

25. Wiench, J.W., et al., *Structure of zinc polyphosphate glasses studied by two-dimensional solid and liquid state NMR.* Journal of Molecular Structure, 2002. 602-603: p. 13.

26. Tischendorf, B., et al., *A study of short and intermediate range order in zinc phosphate glasses.* Journal of Non-Crystalline Solids, 2001. 282: p. 147-158.

27. Brow, R.K., *An XPS study of oxygen bonding in zinc phosphate and zinc borophosphate glasses.* Journal of Non-Crystalline Solids, 1996. 194: p. 267-273.

28. Hoppe, U., et al., *Structure of rare-earth phosphate glasses by X-ray and neutron diffraction.* Journal of Non-Crystalline Solids, 2005. 351: p. 12.

29. Takebe, H., Y. Baba, and M. Kuwabara, *Dissolution behavior of ZnO-P_2O_5 glasses in water.* Journal of Non-Crystalline Solids, 2006. 352: p. 3088-3094.

30. Koudelka, L. and P. Mosner, *Study of the structure and properties of Pb-Zn borophosphate glasses.* Journal of Non-Crystalline Solids, 2001. 293-295: p. 7.

31. Chenu, S., et al., *Structure and properties of $NaPO_3$-ZnO-Nb_2O_5-Al_2O_3 glasses.* Journal of Non-Crystalline Solids, 2012. 358: p. 11.

32. Li, S., P. Chen, and Y. Li, *Structural and physical properties in the system ZnO-B_2O_3-P_2O_5-R_nO_m.* Physica B, 2010. 405: p. 6.

33. Kreidl, N.J. and W.A. Weyl, Journal of American Ceramic Society, 1941. 11.

34. Brow, R.K., *Nature of Alumina in Phosphate Glass: I, Properties of Sodium Aluminophosphate Glass.* Journal of American Ceramic Society, 1993. 76(4): p. 6.

35. Brow, R.K., R.J. Kirkpatrick, and G.L. Turner, *Nature of Alumina in Phosphate Glass: II, Structure of Sodium Aluminophosphate Glass.* Journal of American Ceramic Society, 1993. 76(4): p. 10.

36. Schneider, J., et al., *Short-Range Structure and Cation Bonding in Calcium-Aluminum Metaphosphate Glasses.* Inorganic Chemistry, 2005. 44: p. 8.

37. Tsuchida, J., et al., *Structure of ternary aluminum metaphosphate glasses.* Journal of Physical Chemistry, 2011. 115: p. 15.

38. Fu, C., et al., *Structure and property of ZnO content with Tb^{3+} doped zinc aluminum phosphate glass.* Applied Mechanics and Materials, 2012. 117-119: p. 4.

39. Letcher, J.H. and J.R. Van Wazer, *Theoretical Interpretation of 31P NMR Chemical Shifts. I.* Journal of Chemical Physics, 1966. 44(2): p. 15.

40. Neuville, D.R., L. Cormier, and D. Massiot, *Al environment in tectosilicate and peraluminous glasses: a NMR, Raman and XANES investigation.* Geochimica Cosmochimica Acta, 2004. 68: p. 9.

41. Zhang, L. and H. Eckert, *Short- and medium-range order in sodium aluminophosphate glasses: New insights from high resolution dipolar solid-state NMR spectroscopy.* Journal of Physical Chemistry B, 2006. 110: p. 13.

42. Brow, R.K., C.A. Click, and T.M. Alam, *Modifier coordination and phosphate glass networks.* Journal of Non-Crystalline Solids, 2000. 274: p. 9-16.

43. Rygel, J.L. and C.G. Pantano, *Synthesis and properties of cerium aluminosilicophosphate glasses.* Journal of Non-Crystalline Solids, 2009. 355: p. 8.

44. Sales, B.C., L.A. Boatner, and J.O. Ramey, *Chromatographic studies of the structure of amorphous phosphates: a review.* Journal of Non-Crystalline Solids, 2000. 263&264: p. 12.

45. Mosner, P., et al., *Structure and properties of glasses in ZnO-P_2O_5-TeO_2 system.* Journal of Non-Crystalline Solids, 2010. 357(14): p. 5.

46. Tischendorf, B., et al., *The structure and properties of binary zinc phosphate glasses studied by molecular dynamics simulations.* Journal of Non-Crystalline Solids, 2003. 316: p. 12.

47. Kubo, T., et al., *Thermal properties and structure of zinc phosphate glasses.* Physics and Chemistry of Glasses - European Journal of Glass Science and Technology Part B, 2009. 50(1): p. 4.

48. Schneider, J., et al., *Local Structure of Sodium Aluminum Metaphosphate Glasses.* Journal of American Ceramic Society, 2003. 86(2): p. 8.

49. Metwalli, E. and R.K. Brow, *Cation Effects on Anion Distributions in Aluminophosphate Glasses.* Journal of the American Ceramic Society, 2001. 84: p. 1025-1032.

50. Egan, J.M., R.M. Wenslow, and K.T. Mueller, *Mapping aluminum/phosphorus connectivities in aluminophosphate glasses.* Journal of Non-Crystalline Solids, 2000. 261: p. 115-126.

51. Troy, N., *Materials and Techniques for the Femtosecond Laser Fabrication of Optical Devices in Glass*, in *Applied Science*2012, University of California, Davis: Davis. p. 67.

52. Fletcher, L.B., et al., *Direct femtosecond laser waveguide writing inside zinc phosphate glass.* Optics Express, 2011. 19: p. 7929-7936.

53. Fanderlik, I., *Optical Properties of Glass*. Glass Science and Technology. Vol. 5. 1983, New York: Elsevier.

54. Duffy, J.A. and M.D. Ingram, *An Interpretation of Glass Chemistry in Terms of the Optical Basicity Concept.* Journal of Non-Crystalline Solids, 1976. 21: p. 38.

55. Nelson, B.N. and G.J. Exarhos, *Vibrational spectroscopy of cation-site interactions in phosphate glasses.* Journal of Chemical Physics, 1979. 71(7): p. 9.

56. Popovic, L., D. de Waal, and J.C.A. Boeyens, *Correlation between Raman wavenumbers and P-O bond lengths in crystalline inorganic phosphates.* Journal of Raman spectroscopy, 2005. 36: p. 10.

57. Hoppe, U., *A structural model for phosphate glasses.* Journal of Non-Crystalline Solids, 1996. 195: p. 10.

58. Walter, G., et al., *Intermediate range order in MeO-P_2O_5 glasses.* Journal of Non-Crystalline Solids, 1997. 217: p. 299-307.

59. Metwalli, E. and R.K. Brow, *Modifier effects on the properties and structures of aluminophosphate glasses.* Journal of Non-Crystalline Solids, 2001. 289: p. 10.

60. Ticha, H., et al., *Physical Properties of PbO-ZnO-P_2O_5 Glasses II. Refractive Index and Optical Properties.* Journal of Optoelectronics and Advanced Materials, 2004. 6(3): p. 7.

61. Chen, P., et al., *Sturcture and Crystallization of ZnO-B_2O_3-P_2O_5 Glasses.* Glass Physics and Chemistry, 2011. 37(1): p. 29-33.

2. PHASE RELATIONSHIPS IN THE ZNO-AL_2O_3-P_2O_5 SYSTEM

Charmayne E. Smith, Jeffrey D. Smith, Richard K. Brow
Missouri University of Science and Technology
Rolla, MO 65409 USA

ABSTRACT

Phase relationships in the ZnO-Al_2O_3-P_2O_5 system were determined by heating mixtures of compounds, in air, up to 1000 ˚C for 96 - 122 hours. Stable phases were determined by x-ray diffraction (XRD) and the solidus temperatures for selected stability triangles were determined by differential thermal analysis (DTA). Seven congruently melting binary compounds were identified in the ternary system: $AlPO_4$, $Al(PO_3)_3$, $ZnAl_2O_4$, $Zn(PO_3)_2$, $Zn_3(PO_4)_2$ ZnP_4O_{11} and $Zn_2P_2O_7$. There was no indication for the formation of ternary compounds in the system. The impact of phase stability on glass formation tendency is discussed.

2.1 INTRODUCTION

Materials from the ZnO-Al_2O_3-P_2O_5 (ZAP) system are of interest for a variety of applications, including molecular sieves and mesoporous filtration systems [1]. Wilson et al. showed that aluminophosphates had useful surface selectivity characteristics and structures compared to silicate based zeolites [2]. The addition of metal oxides, such as ZnO or MgO, increases the reactivity of the surface of aluminophosphates and makes them suitable for ion exchange and catalyst applications [1, 3].

Glasses in the ZAP system are of interest as optical materials [4]. Zinc phosphate glasses have been used as substrates for fabrication of waveguides and embedded optical devices created by femto-second laser irradiation [5-7] and alumina is added to improve the chemical durability [8, 9].

Relevant binary phase diagrams have been reported for the Al_2O_3-P_2O_5 [10-12], ZnO-P_2O_5 [13-15] and the ZnO-Al_2O_3 systems [16], either individually or as part of other ternary systems, and in all cases there is general agreement about the binary compounds that exist.

In the ZnO-P_2O_5 system, four stable and congruently melting compounds have been reported: zinc ultraphosphate (ZnP_4O_{11}), zinc metaphosphate ($Zn(PO_3)_2$), zinc pyrophosphate ($Zn_2P_2O_7$) and zinc orthophosphate ($Zn_3(PO_4)_2$) [15]. $Zn(PO_3)_2$ and $Zn_2P_2O_7$ each have two polymorphic forms and $Zn_3(PO_4)_2$, which was previously described as not exhibiting solid state phase transformations, has a sluggish transition at 942 ˚C [15]. ZnP_4O_{11} is difficult to prepare, due to the tendency of ultraphosphates to react with water vapor in the air, requiring its synthesis to be completed in a sealed furnace or ampoule [17]. Attempts to produce ultraphosphates generally result in the

formation of the zinc metaphosphate compound from accumulation of atmospheric water in the network, the development of phosphoric acid or after loss of P_2O_5 [3, 18]. Little is known of the zinc ultraphosphate compound although it has been shown to be isomorphic with magnesium ultraphosphate [19], which exhibits a transition to a high temperature phase near 850 ˚C [20].

Interest in the phase relationships in the ZnO-Al_2O_3 system is due in part to the formation of spinel phases [21, 22]. Spinels are useful in numerous high temperature applications [23]. Gahnite ($ZnAl_2O_4$) is the only known compound on the zinc aluminate binary and has been shown to melt congruently at 1950˚C [16].

Ternary aluminophosphate compositions have been investigated for cements, fertilizers, dental materials, mineralogy and other applications [10, 11]. Stone described the phase relationships in the CaO-Al_2O_3-P_2O_5 system and found two stable crystalline compound mixtures in the Al_2O_3- P_2O_5 binary system; $Al(PO_3)_3$ and $AlPO_4$ [10].

2.1.1 Ternary Phase Stability Diagrams. The combination of binary phase diagrams is an important approach to understanding reactions that occur in the ternary system. Compounds that are mutually stable are must share an Alkemade line on a phase diagram [24]; e.g., the dashed lines in Figure 1. These lines indicate an intersection of phase fields. When compounds that share an Alkemade line are mixed and heated, they will not react to form a new phase. Similarly, three Alkemade lines combine to form an Alkemade triangle, indicating compositions for which the three phases are mutually stable [25]. For example, in Figure 1, three Alkemade triangles exist: A-AC-AB, AB-AC-B and AC-B-C, and seven Alkemade lines are present. The AB-AC Alkemade line indicates that these two compounds are stable together, whereas the lack of an Alkemade

line connecting A and C indicates that these two materials are not stable together and must react to form AC by the following reaction:

$$A + C \rightarrow AC$$

The compounds A, AC, and AB form an Alkemade triangle and this indicates that for any composition found within this region, neither phase C nor phase B will form. The equilibrium phases that crystallize from melts with compositions defined within a particular Alkemade triangle, or the equilibrium phases that form from solid-state reactions of components within an Alkemade triangle, will be established by the compounds at the triangle corners [23]. Phase stability diagrams thus can provide useful information about compound reactions and system stability. Additionally, mixing and heating a combination of AB and C will cause the following reaction to occur:

$$AB + C \rightarrow AC + B$$

If the reaction is stoichiometric, all AB + C will be eliminated by the reaction and only the two phases AC and B will remain. If, however, AB or C were present in excess, then the resulting equilibrium would involve three phases.

Each individual Alkemade triangle will also include characteristic temperatures where transitions from solids to solid + liquid or solids to liquid occur. The temperature below which no liquid is present is termed the solidus temperature [23]. Each of the three phase Alkemade triangles shown in Figure 1 have a unique solidus temperature and once these temperatures are measured, information of melting behavior and liquid/solid interactions can be understood.

Phase stability information has been used to understand the properties, structure and crystallization behavior of glasses in the ZnO-B_2O_3-P_2O_5 system [26]. Phase

stability is not only useful in understanding equilibrium conditions but can also be utilized for investigations involving metastability, or glass formation.

To date, there has been no comprehensive investigation of the phase stability in the ZAP ternary system. The purpose of this work is to identify the stable phases in the ZnO-Al_2O_3-P_2O_5 system, map them on a ternary diagram and use the resulting diagram to understand how the phases interact with each other. In addition, the onset of melting for Alkemade triangles, through determination of solidus temperatures, are established and the diagram is used to understand glass forming behavior.

2.2 EXPERIMENTAL AND METHODS SECTION

The raw materials used were Al_2O_3 (Alfa Aesar, 99.5%), $NH_4H_2PO_4$ (Alfa Aesar, 98%), $Zn_3(PO_4)_2 \cdot xH_2O$ (Alfa Aesar, technical grade), ZnO (Sigma Aldrich, ≥99.0%), $Al(PO_3)_3$ (Alfa Aesar) and $AlPO_4$ (Sigma Aldrich, reagent grade). Raw materials were batched as necessary, saturated with acetone and mixed with a mortar and pestle until dry. The batch was either placed in alumina crucibles (AdValue Technology, 99.9%), or pressed into pellets (½" diameter by ¼" height), and heated to temperatures up to 1000 °C and held for up to 122 hours. Compositions with more than 40 mole% P_2O_5 were heated in alumina crucibles that were covered with alumina discs to minimize volatilization of P_2O_5. Due to the relatively low melting temperature of P_2O_5, some samples melted during processing and did not crystallize upon quenching. These samples were not used to define phase regions

As part of a parallel glass-formation study [9], many compositions were heated in alumina crucibles up to temperatures of 1500 °C and held for approximately two hours. Information about compositions that crystallized is included in this study.

Crystalline $Zn_2P_2O_7$ was prepared by heating a stoichiometric mixture of $NH_4H_2PO_4$ and ZnO to 800°C for ~15 hrs. following Maadi, et al. [27], and reacted with alumina powder (20 mole%) at 900 °C for nine days, in a covered alumina crucible, to test a prediction of the formation of equilibrium phases.

Weight loss was monitored for all experiments due to concern of P_2O_5 volatility, and no samples discussed here exhibited weight loss greater than 2.5%. After heat treatments, the products were crushed to particle sizes between 100-300 microns and the phases were analyzed by x-ray diffraction (XRD) using a Phillips Panalytical X'pert Multipurpose Diffractometer with a Cu K-α source.

The solidus temperatures for each Alkemade triangle were determined by differential thermal analysis (DTA). Approximately 30 mg of powder (<75 μm), with phases confirmed by XRD, was heated in an open, alumina crucible at a rate of 10 ˚C/min, in nitrogen atmosphere, to a maximum of 1500 ˚C using a Perkin-Elmer DTA 7 system. The solidus temperature for each triangle was determined by the onset method; the estimated error is ±10 °C.

Except for the P_2O_5-rich compositions, the Alkemade triangles presented below are based on three or more different compositions to confirm the formation of the specified phases in the triangle. Due to volatilization of P_2O_5, triangles in the P_2O_5-rich corner are proposed by the phase assignments of the neighboring triangles, using the rule that Alkemade lines do not cross one another [23].

2.3 RESULTS AND DISCUSSION

The binary compounds reported in the literature for the ZnO-Al_2O_3-P_2O_5 system are given in Table 1. Ternary compounds are not reported in the literature and none were

found in this work. The compositions tested, and the raw materials used to prepare them, are shown in Table 2, along with the times and temperatures at which each mixture was treated. Table 2 also summarizes the phases detected from each sample analyzed. There was no evidence for any new crystalline phases in the samples studied.

Figure 2 shows the phase stability diagram for the ZnO-Al_2O_3-P_2O_5 system, based on the results of the XRD study, and using the binary compounds reported in the literature. This diagram is similar to that reported for the MgO-Al_2O_3-P_2O_5 system at 1000 °C, for which no ternary compounds are known [28]. That MgO-Al_2O_3-P_2O_5 phase stability diagram did not include the ultraphosphate MgP_4O_{11} [29].

Figure 3 shows an example of a DTA experiment on a reacted sample with the nominal composition 55 mol% ZnO·19 mol%Al_2O_3·26 mol% P_2O_5; the exotherm associated with initial melting (the solidus temperature) is indicated. Table 3 summarizes the solidus temperature measurements for each Alkemade triangle where melting could be detected. For the Al_2O_3-$ZnAl_2O_4$-$AlPO_4$ triangle, no evidence for sample melting was found for DTA and thermal treatments up to 1500˚C.

If the three compounds that constitute an Alkemade triangle melt congruently, there will be a eutectic point associated with that triangle and the eutectic temperatures in binary and ternary systems will be lower than those congruent melting temperatures [23]. Thus, the initial melting temperature (solidus temperature) indicated in the thermal analysis of a mixture of compounds should not be greater than the temperature of the lowest melting compound. From these relationships, eutectic temperatures can still be estimated. For example, from Table 3 and Figure 2, any composition in the Alkemade triangle formed by $AlPO_4$, $ZnAl_2O_4$ and $Zn_3(PO_4)_2$, will exhibit the first signs of liquid

formation, upon heating, at temperatures near 1025 °C (±5 °C). While the compounds in this system are known to melt congruently, there is a tendency for volatilization of P_2O_5 [30] and, to a lesser extent, ZnO [31], especially at temperatures above 1200 ˚C. Volatilization of compounds will result in a change in composition and processing temperatures shift to greater values due to loss of lower melting components.

ZnO and Al_2O_3 melt at high temperatures (1975 ˚C and 2072 ˚C, respectively [32]), whereas P_2O_5 has a melting temperature near 580 ˚C [3, 33, 34]. There is an overall decrease in the solidus temperatures for the Alkemade triangles as the amount of P_2O_5 increases (Figure 2). In addition, the aluminum phosphate binary, which has fewer stable compounds, has greater melting temperatures than the zinc phosphate binary. Therefore the eutectic temperatures in each triangle will most likely be closer to the melting (and eutectic) temperatures indicated in the zinc phosphate binary diagram, as those compounds melt at temperatures closer to the solidus temperatures.

Phase stability diagrams can also be used to predict equilibrium phases from mixtures of compounds. To illustrate this, a composition within the $ZnAl_2O_4$-$AlPO_4$-$Zn_3(PO_4)_2$ triangle, with 20 mol% Al_2O_3 and 80 mol% $Zn_2P_2O_7$, shown as the ‘X’ on Figure 2, was heated at 900 °C for nine days, . The XRD pattern from this sample, Figure 4, confirms the expected phases have formed. Figure 2 also shows that if a line is drawn from $Zn_2P_2O_7$ to Al_2O_3, two Alkemade lines are crossed as a result of passing through three Alkemade triangles. Any combination of a variety of relative percentages of these two compounds can produce three different sets of stable phases, depending on where that composition is located on the diagram.

2.3.1 Glass Formation. Determination of the phase stability of the system can also contribute to understanding glass formation. The glass formation region for the zinc aluminophosphate system has recently been investigated [9], and is shown in Figure 5. Included in Figure 5 are the Alkemade lines established in the present work. The ZAP ternary can be divided into two, separate glass-forming binaries: the zinc phosphate and the aluminophosphate systems.

Phase equilibria diagrams can provide insight to glass formation tendencies. For example, Weinch et al. and Tischendorf et al. investigated glasses in the binary zinc phosphate system [35, 36]. Although glass formation was found to extend to 80 mol% ZnO, as can be seen in Figure 5, there was difficulty in quenching a glass from a melt with the composition of 75 mol% ZnO 25 mol% P_2O_5. Both studies used roller quenching techniques to cool the melt at rates of 10^7 K/s, but samples still showed evidence of phase separation and crystallization [35, 36]. Through understanding the phase stability diagram it can be noted that this difficulty is not unexpected, due to the formation of the compound, $Zn_3(PO_4)_2$, at 75 mol% ZnO. Additionally, the presence of a stable crystalline phase at certain compounds will not prohibit glass formation, but it may indicate the need for faster cooling rates to ensure a pure glassy phase is prepared.

The aluminophosphate binary shows that the maximum amount of alumina in a glass forming composition is at ~ 35 mol% Al_2O_3, between the aluminum metaphosphate and aluminum orthophosphate compounds (Figure 5). It is clear that the presence of a crystalline compound is not impeding glass formation; so to understand why glass formation is limited to a maximum of 34.7 mol% Al_2O_3 (±2.5%) it is useful to determine how the temperatures are changing. Figure 6 shows the phase diagram between $Al(PO_3)_3$

and $AlPO_4$ as a function of temperature, including the composition indicated as the maximum glass forming alumina concentration [9] (dash-dot line). Glass formation is enhanced for compositions near deep eutectics [23], like that shown in Figure 6. The steep rise in melting temperature as the Al_2O_3 concentration increases limits the processing of glasses in the Al_2O_3-P_2O_5 binary and, therefore, limits the glass forming due to the necessity of higher melting temperature. Indeed, Smith et al. [9] were limited to 1500 ˚C and it can be seen that as the compositions move towards the $AlPO_4$ stoichiometry, melting temperatures increase dramatically (Figure 6).

2.4. CONCLUSIONS

The first phase stability diagram for the ZnO-Al_2O_3-P_2O_5 system has been proposed. No evidence for the formation of stable ternary compounds exists and the binary compounds found in this work are the same as those previously reported in the literature. Alkemade triangles were established for all compounds, and solidus temperatures were determined for most of these triangles. Connections between glass-forming tendencies and phase stability were made and the usefulness of phase stability diagrams for solid state reactions was demonstrated.

2.5 ACKNOWLEDGEMENTS

The authors acknowledge the Department of Education for the Graduate Assistance in Areas of National Need (GAANN) fellowship and the National Science Foundation (DMR 1207520) for funding this work. The contributions of Dr. Kelley R. Wilkerson for useful discussions and proof-reading, Eric Bohannon for guidance with the x-ray diffraction measurements, and Ryan Jones for assistance with the sample synthesis are also greatly appreciated.

Tables

Table 1: Unary and binary compounds in the ZnO-Al_2O_3-P_2O_5 system and their melting temperatures

Compound	Melting Temp °C	Reference
*P_2O_5 (O)	~580	[3, 33, 34]
$Al(PO_3)_3$	1480	[10]
$AlPO_4$	2000	[37]
ZnP_4O_{11}	~680	[38]
$Zn(PO_3)_2$	872	[15]
$Zn_2P_2O_7$	~1020	[15, 39]
$Zn_3(PO_4)_2$	1060	[15]
ZnO	1975	[32]
$ZnAl_2O_4$	1950	[32]
Al_2O_3	2072	[32]

* - certain phases also sublime (400-500 °C) (O)-orthogonal structure

Table 2: Compositions, treatment parameters and measured phases

Compositions			Treatment Parameters			
Mol% ZnO	Mol% Al_2O_3	Mol% P_2O_5	Time (hrs.)	Temperature (°C)	Raw materials	Phases Present
55	30	15	122	1000	ZnO, $Zn_2P_2O_7$, Al_2O_3	$ZnAl_2O_4$, $AlPO_4$, $Zn_3(PO_4)_2$
42	43	15	96	1000	$Al(PO_3)_3$, Al_2O_3, ZnO	$AlPO_4$, $Zn_3(PO_4)_2$, $ZnAl_2O_7$
80	10	10	96	1000	Al_2O_3, ZnO, $NH_4H_2PO_4$	$Zn_3(PO_4)_2$, ZnO, $ZnAl_2O_7$
82	14	4	96	1000	ZnO, $Zn_2P_2O_7$, Al_2O_3	ZnO, $Zn_3(PO_4)_2$, $ZnAl_2O_4$
32	66	2	122	1000	ZnO, $Zn_2P_2O_7$, Al_2O_3	$ZnAl_2O_4$, $AlPO_4$, Al_2O_3
11	32	57	122	1000	$AlPO_4$, $Al(PO_3)_3$, ZnO	$Al(PO_3)_3$, $AlPO_4$, $Zn(PO_3)_2$
55	19	26	122	1000	Al_2O_3, ZnO, $NH_4H_2PO_4$	$Zn_3(PO_4)_2$, $ZnAl_2O_4$, $AlPO_4$
20	10	70	240	390	$Al(PO_3)_3$, $Zn_3(PO_4)_2$, $NH_4H_2PO_4$	$Zn(PO_3)_2$, $Al(PO_3)_3$
85	0	15	2.5	1300	ZnO, $NH_4H_2PO_4$	ZnO, $Zn_3(PO_4)_2$
75	0	25	2.5	1200	ZnO, $NH_4H_2PO_4$	$Zn_3(PO_4)_2$
70	10	20	2	1500	$AlPO_4$, ZnO, $NH_4H_2PO_4$	$Zn_3(PO_4)_2$, $ZnAl_2O_4$
60	15	25	2	1500	$AlPO_4$, ZnO, $NH_4H_2PO_4$	$AlPO_4$, $ZnAl_2O_4$, $Zn_3(PO_4)_2$
55	15	30	2	1500	Al_2O_3, ZnO, $NH_4H_2PO_4$	$AlPO_4$, $ZnAl_2O_4$, $Zn_3(PO_4)_2$
40	20	40	2	1500	Al_2O_3, ZnO, $NH_4H_2PO_4$	$Zn_2P_2O_7$, $AlPO_4$

Table 3: Estimated solidus temperatures of ZAP Alkemade triangles

Alkemade Triangle	$T_{solidus}$
P_2O_5, ZnP_4O_{11}, $Al(PO_3)_3$ ZnP_4O_{11}, $Zn(PO_3)_2$, $Al(PO_3)_3$	nm
$Al(PO_3)_3$, $Zn(PO_3)_2$, $AlPO_4$	785
$Zn(PO_3)_2$, $AlPO_4$, $Zn_2P_2O_7$	nm
$Zn_2P_2O_7$, $AlPO_4$, $Zn_3(PO_4)_2$	990
$Zn_3(PO_4)_2$, $ZnAl_2O_4$, ZnO	960
$Zn_3(PO_4)_2$, $AlPO_4$, $ZnAl_2O_4$	1025
$AlPO_4$, $ZnAl_2O_4$, Al_2O_3	>1500

Figures

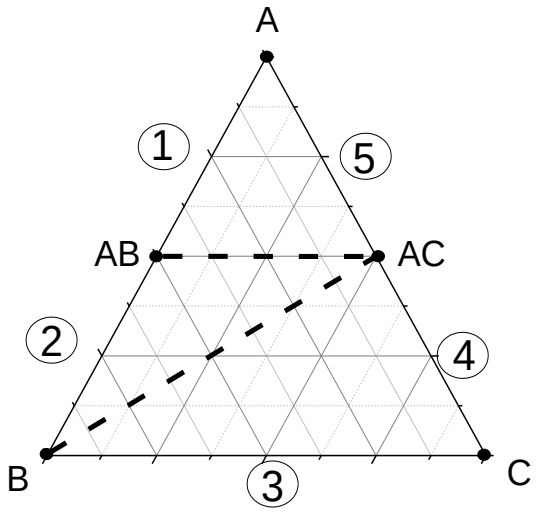

Figure 1: Example phase stability triangle of compounds A, AB, B, C, and AC.

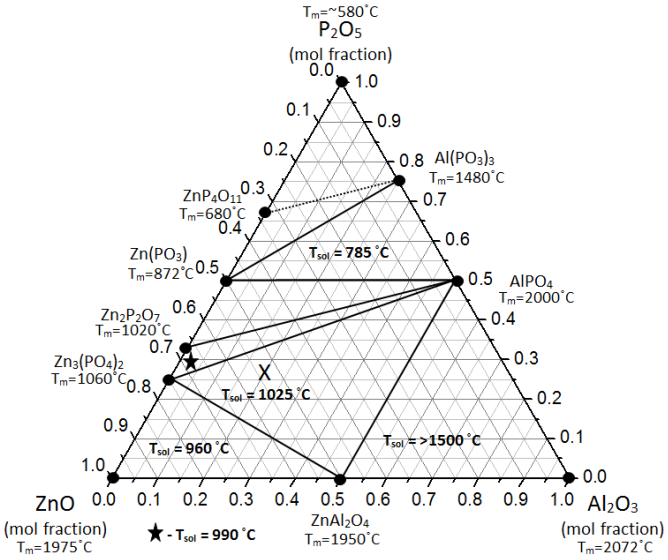

Figure 2: Phase stability diagram for the ZnO-Al_2O_3-P_2O_5 system with reported compound melting temperatures and measured solidus temperatures (solid lines = confirmed; dashed lines = proposed). (The "X" indicates mixture 20 mol% $Zn_2P_2O_7$ 80 mol% Al_2O_3)

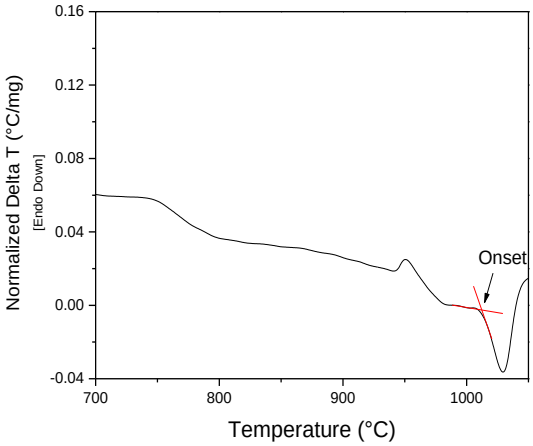

Figure 3: Differential thermal analysis spectrum for 55 mol% ZnO•19 mol% Al_2O_3 26 mol% P_2O_5 [solidus temperature determined by the onset method]

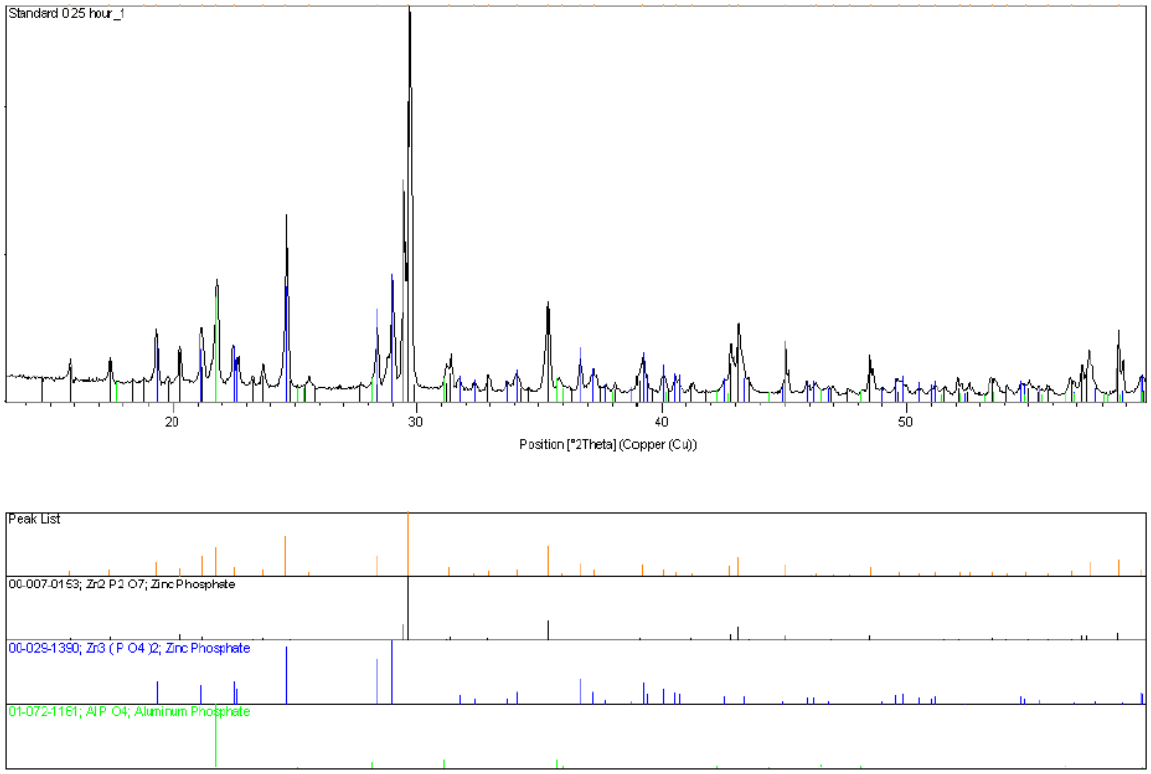

Figure 4: X-ray diffractogram of ZnP_2O_7 + Al_2O_3 at 900 ˚C for 9 days producing $Zn_2P_2O_7$ (black), $Zn_3(PO_4)_2$ (blue) and $AlPO_4$ (green)

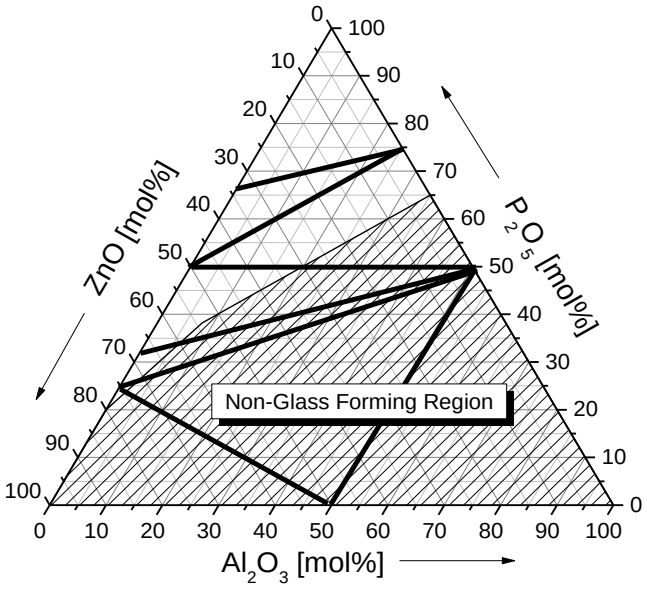

Figure 5: Zinc aluminophosphate ternary diagram with expected glass forming region [9] and the Alkemade triangles from this work.

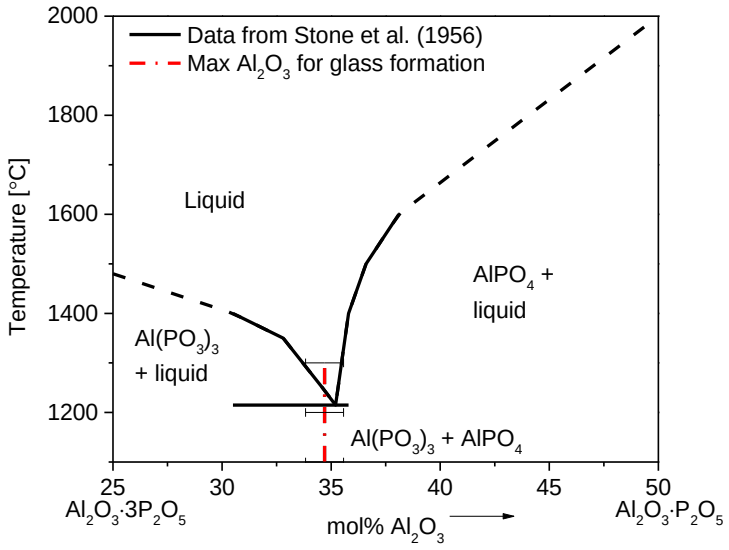

Figure 6: $Al(PO_3)_3$ - $AlPO_4$ binary [10] with maximum Al_2O_3 allowed for glass formation [9] (Dashed lines are extrapolated to the reported compound melting temperatures)

REFERENCES

1. Elangovan, S.P., V. Krishnasamy, and V. Murugesan, *Synthesis, characterization and catalytic activity of ZAPO-5 and ZAPO-11.* Catalysis Letters, 1996. 36: p. 271-277.

2. Wilson, S.T., et al., *Aluminophosphate Molecular Sieves: A New Class of Microporous Crystalline Inorganic Solids.* Journal of American Chemical Society, 1982. 104: p. 2.

3. Barrie, P.J. and J. Klinowski, *Ordering in the framework of a magnesium aluminophosphate molecular sieve.* The Journal of Physical Chemistry, 1989. 93(16): p. 3.

4. Fu, C., et al., *Structure and property of ZnO content with Tb^{3+} doped zinc aluminum phosphate glass.* Applied Mechanics and Materials, 2012. 117-119: p. 4.

5. Canioni, L., et al., *Three-dimensional optical data storage using third-harmonic generation in silver zinc phosphate glass.* Optics Letters, 2008. 33(4): p. 3.

6. Fletcher, L.B., et al., *Direct femtosecond laser waveguide writing inside zinc phosphate glass.* Optics Express, 2011. 19: p. 7929-7936.

7. Fletcher, L.B., et al., *Femtosecond laser writing of waveguides in zinc phosphate glasses.* Optical Materials Express, 2011. 1: p. 845-855.

8. Kreidl, N.J. and W.A. Weyl, Journal of American Ceramic Society, 1941. 11.

9. Smith, C.E., et al., *The structure and properties of zinc aluminophosphate glasses.* Journal of Non-Crystalline Solids, 2014.

10. Stone, P.E., E.P. Egan Jr., and J.R. Lehr, *Phase Relationships in the System CaO-Al_2O_3-P_2O_5.* Journal of the American Ceramic Society, 1956. 39(3): p. 89-98.

11. Yuh, S.J. and T.J. Rockett, *The system CaO-Al_2O_3-P_2O_5-H_2O at 200^oC.* Journal of the American Ceramic Society, 1981. 64(8): p. 491-493.

12. Gonzalez, F.J. and J.W. Halloran, *The Ternary System MgO-Al_2O_3-P_2O_5* Journal of American Ceramic Society, 1980. 63(9-01).

13. Carbajal, L., et al., *Solid-state compatability in two regions of the system ZnO-CaO-P_2O_5.* Journal of the American Ceramic Society, 2011. 94(7): p. 2213-2219.

14. Hoffman, M.V., *The systems BaO-MgO-P_2O_5 & BaO-ZnO-P_2O_5 compounds and fluorescence.* Journal of the Electrochemical Society, 1963. 110(12): p. 1223-1227.

15. Katnack, F.L. and F.A. Hummel, *Phase Equilibria in the System ZnO-P_2O_5.* Journal of the Electrochemical Society, 1958. 105(3): p. 125-133.

16. Hansson, R., et al., *A Reinvestigation of Phase Equilibria in the System Al_2O_3-SiO_2-ZnO.* Metallurgical and Materials Transactions B, 2005. 36B: p. 187-193.

17. Van Wazer, J.R., *Phosphorus and its Compounds Volume I: Chemistry*. Vol. 1. 1958, New York: Interscience Publishers, Inc. 954.

18. Martinez-Martinez, R., et al., *White light generation through the zinc metaphosphate glass activated by Ce^{3+}, Tb^{3+} and Mn^{2+} ions.* Journal of Luminescence, 2009. 129: p. 5.

19. Baez-Doelle, C., et al., *Crystal structure of zinc ultraphosphate, ZnP_4O_{11}.* Zeitschrift für Kristallographie, 1993. 203: p. 2.

20. Meyer, K., A. Barz, and D. Stachel, *A Study of the Structure of Binary Magnesium Ultraphosphate Glasses by Vibrational Spectroscopy.* Ceramics-Silikaty, 1999. 43(4): p. 5.

21. Ha, L.H., et al., *Some physical properties of $ZnAl_2O_4$: Cr^{3+} (Co^{2+}) powders prepared by hydrothermal method.* Journal of Physics: Conference Series, 2009. 187: p. 6.

22. Petrova, M.A., et al., *Spinel solid solutions in the systems $MgAl_2O_4$-$ZnAl_2O_4$ and $MgAl_2O_4$-Mg_2TiO_4.* Journal of Materials Research, 1997. 12(10): p. 5.

23. Bergeron, C.G. and S.H. Risbud, *Introduction to Phase Equilibria in Ceramics*. 1984, Westerville, Ohio: The American Ceramic Society.

24. Smith, J.D., *Phase equilibria diagrams of three components - Systems containing limited (or no) solid solution.* Refractories Applications and News, 2009. 14(1): p. 6.

25. van Rijn van Alkemade, A.C., Zeitschrift für physikalische Chemie, 1893. 11: p. 289-327.

26. Chen, P., et al., *Structure and crystallization of ZnO-B_2O_3-P_2O_5.* Glass Physics and Chemistry, 2011. 37(1): p. 5.

27. Maadi, A.E., et al., *Synthesis and characterization of $(Zn,M)_2P_2O_7$ (M=Mn,Cu).* Jounal of Alloys and Compounds, 1994. 205: p. 243-247.

28. Ust'yantsev, V.M., M.G. Tretnikova, and L.S. Zholobova, Inorganic Materials (Engl. Transl.), 1973. 9(3).

29. Stachel, D., et al., *Crystal structure of magnesium ultraphosphate, MgP_4O_{11}.* Zeitschrift für Kristallographie - Crystalline Materials, 1992. 199: p. 2.

30. Syritskaya, Z.M. and V.V. Yakubik, *Toward the study of the glass region in the system P_2O_5-Al_2O_3-ZnO.* Steklo i Keramika (translated), 1960. 17(2): p. 3.

31. Brown, H.E., *Zinc oxide rediscovered*. 1957: New Jersey Zinc Company. 99.

32. Bunting, E.N., *Phase equilibria in the system SiO_2-ZnO-Al_2O_3.* Bureau of Standards Journal of Research, 1932. 8: p. 11.

33. Hill, W.L., G.T. Faust, and S.B. Hendricks, *Polymorphism of Phosphoric Oxide.* Journal of American Chemical Society, 1943. 65: p. 794-802.

34. Jung, I.-H. and P. Hudon, *Thermodynamic Assessment of P_2O_5.* Journal of American Ceramic Society, 2012. 95(11): p. 8.

35. Wiench, J.W., et al., *Structure of zinc polyphosphate glasses studied by two-dimensional solid and liquid state NMR.* Journal of Molecular Structure, 2002. 602-603: p. 13.

36. Tischendorf, B., et al., *A study of short and intermediate range order in zinc phosphate glasses.* Journal of Non-Crystalline Solids, 2001. 282: p. 12.

37. Tananaev, I.V., et al., Inorganic Materials (Engl. Transl.), 1978. 14(4): p. 4.

38. Meyer, K., et al., *Infrared spectra and structure of various crystalline ultraphosphates and their glasses.* Vibrational Spectroscopy, 1994. 6: p. 10.

39. Petrova, M.A., G.A. Mikirticheva, and R.G. Grebenshichikov, *Phase Equilibria in the $Zn_2P_2O_7$-$M_2ZnP_2O_7$ and $M'_2ZnP_2O_7$-$M''_2ZnP_2O_7$ (M, M', M'' = Li, Na, K) Glass-forming systems.* Inorganic Materials, 2007. 43(9): p. 8.

3. THE PROPERTIES AND STRUCTURE OF ZINC MAGNESIUM PHOSPHATE GLASSES

Charmayne E. Smith, Richard K. Brow
Missouri University of Science and Technology
Rolla, MO 65409, US

ABSTRACT

Zn-Mg-phosphate (ZMP) glasses were prepared and properties such as density, refractive index, coefficient of thermal expansion and glass transition temperature (T_g), were measured. The glass transition temperature increases by 100-150 ˚C and the room temperature dissolution rates in water decrease by 1-2 orders of magnitude when MgO replaces ZnO in compositional series with constant (40 or 50 mole%) P_2O_5 content. Glass structures were characterized by Raman spectroscopy and there were no significant changes in the phosphate anion distributions when ZnO was replaced by MgO. The significant changes in properties cannot be explained by a simple cation field strength argument since Mg^{2+} and Zn^{2+} have similar sizes; instead, the effect of 3d electrons on the nature of the bonds between Zn^{2+} ions and non-bridging oxygens on the phosphate tetrahedra must be considered.

3.1 INTRODUCTION

Zinc phosphate glasses have been developed for use as LED light sources [1], and as substrates for optical waveguides written by f-sec lasers [2-5]. These glasses possess a UV-edge below 400 nm, which is useful for some optical applications [6]. Zinc phosphate glasses also tend to have higher coefficients of thermal expansion with low processing temperatures which make them useful as sealing glasses [7, 8].

A drawback to the use of binary zinc phosphate glasses is their susceptibility to chemical attack because of the ease of hydrolysis of the P-O-Zn bonds [9]. It is known that the addition of other oxides can improve the chemical durability of phosphate glasses; one in particular is magnesium oxide which has been shown to reduce corrosion rates of zinc phosphate glasses, presumably due to the formation of more chemically resistant P-O-Mg bonds [10].

The properties and structures of binary zinc [9, 11-24] and magnesium phosphate [14, 18, 25-30] glasses have been studied. Both the $ZnO\text{-}P_2O_5$ and the $MgO\text{-}P_2O_5$ binary systems have been classified as anomalous because of discontinuities in composition-property trends near the metaphosphate (50 mol% P_2O_5) composition [26]. The addition of either ZnO or MgO to P_2O_5 results in systematic changes in properties that can be related to changes in the phosphate network structure. Glasses from the $ZnO\text{-}P_2O_5$ binary have a minimum in T_g and CTE near 60 mol% ZnO [13], behavior that is not found in the $MgO\text{-}P_2O_5$ system [19].

Phosphate anionic structures can be described using the Q^n-terminology, where 'n' represents the number of bridging oxygens on a phosphate tetrahedron [31]. For

example, changes in the types of phosphate tetrahedra with the addition of MeO (where Me=Zn, Mg) can be described by the reaction:

$$2Q^n + MeO \rightarrow 2Q^{n-1} \quad (1)$$

Binary phosphates with increasing MeO-content (increasing O/P ratio) have shorter average phosphate anion lengths as nonbridging oxygens replace bridging oxygens on the P-tetrahedra. Evidence of these structural changes can be seen in the many spectroscopic studies, including Raman and/or infrared (IR) spectroscopies [11, 25, 28] and ^{31}P nuclear magnetic resonance (NMR) spectroscopy [20, 32-34].

Khor and colleagues have described the effects of the composition of ternary zinc-magnesium-phosphate (ZMP) glasses on the optical, dielectric and physical properties [6, 10, 29, 30, 35]. They showed that the replacement of P_2O_5 by MgO decreases the aqueous dissolution rates of zinc phosphate glasses [10], although it is unclear if this improvement in chemical durability is due to the replacement of P-O-Zn bonds by P-O-Mg bonds, or to the overall decrease in the P_2O_5 content [9, 36, 37].

The goal of this study is to determine the effects of substituting MgO for ZnO, while maintaining a constant P_2O_5 content (constant O/P ratio), on the properties and structures of zinc phosphate glasses, including compositions originally developed as substrates for femto-second processing. A constant O/P ratio fixes the average chain length of the phosphate units in the structure [31] and so property changes can then be related to the nature of the P-O-Me bonds that link neighboring anions. The focus of this paper is to report the glass-forming range of several series of $xZnO\text{-}(1\text{-}x)MgO\text{-}P_2O_5$ compositions, to describe the property trends due to the systematic replacement of ZnO by MgO, and to relate those property trends to the glass structures.

3.2 EXPERIMENTAL

The glasses were prepared by mixing appropriate amounts of MgO (Alfa Aesar, 96%), $NH_4H_2PO_4$ (ACS, 98.0% - Alfa Aesar), and ZnO (reagent grade, ≥ 99.0% - Sigma Aldrich), calcining the batches in an alumina crucible for ~15 hrs. at 500°C, then melting the batches between 1000-1500°C for approximately two hours in air. Melts were quenched on copper plates, and these glasses were remelted in alumina using similar conditions to improve glass homogeneity. The final glass samples were obtained by pouring the melts into a steel mold (10 mm in diameter and 2.5 cm tall), or splat quenching between copper plates if necessary, and annealing near T_g for approximately two hours, before slowly cooling to room temperature.

The density of each bubble-free glass was measured using Archimedes' method with distilled water as the buoyancy liquid. Three samples of each glass were measured and the standard deviation is reported as the experimental uncertainty. The molar volume (MV) was calculated by dividing the density of each glass by the molecular weight, calculated from analyzed glass compositions. The compositions of polished samples were calculated from cation ratios determined using energy dispersive spectroscopy (EDS, Helios NanoLab 600 FIB/FESEM with an Oxford EDS attachment). The compositional uncertainty was determined by analyzing three or more areas of at least three different samples of the same composition and was found to be a maximum of ±0.6 mol% for each oxide [Table 1]. The glasses will be described using their nominal compositions.

Differential thermal analysis (DTA, Perkin-Elmer DTA7) was used to determine the glass transition temperature (T_g) by placing 30-40mg of glass powder (<75 μm) in an

open, alumina crucible, then heating at a rate of 10˚C/min in nitrogen atmosphere; the onset temperatures were determined with the accompanying software and the estimated uncertainty of this characteristic temperature is ±5 ˚C.

The refractive indices (n) were measured using a prism coupler (Metricon model 2010/M) at 632.8 nm on samples that were ~1 mm thick and polished to a 1 μm finish (diamond paste, Allied High Tech); the uncertainty of these measurements is ±0.0004.

The dilatometric softening temperature (T_d) and the coefficient of thermal expansion (CTE) were determined using an Orton dilatometer (Model 1600D) on cylindrical samples approximately 2.54 cm in length, heated at a rate of 10°C/min in air. The T_d is established as the maximum of the dilatometric data with a reproducibility of ±5 ˚C. The CTE is reported as the linear slope of data from 200-400 ˚C and these measurements were reproducible to ±0.2 ppm/˚C.

Weight loss measurements from bulk glasses immersed in deionized (DI) water at 21˚C for up to 48 hours were made to determine relative chemical durability. Polished disks (10 mm in diameter, 1 mm thick, 5 μm finish) were rinsed with acetone and dried before testing. A constant sample surface area (SA) to solution volume ratio of 0.035 cm^{-1} was used for each experiment. Samples were removed periodically from the polypropylene containers used for the corrosion tests, dried and weighed, and then returned to the original solution. Three samples were tested for each condition and the average weight loss and standard deviation are reported. Dissolution rates are reported as the linear slope of the weight loss data over the entire 48 hours of each experiment.

Raman spectra were collected from a polished sample of each glass using a Jobin-Yvon micro-Raman spectrometer with a 632.8 nm He–Ne laser (17 mW) as the excitation source.

3.3 RESULTS

3.3.1 Glass-Forming Region. The as-batched and measured compositions of the glasses are given in Table 1 and shown in Figure 1 along with other compositions melted to confirm the glass forming region. Small amounts of alumina (<5 mol%) were dissolved into the glasses because of reactions between the melts and the alumina crucible (Table 1). The binary magnesium phosphate glass with an intended O/P ratio of 3.25 had the largest alumina content (4.7 mol%) because of the high melting temperatures used (1500 ˚C). P_2O_5-loss was limited and so compositions are grouped by their batched O/P ratios. Glasses with an O/P ratio below 2.8, in the ultraphosphate region, were not prepared in this study. Studies of binary compositions prepared by traditional splat quenching methods produced glasses with up to ~71 mol% ZnO [11, 19, 21] and ~65 mol% MgO [18, 25, 27, 29], which coincide with the forming ranges found in this work (Figure 1).

The binary compositions with between 70-80 mol% MgO melted below 1500 ˚C, but the melts had very low viscosities and crystallized immediately upon quenching. The use of roller quenching has been shown to push the glass forming region of binary phosphate glasses with both ZnO [17] and MgO [28] up to 80 mol% and these reported roller-quenching limits of glass formation for the respective binaries are also shown in Figure 1.

3.3.2 Physical and Thermal Properties. The densities of ZMP compositions with O/P ratios = 3.0 and 3.25 are shown in Figure 2a and their molar volumes are shown in Figure 2b. Also shown are properties of glasses with similar compositions reported in the literature. For glasses with similar O/P ratios, the replacement of ZnO by MgO systematically decreases density but has no significant effect on molar volume. Glasses with greater P_2O_5 contents (lower O/P ratios) have lower densities and greater molar volumes. Figure 3a and 3b show that the glass transition temperatures (T_g) and dilatometric softening temperatures (T_d), respectively, increase systematically with the replacement of ZnO by MgO, and do not vary significantly with O/P ratio. Figure 4 shows that there is a small increase in the coefficients of thermal expansion (CTE) as a function of MgO content, and glasses with O/P=3.25 have slightly greater CTEs than glasses with O/P=3.0.

The refractive indices measured at 632.8 nm are shown in Figure 5. With the replacement of ZnO by MgO, there is a systematic decrease in the refractive index. Glasses with greater P_2O_5 contents (lower O/P ratios) have lower refractive indices.

3.3.3 Chemical Durability. The weight loss data in room temperature water for the ZMP glasses with O/P ratios = 3.0 and 3.25 are shown in Figure 6a and Figure 6b, respectively. In general, the glasses exhibit a linear weight loss behavior over the 48 hours of the tests. There is an overall decrease in weight loss rate with the replacement of ZnO by MgO in the composition, as can be seen in Figure 6c.

3.3.4 Raman Spectroscopy. The Raman spectra of the metaphosphate (O/P = 3.0) and polyphosphate (O/P = 3.25) glasses are shown in Figure 7a and Figure 7b, respectively.

Raman spectra of the binary zinc phosphate glasses are similar to spectra from similar compositions reported in the literature [11]. The spectrum from the 50MgO-$50P_2O_5$ composition also is similar to a previously reported spectrum of similar glass, however the spectrum from the 60MgO-$40P_2O_5$ glass is more similar to a glass with a greater MgO content (65MgO-$35P_2O_5$) [38], likely due to the relatively high alumina content in the present glass.

The spectra of glasses in the metaphosphate compositional range have the following features: peaks at 704 cm^{-1} and 1204 cm^{-1}, and a broad shoulder in the range 1240-1350 cm^{-1}; these peaks are assigned to the POP_{sym} stretching mode of bridging oxygens in Q^2 units, the $(PO_2)_{sym}$ stretching mode of non-bridging oxygens in Q^2 units, and the $(PO_2)_{asym}$ stretching mode of non-bridging oxygens in Q^2 units, respectively [11, 23]. When MgO replaces ZnO in this series (Figure 7a), the main peak at 1200 cm^{-1} narrows slightly and a peak near 1282 cm^{-1} becomes more distinct and intense.

The Raman spectra for the ZMP polyphosphate glasses (O/P = 3.25), shown in Figure 7b, have peaks at ~700 cm^{-1}, an intense peak at 1200 cm^{-1} and a broad shoulder centered near 1310 cm^{-1}, similar to what was observed in the spectra from the metaphosphate glasses. In addition, there is a shoulder at ~750 cm^{-1} due to the POP stretching mode associated with Q^1 sites and a broad shoulder centered near ~1050 cm^{-1} which is due to the PO_3 stretching modes of nonbridging oxygens in Q^1 end groups [11, 23]. There are no significant changes in the Raman spectra of the ZMP polyphosphate glasses when MgO replaces ZnO, although the relative intensity of the shoulder between 900-1100 cm^{-1} in the spectrum from the ZnO-free ZMP_60_3.25 glass is greater than it is

in the spectra from the other glasses. Again, this is related to the greater O/P ratio measured for this glass (3.44, Table 1) than from the others.

3.4. DISCUSSION

3.4.1 Glass Properties. The decrease in density with the replacement of ZnO by MgO (Figure 2a) is due to the smaller mass of Mg compared to Zn. The molar volume (Figure 2b), however, shows no significant changes with MgO substitution which indicates that this substitution is not accompanied with significant structural reorganization. A substantial decrease in molar volume is noted for glasses with greater O/P ratios. Some of the variability in the molar volumes of glasses within a series may be due to small variations in O/P ratios due to differences in the residual alumina content and P_2O_5 volatility during melting.

The lower molar volumes for the zinc-magnesium polyphosphate (O/P=3.25) glasses compared to the metaphosphate (O/P=3.00) glasses are consistent with the smaller phosphate anions associated with the former series. For both the binary Zn- and Mg-phosphate glasses, there is a systematic decrease in the molar volumes with increasing O/P ratios (Figure 9). The Raman spectra of the ZMP glasses are consistent with the formation of smaller phosphate anions with increasing O/P ratios, following Equation 1. The smaller average phosphate anions, and the larger relative fractions of Zn- and Mg-polyhedra, pack more efficiently in the structures of glasses with greater O/P ratios, decreasing the overall molar volume of the glass.

The replacement of ZnO by MgO in the ZMP glasses decreases the refractive index with increasing MgO for both O/P ratio series (Figure 5), which is in agreement with previous studies [35], and is explained by the greater ionic refractivity (R_i) of Zn^{2+}

(R_i=0.70) compared to Mg^{2+} (0.25) and P^{5+} (0.05) [39]. Molar refraction (R_m) values were calculated from the measured refractive indices and calculated molar volume (MV) from [40]:

$$R_m = MV*((n^2-1)/(n^2+2)) \quad (2)$$

As shown in Figure 10a, molar refraction decreases when MgO replaces ZnO in both series of glasses, indicating an overall decrease in the polarizability of the Mg-glasses. The individual ionic contributions to R_m can be determined from the ion concentrations (c_i) and individual ionic refractivities from [39]:

$$R_m = \sum_i R_i \cdot c_i \quad (3)$$

Assuming constant ionic refractivities for all cations (including Al^{3+}), the oxygen refractivity can be determined from the values of R_m and the measured glass compositions (Table 1). The oxygen refractivities are shown as a function of MgO content for both O/P ratio series in Figure 10b. The systematic decrease in oxygen refractivity indicates that there is a decrease in the polarizability of the average nonbridging oxygen when MgO replaces ZnO in both series of glasses. The oxygen refractivities of the polyphosphate glasses are greater than that of the metaphosphate glasses because the former have a greater fraction of more polarizable nonbridging oxygens.

The replacement of ZnO by MgO has a significant effect on the glass transition (Figure 3a) and the dilatometric softening temperatures (Figure 3b). The thermal properties of phosphate glasses are often discussed in terms of the relative field strengths (charge/(ionic radius)^2) of the cations added. High field strength cations, like Al^{3+}, form strong bonds with the non-bridging oxygens on the phosphate anions [41, 42] and these

bonds have a great effect on thermal properties. Metwalli et al. reported an increase in T_g of ~200 ˚C with the replacement of MgO by Al_2O_3 for a series of metaphosphate glasses with a constant O/P ratio [43]. The field strength argument, however, does not explain the large increase in T_g when MgO replaces ZnO because these two cations have the same charge and similar sizes: in tetrahedral sites, 0.71 nm for Mg^{2+} and 0.74 nm for Zn^{2+} [44].

The systematic changes in glass properties with the replacement of ZnO by MgO should be understood by the differences in ion properties other than size. Weyl and Marboe have noted that oxide melting temperatures can be affected by a few key factors, i.e. differences in cation charge, anion size to cation size ratio, cation size and ion polarizability [45]. Mg^{2+} and Zn^{2+} have similar sizes and the same charge, but have different polarizabilities, as reflected by their different ionic refractivities. A comparison of the melting temperatures of ZnO (1975 ˚C) and MgO (2800 ˚C) shows that cation polarizability has a strong effect on thermal properties and it has been noted before that oxides of cations with noble-gas configurations (MgO) tend to have greater melting temperatures than oxides with d-electrons (ZnO) [45]. The $3d^{10}$ electrons contribute to the greater polarizability of Zn^{2+}, compared to Mg^{2+}. The greater shielding effects of the d-electrons lead to weaker coulombic interactions with neighboring anions. The stronger coulombic interactions between Mg^{2+} and nonbridging oxygens on a phosphate tetrahedron, compared with Zn^{2+}, leads to the significant increase in the glass transition (Figure 3a) and dilatometric softening (Figure 3b) temperatures when MgO replaces ZnO for both O/P ratio series. These trends in characteristic temperatures are also consistent

with the relative melting points of the respective crystal compounds: $Mg(PO_3)_2$ (1160 ˚C) [46] and $Zn(PO_3)_2$ (872 ˚C) [47] and $Mg_3(PO_4)_2$ (1357 ˚C) and $Zn_3(PO_4)_2$ (1060 ˚C) [48].

3.4.2 Chemical Durability. The linear trends in weight loss with time are typical for many phosphate glasses [36, 49]. When phosphate glasses react in water, the bonds between metal cations and non-bridging oxygens (P-O-Me) are attacked by hydration. Due to this process, the phosphate chains are unbroken and only the nonbridging oxygen sites of the structure are affected, disconnecting entire phosphate anions which are then released, intact, into the solution [15, 50, 51]. Thus the dissolution rates of phosphate glasses depend on the hydration rates of the interchain linkages. The replacement of P-O-Zn bonds by P-O-Mg bonds for glasses with constant average chain lengths leads to a decrease in the dissolution rates of the ZMP glasses in water (Figure 6c). This is consistent with the study by Khor, et al., who also showed that the addition of MgO to zinc phosphate glasses decreased dissolution rates [10], although the decrease noted in their work could also be the result of the concomitant replacement of P_2O_5 by MgO and ZnO.

The overall decrease in dissolution rates when MgO replaces ZnO indicates that the P-O-Mg bonds are more resistant to hydration than the P-O-Zn bonds. Takebe, et al. [52] have related the relative dissolution rates of binary phosphate glasses to the polarizability of the nonbridging oxygens in the P-O-Me bonds that link neighboring P-anions. They discuss that the more polarizable bonds react more readily with water to reduce chemical durability. If the oxygen refractivity data in Figure 10b is a measure of the relative polarizability of P-O-Zn and P-O-Mg bonds, then replacing ZnO with MgO

reduces the average polarizability of oxygens in the glass and so would make the glass less reactive in water.

It should be noted that the Mg-free zinc polyphosphate glass (ZMP_0_3.25) has a much lower dissolution rate ($1.5x10^{-5}$ g/cm^2*hr) than several others in the polyphosphate series. A white corrosion film formed on this sample (inset to Figure 8) that did not form on any other sample. The film was x-ray amorphous, but Raman spectroscopy (Figure 8) indicates that it has a chemical structure that is similar to the crystalline compound $Zn_2P_2O_7$. Zinc phosphate glasses have been reported to exhibit two different dissolution behaviors in water, either by progressive dissolution and the precipitation of material in solution (Type I) or by dissolution and the formation of a precipitation layer on the reacting glass surface (Type II) [9]. The ZMP_0_3.25 sample was the only sample to exhibit this Type II dissolution behavior, and the formation of the amorphous corrosion layer appears to have slowed down the overall dissolution rate of this glass.

3.4.3 Glass Structure. It is important to recall that the trends in thermal and chemical properties are not associated with significant reorganization of the phosphate network structure. There are no significant changes in the molar volumes and the Raman spectra are similar for both glass series when MgO replaces ZnO, although there are systematic changes in Raman peak positions. For the metaphosphate (O/P = 3.0) series, the peak for the PO_2 symmetric stretching mode near 1200 cm^{-1} increases in frequency with increasing MgO (Figure 11). The peak for the PO_2 asymmetric stretching mode also increases in frequency, from the shoulder near 1247 cm^{-1} from the Zn-metaphosphate glass to the sharp peak at 1282 cm^{-1} for the Mg-metaphosphate glass [Figure 7a]. Popovic et al. [53] and Nelson et al. [54] relate these increases in frequency to a decrease

in the average P-nonbridging oxygen bond lengths. This is consistent with diffraction studies which show that the P-NBO bond length in a Mg-metaphosphate glass is shorter (0.149±0.001 nm [33]) than that in a Zn-metaphosphate glass (0.150±0.002 nm [12]).

For the series of ZMP glasses with O/P ratio = 3.25, there is a significant decrease in the frequency of the $(PO_2)_{sym}$ stretching mode (Figure 11a) and an increase in the frequency of the PO_3 stretching mode with increasing MgO, as determined by peak deconvolution. Using the Popovic correlation [53], these trends in respective peak positions indicate that the average P-NBO bond lengths associated with Q^2 units are getting longer and the average P-NBO bond lengths associated with the Q^1 units are becoming shorter as MgO replaces ZnO in the polyphosphate glass series. The shorter P-O bonds are consistent with the lower average polarizabilities of the oxygen ions, implied by the lower oxygen ionic refractivity shown in Figure 10b.

The shorter P-NBO bonds on Q^2 tetrahedra for the metaphosphate series and shorter P-NBO bonds on Q^1 tetrahedra for the polyphosphate may also be related to the increases in glass transition (Figure 3a) and dilatometric softening temperatures (Figure 3b) as ZnO is replaced by MgO. Shorter bonds imply stronger bonds that may require more thermal energy to deform.

3.5 CONCLUSIONS

The properties and structures of ZnO-MgO-P_2O_5 glasses where ZnO was systematically replaced by MgO have been described. Zinc and magnesium ions have similar sizes and this compositional substitution has little effect on the molar volumes of the glasses. Raman spectroscopy indicates that these compositional changes do not significantly affect the overall phosphate network. However, substantial changes in glass

properties, including increases by over 100°C in the glass transition temperature and reductions by 1-2 orders of magnitude in aqueous dissolution rates, indicate that ZnO and MgO affect the glasses in different ways.

The $3d^{10}$ electrons with the Zn^{2+} ion makes it more polarizable than the Mg^{2+} ion. This polarizability accounts for the greater ionic refractivity of Zn^{2+} and so the greater refractive indices for the Zn-rich glasses. The $3d^{10}$ electrons also screen the zinc nucleus, reducing the coulombic attraction between Zn^{2+} ions and nonbridging oxygens on phosphate tetrahedra compared to the Mg^{2+} ions, accounting for the systematic increases in T_g with MgO-substitution.

The average ionic refractivity of the oxygen ions decreases with increasing MgO-substitution, indicating that the non-bridging oxygens associated with the P-O-Mg bonds are becoming less polarizable. This lower polarizability may make the P-O-Mg bonds less susceptible to hydration reactions to account for the improved chemical durability of these glasses when MgO replaces ZnO.

3.6 ACKNOWLEDGEMENTS

The authors acknowledge the Department of Education for the Graduate Assistance in Areas of National Need (GAANN) fellowship and the National Science Foundation (DMR 1207520) for funding this work. The contributions of Dr. Jen Hsien Hsu for the compositional analysis by EDS and Ryan Jones for assistance with the synthesis and characterization of the ZMP glasses are greatly appreciated.

Tables

Table 1: Nomenclature and compositions of the Zinc Magnesium Phosphate glasses

Designation (mol%)	Batched Compositions (mol%)	Measured Analyzed Compositions [mol%]				
ZMP_mol% MgO_O/P	ZnO-MgO-P_2O_5 [O/P ratio]	ZnO (±0.6)	MgO (±0.5)	P_2O_5 (±0.3)	Al_2O_3 (±0.2)	O/P
ZMP_0_3.0	50-0-50 [3.0]	48.5	0	49.4	2.1	3.05
ZMP_13_3.0	37.5-12.5-50 [3.0]	37.3	12.0	48.9	1.8	3.06
ZMP_25_3.0	25-25-50 [3.0]	25.0	23.4	50.0	1.6	3.03
ZMP_38_3.0	12.5-37.5-50 [3.0]	13.1	35.0	51.1	0.9	3.00
ZMP_50_3.0	0-50-50 [3.0]	0	46.1	53.1	0.8	2.96
ZMP_0_3.25	60-0-40 [3.25]	60.5	0	36.7	2.8	3.44
ZMP_15_3.25	45-15-40 [3.25]	38.7	19.1	41.2	1.0	3.24
ZMP_30_3.25	30-30-40 [3.25]	30.3	27.8	41.3	0.6	3.23
ZMP_45_3.25	15-45-40 [3.25]	15.5	42.0	41.6	0.9	3.22
ZMP_60_3.25	0-60-40 [3.25]	0	55.5	39.8	4.7	3.37

Figures

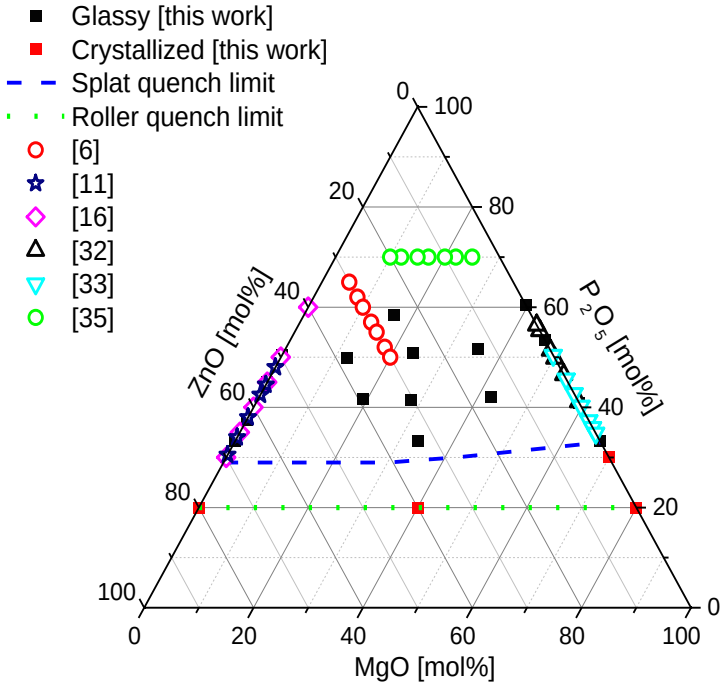

Figure 1: Glass forming diagram of the zinc magnesium phosphate system. Non glass forming region by splat quenching (blue dashed line) [this work] and the estimated non glass forming region by roller quenching (green dotted line). Diagram includes glasses reported in the literature [6, 11, 16, 32, 33, 35].

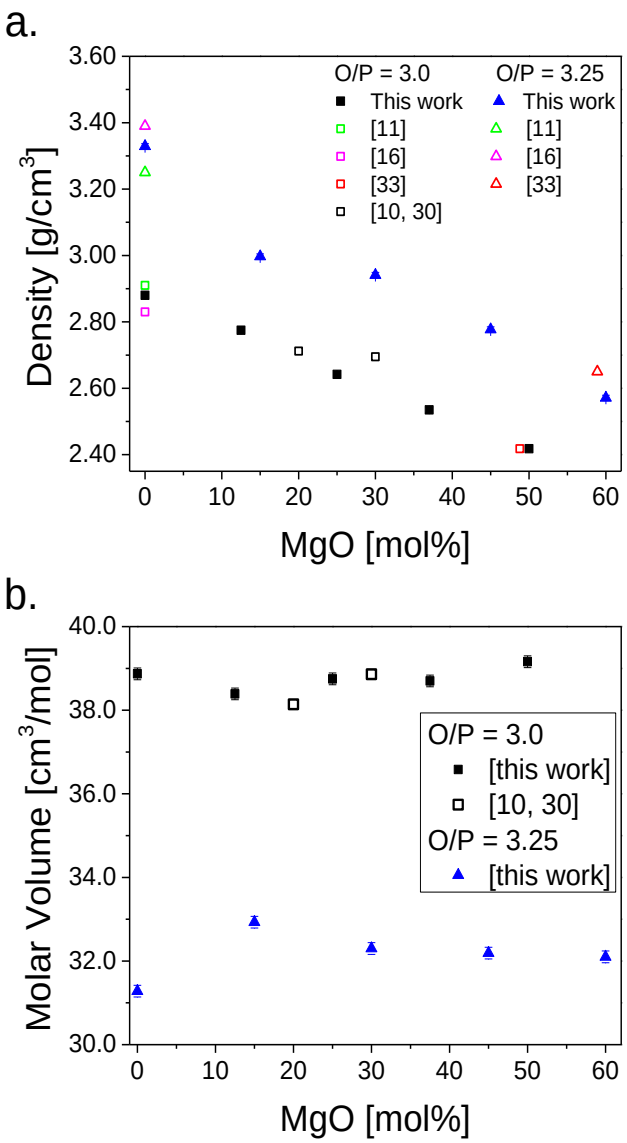

Figure 2: a) Density and b) molar volume of ZMP glasses with O/P = 3.0 [squares] and 3.25 [triangles]. (Data from the literature are given as open symbols)

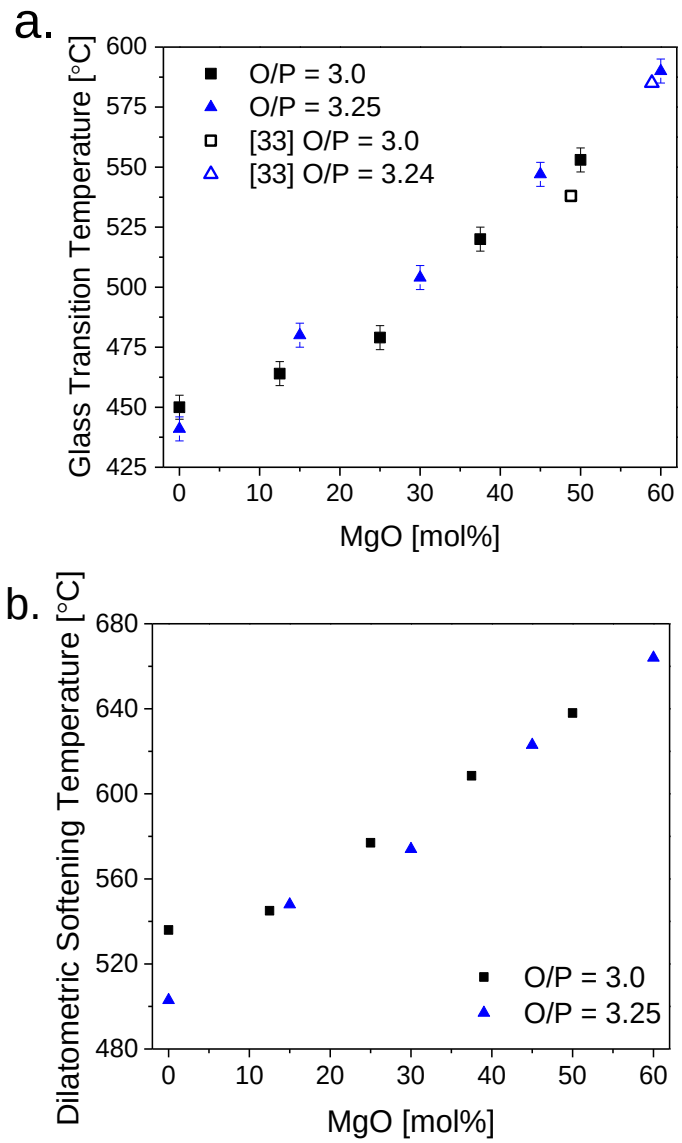

Figure 3: a) The glass transition temperatures and b) dilatometric softening temperatures [error = ±5˚C] for the ZMP glasses with O/P = 3.0 [squares] and 3.25 [triangles]. (Data from the literature as open symbols)

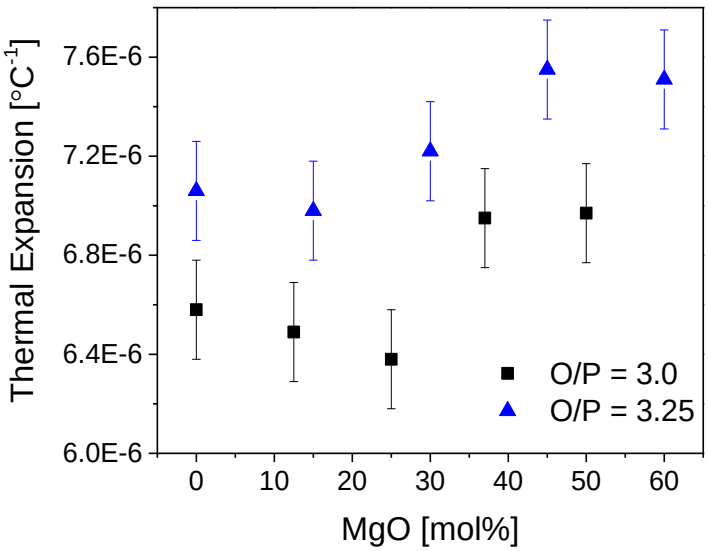

Figure 4: Coefficient of thermal expansion for the ZMP glasses

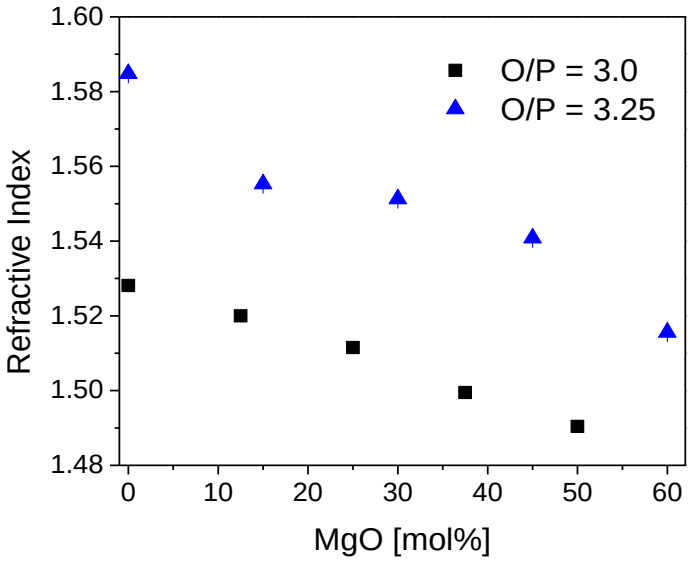

Figure 5: Refractive indices of glasses in the ZnO-MgO-P_2O_5 system

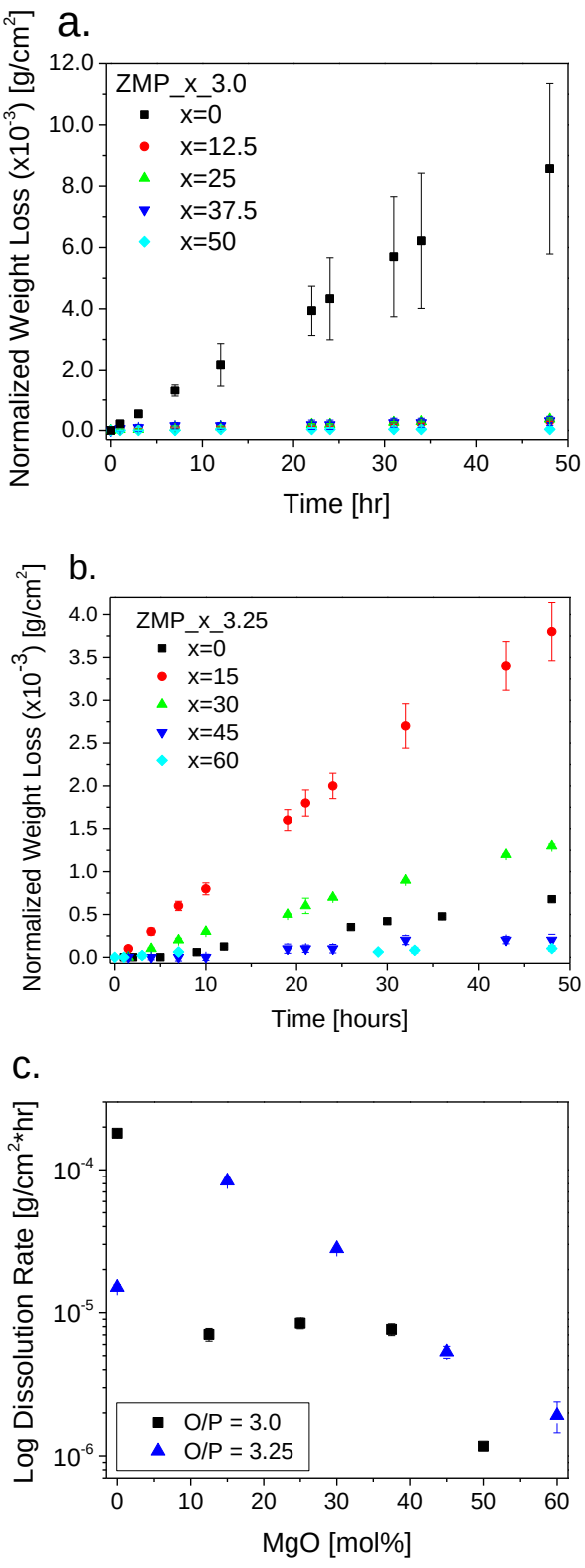

Figure 6: Weight loss data in room temperature water for ZMP glasses with a) O/P = 3.0 and b) O/P = 3.25; c) dissolution rates calculated from the weight loss data.

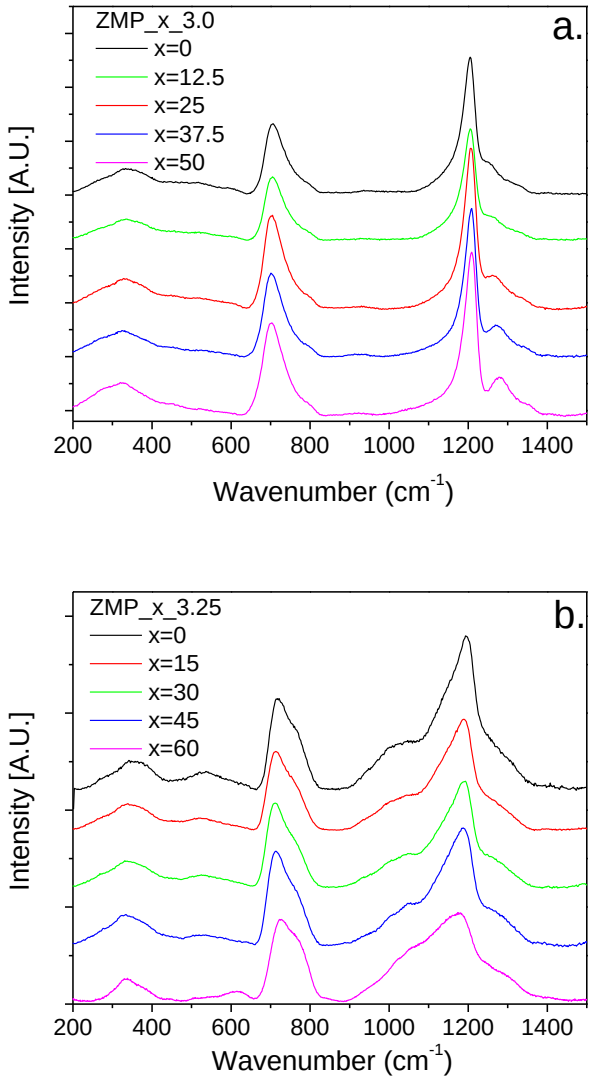

Figure 7: Raman spectra of ZMP glasses with a) O/P = 3.0 and b) O/P = 3.25

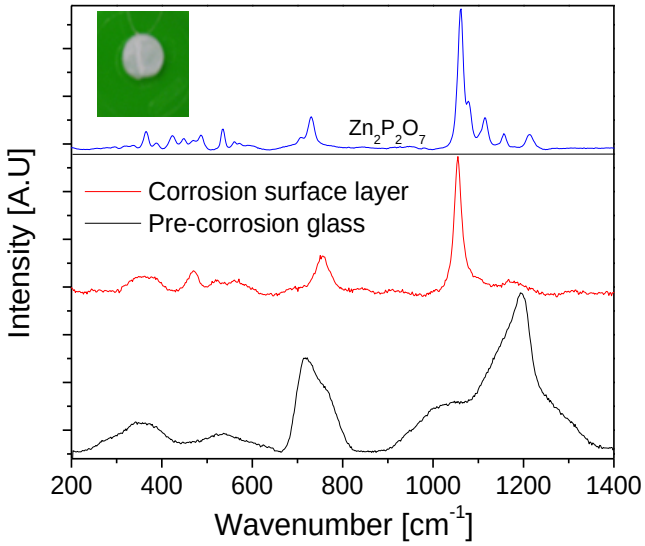

Figure 8: Raman spectra of the ZMP_0_3.25 glass surface before (bottom) and after (middle) 48 hours in room temperature water, compared to the spectrum from crystalline $Zn_2P_2O_7$ (top). The inset shows an optical image of a sample of this glass after corrosion testing.

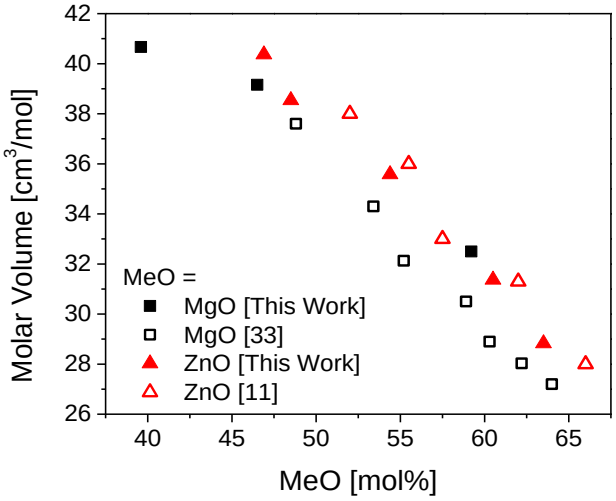

Figure 9: Molar volume plotted as a function of MeO content for binary MeO-P_2O_5 glasses [Me = Zn (red triangles) or Mg (black squares)] from this work. (Data from the literature are shown as open symbols)

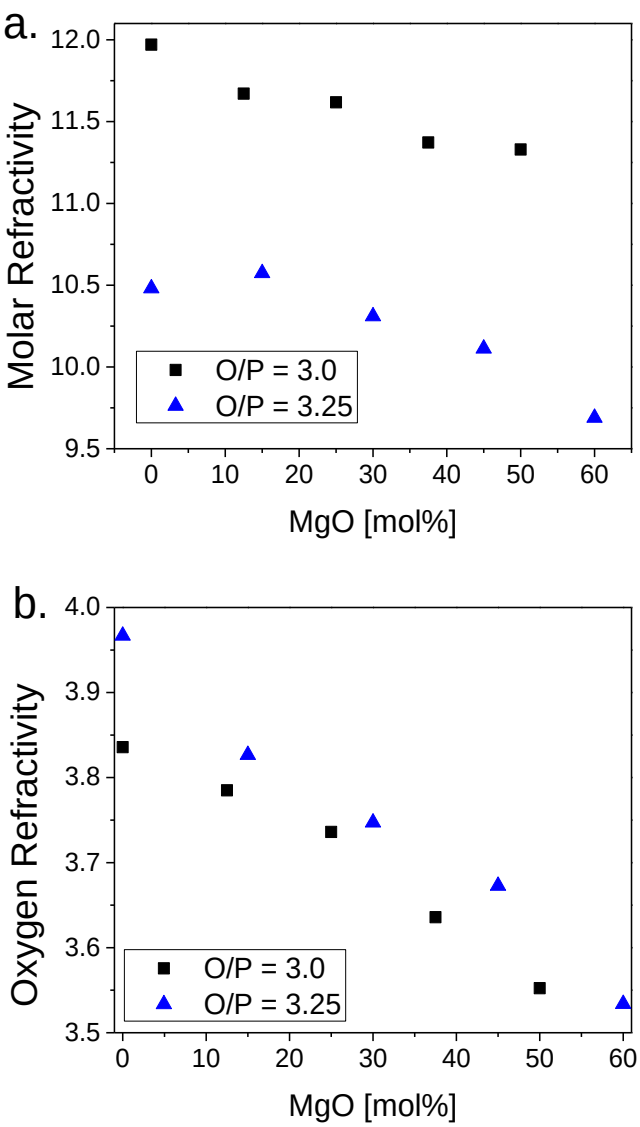

Figure 10: a) Molar refractivity and b) oxygen refractivity of ZMP glasses with O/P = 3.0 (black squares) and 3.25 (blue triangles)

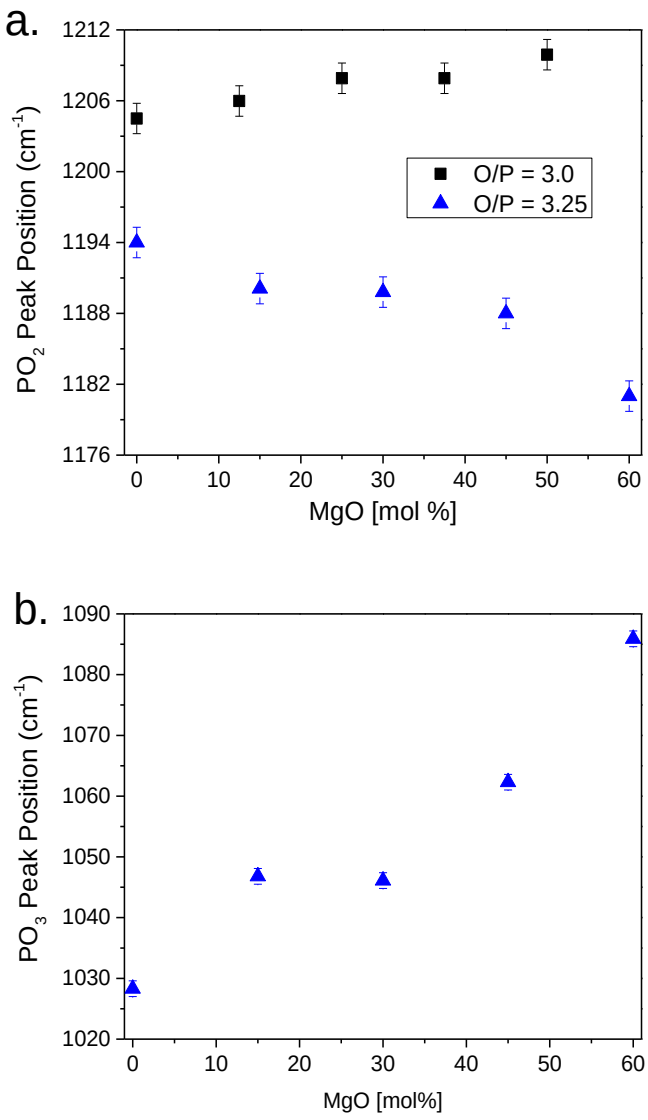

Figure 11: Raman peak positions of the a. PO_2 symmetric stretching mode for ZMP glasses with O/P = 3.0 [black squares] and O/P = 3.25 [blue triangles] and b. PO_3 asymmetric stretching mode for O/P = 3.25

REFERENCES

1. Martinez-Martinez, R., et al., White light generation through the zinc metaphosphate glass activated by Ce^{3+}, Tb^{3+} and Mn^{2+} ions. Journal of Luminescence, 2009. 129: p. 5.

2. Fletcher, L.B., et al., Effects of rare-earth doping on femtosecond laser waveguide writing in zinc polyphosphate glass. Journal of Applied Physics, 2012. 112.

3. Fletcher, L.B., et al., Direct femtosecond laser waveguide writing inside zinc phosphate glass. Optics Express, 2011. 19(9).

4. Fletcher, L.B., et al., Femtosecond laser writing of waveguides in zinc phosphate glasses. Optical Materials Express, 2011. 1: p. 845-855.

5. Canioni, L., et al., Three-dimensional optical data storage using third-harmonic generation in silver zinc phosphate glass. Optics Letters, 2008. 33(4): p. 3.

6. Khor, S.F., Z.A. Talib, and W.M. Mat Yunus, Optical properties of ternary zinc magnesium phosphate glasses. Ceramics International, 2012. 38: p. 6.

7. Aitken, B.G., et al., Non-lead sealing glasses, 1993, Corning Incorportated: United States.

8. Morena, R.M., Phosphate glasses as alternatives to Pb-based sealing frits. Journal of Non-Crystalline Solids, 2000. 263&264: p. 6.

9. Takebe, H., Y. Baba, and M. Kuwabara, Dissolution behavior of ZnO-P_2O_5 glasses in water. Journal of Non-Crystalline Solids, 2006. 352: p. 3088-3094.

10. Khor, S.F., et al., Degradation study on ternary zinc magnesium phosphate glasses. Journal of Materials Science, 2011. 46: p. 6.

11. Brow, R.K., et al., The short-range structure of zinc polyphosphate glass. Journal of Non-Crystalline Solids, 1995. 191: p. 45-55.

12. Hoppe, U., et al., Structure of zinc phosphate glasses probed by neutron and X-ray diffraction of high resolving power and by reverse Monte Carlo simulations. Journal of Non-Crystalline Solids, 2005. 351: p. 12.

13. Kubo, T., et al., Thermal properties and structure of zinc phosphate glasses. Physics and Chemistry of Glasses - European Journal of Glass Science and Technology Part B, 2009. 50(1): p. 4.

14. Matsubara, E., et al., Structural study of binary phosphate glasses with MgO, ZnO, and CaO by X-ray diffraction. Journal of Non-Crystalline Solids, 1988. 103: p. 8.

15. Sales, B.C., et al., Structure of zinc polyphosphate glasses. Journal of Non-Crystalline Solids, 1998. 226: p. 287-293.

16. Tischendorf, B., et al., The structure and properties of binary zinc phosphate glasses studied by molecular dynamics simulations. Journal of Non-Crystalline Solids, 2003. 316: p. 12.

17. Tischendorf, B., et al., A study of short and intermediate range order in zinc phosphate glasses. Journal of Non-Crystalline Solids, 2001. 282: p. 147-158.

18. Walter, G., et al., Intermediate range order in $MeO-P_2O_5$ glasses. Journal of Non-Crystalline Solids, 1997. 217: p. 299-307.

19. Walter, G., et al., The structure of zinc polyphosphate glass studied by diffraction methods and ^{31}P NMR. Journal of Non-Crystalline Solids, 2004. 333: p. 11.

20. Wiench, J.W., et al., Structure of zinc polyphosphate glasses studied by two-dimensional solid and liquid state NMR. Journal of Molecular Structure, 2002. 602-603: p. 13.

21. Suzuya, K., et al., The structure of binary zinc phosphate glasses. Journal of Non-Crystalline Solids, 2004. 345&346: p. 80-87.

22. Meyer, K., Characterization of the structure of binary zinc ultraphosphate glasses by infrared and Raman spectroscopy. Journal of Non-Crystalline Solids, 1997. 209: p. 227-239.

23. Schwarz, J., et al., Physical properties of $PbO-ZnO-P_2O_5$ glasses. I.Infrared and Raman Spectra. Journal of Optoelectronics and Advanced Materials, 2004. 6(3): p. 737-746.

24. Crobu, M., et al., Chain-length-identification strategy in zinc polyphosphate glasses by means of XPS and ToF-SIMS. Anal Bioanal Chem, 2012. 403: p. 8.

25. Meyer, K., Structural characterisation of binary magnesium ultraphosphate glasses by vibrational spectroscopy. Physical Chemistry of Glasses, 2001. 42(2): p. 9.

26. Kordes, E., W. Vogel, and R. Feterowsky, Z. Elektrochem, 1953. 57: p. 282.

27. Suzuya, K., et al., The structure of magnesium phosphate glasses. Journal of Physics and Chemistry of Solids, 1999. 60: p. 4.

28. Meyer, K., A. Barz, and D. Stachel, A study of the structure of binary magnesium ultraphosphate glasses by vibrational spectroscopy. Ceramics - Silikaty, 1999. 43(4): p. 6.

29. Khor, S.F., et al., Effects of MgO on dielectric properties and electrical conductivity of ternary zinc magnesium phosphate glasses. Journal of Non-Crystalline Solids, 2009. 355: p. 7.

30. Khor, S.F., et al., Effects of ZnO on Dielectric Properties and Electrical Conductivity of Ternary Zinc Magnesium Phosphate Glasses. American Journal of Applied Sciences, 2009. 6(5): p. 5.

31. Brow, R.K., Review: the structure of simple phosphate glasses. Journal of Non-Crystalline Solids, 2000. 263&264: p. 1-28.

32. Fayon, F., et al., ^{31}P NMR study of magnesium phosphate glasses. Journal of Non-Crystalline Solids, 2001. 283: p. 7.

33. Walter, G., et al., Structural study of magnesium polyphosphate glasses. Journal of Non-Crystalline Solids, 2003. 320: p. 13.

34. Wiench, J.W., et al., Structural studies of zinc polyphosphate glasses by nuclear magnetic resonance. Journal of Non-Crystalline Solids, 2000. 263&264: p. 10.

35. Khor, S.F., et al., Optical properties of ultraphosphate glasses containing mixed divalent zinc and magnesium ions. Optical Materials, 2013. 35: p. 5.

36. Tosic, M.B., et al., Dissolution behavior of a polyphosphate glass into an aqueous solution under static leaching conditions. Journal of Non-Crystalline Solids, 2013. 362: p. 10.

37. Marino, A.E., et al., Durable phosphate glasses with lower transition temperatures. Journal of Non-Crystalline Solids, 2001. 289: p. 5.

38. Karakassides, M.A., A. Saranti, and I. Koutselas, Preparation and structural study of binary phosphate glasses with high calcium and/or magnesium content. Journal of Non-Crystalline Solids, 2004. 347: p. 11.

39. Fanderlik, I., Optical Properties of Glass. Glass Science and Technology. Vol. 5. 1983, New York: Elsevier.

40. Duffy, J.A., The refractivity and optical basicity of glass. Journal of Non-Crystalline Solids, 1986. 86: p. 12.

41. Ray, N.H., Composition-Property Relationships in Inorganic Oxide Glasses. Journal of Non-Crystalline Solids, 1974. 15: p. 12.

42. Ray, N.H., The structure and properties of inorganic polymeric phosphates. British Polymer Journal, 1979. 11(4): p. 14.

43. Metwalli, E. and R.K. Brow, Modifier effects on the properties and structure of aluminophosphate glasses. Journal of Non-Crystalline Solids, 2001. 289: p. 10.

44. Shannon, R.D., Revised effective ionic radii and systematic studies of interatomic distances in halides and chalcogenides. Acta Crystallographica, 1976. A32: p. 7.

45. Weyl, W.A. and E.C. Marboe, The Constitution of Glasses: A Dynamic Interpretation, ed. W.a. Sons. Vol. 1: Fundamentals of the Structure of Inorganic Liquids and Solids. 1962, New York: Interscience Publishers.

46. Sarver, J.F. and F.A. Hummel, Journal of the Electrochemical Society, 1959. 106(11).

47. Katnack, F.L. and F.A. Hummel, Phase Equilibria in the System ZnO-P_2O_5. Journal of the Electrochemical Society, 1958. 105(3): p. 125-133.

48. Sarver, J.F. and F.A. Hummel, Journal of the Electrochemical Society, 1959. 106.

49. Knowles, J.C., Phosphate based glasses for biomedical applications. Journal of Materials Chemistry, 2003. 13: p. 7.

50. Sales, B.C., L.A. Boatner, and J.O. Ramey, Chromatographic studies of the structures of amorphous phosphates: a review. Journal of Non-Crystalline Solids, 2000. 263&264: p. 12.

51. Van Wazer, J.R., Phosphorus and its Compounds Volume I: Chemistry. Vol. 1. 1958, New York: Interscience Publishers, Inc. 954.

52. Takebe, H., Y. Baba, and M. Kuwabara. Compositional dependence of water durability in metaphosphate glasses. in ICG. 2007. Strasbourg, France.

53. Popovic, L., D. de Waal, and J.C.A. Boeyens, Correlation between Raman wavenumbers and P-O bond lengths in crystalline inorganic phosphates. Journal of Raman spectroscopy, 2005. 36: p. 10.

54. Nelson, B.N. and G.J. Exarhos, Vibrational spectroscopy of cation-site interactions in phosphate glasses. Journal of Chemical Physics, 1979. 71(7): p. 9.

4. COMPOSITIONAL DEPENDENCE OF IRRADIATION INDUCED DEFECTS IN ZINC ALUMINOPHOSPHATE GLASSES

Charmayne E. Smith, Richard K. Brow
Missouri University of Science and Technology
Rolla, MO 65409, USA
D. Blane Baker
William Jewell College
Liberty, MO 64068, USA

ABSTRACT

The formation of electronic defects, including phosphorus oxygen hole centers and PO_3^{2-} electron centers, in zinc-aluminophosphate (ZAP) glasses by ultra-violet (UV) (λ = ~260 nm) and x-ray (λ = 0.1548 nm) radiation were studied by optical and electron spin resonance (ESR) spectroscopies. The types and number of defects were found to depend on glass composition. With the addition of alumina, a new defect, the PO_4^{4-} center, is generated with x-ray exposure and glasses with greater alumina contents are generally more susceptible to defect formation with UV exposure. For glasses with greater O/P ratios, x-ray exposure produces fewer PO_4^{4-} defects and more PO_2^{2-} defects.

4.1 INTRODUCTION

Phosphate glasses are used for different optical applications because they can possess useful refractive indices, transmit into the UV spectrum, and be doped with large concentrations of rare earth ions [1-4]. Recently it was shown that the refractive index of zinc phosphate glasses could be spatially modified by a femto-second (fs) laser to produce optical waveguides [4, 5]. A drawback to the use of zinc phosphate glasses is their poor chemical durability, compared to silicate glasses [6]. The addition of alumina to zinc phosphate glasses improves the chemical durability [7] and waveguides have been written into these more durable zinc aluminophosphate glasses [8].

Phosphate anionic structures are built from phosphorus tetrahedra that form chains of varying lengths. The phosphate tetrahedra are connected through covalent bridging oxygen bonds and the oxygen to phosphorus (O/P) ratio sets the average number of tetrahedral linkages in these anions [9]. The properties of zinc phosphate glasses depend on the O/P ratio and can be related to systematic changes in the average phosphate anionic structure [10-13]. Glasses with different O/P ratios that were irradiated with a fs laser had refractive index changes that were related to structural changes and electronic defect formation [4, 14]. The glasses that had lower defect concentrations induced by the f-sec laser were more likely to readily form optical waveguides [4].

Electron spin resonance (ESR) spectroscopy and optical absorption spectroscopy are useful tools to characterize intrinsic and extrinsic defects in glasses and crystals [7, 15-22]. ESR is sensitive to changes in electric fields near unpaired electrons and so can distinguish different electronic defects created by ionizing radiation. Radiation induced

defects, from gamma [12], x-ray [23, 24], UV [14] and laser sources [25], or combinations of sources [26], have been studied for many phosphate glass systems. Some other works have investigated to the effects of x-ray and/or gamma-ray exposure to ultraphosphate and metaphosphate glasses [27], including binary zinc and aluminum phosphate compositions [28]. The types of defects that form are electron centers [EC] and hole centers [HC] associated with ^{31}P nuclei. UV-radiation causes photoreaction processes to occur from excited electrons and typically induces only UV absorbing species [29], whereas x-ray and gamma-rays are known to cause partial rupture of chemical bonds, discoloration, reductions of certain ions and other responses due to their greater energies [26].

In this study, the effects of UV and x-ray radiation of zinc aluminophosphate glasses are investigated as a function of glass composition. Optical spectroscopy and electron spin resonance (ESR) spectroscopy were used to identify and quantify systematic changes in defect types and concentrations. The ultimate goal of this work is to identify compositions most resistant to defect generation that might be most useful for femtosecond laser applications.

4.2 EXPERIMENTAL

Zinc aluminophosphate (ZAP) glasses were prepared by batching appropriate mixtures of $NH_4H_2PO_4$ (ACS, 98.0% - Alfa Aesar), ZnO (reagent grade, ≥99.0% - Sigma Aldrich) and Al_2O_3 (99.5% metals basis – Alfa Aesar). The raw materials were batched to prepare 15-25 grams of glass, thoroughly mixed and calcined in high purity alumina crucibles (AdValue Technology, 99.9%) for 15-18 hours at 500 °C to evolve water and NH_3, before melting between 1000-1300 °C for 1-3 hours, depending on the composition.

Melts were initially quenched on steel plates, then remelted in the same crucible, before being poured into cylindrical steel molds (10 mm in diameter and 2.5 cm). Samples were annealed near their glass transition temperatures (T_g) for two hours. Sample compositions were determined from polished samples using energy dispersive spectroscopy (Helios NanoLab 600 FIB/FESEM). Compositions were determined from at least three areas on three different samples for each composition and the average compositions are reported (Table 1).

Sample discs (thickness = ~1 mm, polished to a 5 micron finish) were irradiated by X-rays from Cu-Kα (λ = 0.1548nm) source for 4 hrs. or by a Xe lamp (λ = ~240-280 nm) for 24-96hrs. Optical spectra were collected from 190-1100 nm from irradiated and un-irradiated samples using a Thermoscientific Genesys 10-S spectrophotometer. Induced absorbance, defined as the difference between spectra from pre- and post-irradiated samples, is used to describe spectra changes.

The refractive indices of these polished samples, before and after exposure, were measured (Metricon Refractometer model 2010/M) at 632.8 nm [uncertainty = ±0.0004].

Electron spin resonance (ESR) measurements were performed on the bulk irradiated samples after they were crushed to powder (mass = ~0.5 grams, particle sizes = 150-300 microns) with a Bruker EMX EPR spectrometer at room temperature at frequencies of ~9.5 GHz. All runs were done at a power of 1.97 mW, with 20 dB attenuation. The spectra are displayed as the observed first derivative curves. The parameters used to identify specific features, explained elsewhere [16, 17, 23], are the hyperfine splitting (A_{iso}), calculated by subtracting the magnetic field of the inflection

point of the low field feature of a doublet from high field feature; and the g-value, which is given by

$$g = \frac{h\nu}{\mu B} \quad (1)$$

where h is Planck's constant (6.682×10^{-34} J·s), ν is the frequency of resonance, μ_B is the Bohr magneton (9.27e-28 $J \cdot G^{-1}$) and B_0 is the magnetic field [Gauss]. The magnetic field used is taken as the averages of the inflection points of high field and low field signatures for each doublet.

4.3 RESULTS

Compositions and refractive indices of the ZAP glasses are shown in Table 1. The un-irradiated glasses were clear and were paramagnetically inactive, but they turned pink after x-ray exposure. UV radiation had no impact on visible color. The color of the x-irradiated samples was unchanged six months after exposure.

The un-irradiated glasses were paramagnetically inactive and, therefore, have no ESR active features. Table 2 provides a summary of the radiation-induced electronic defects that have been identified in phosphate-containing glasses, along with their reported ESR and UV/Vis parameters. These assignments have been explained and depicted elsewhere [21, 23, 26, 27, 30, 31]. These parameters were used to assign the radiation-induced defects discussed below.

4.3.1 UV Exposure. ESR spectra for ZAP_3.06 after 24 hrs. and 96 hrs. of UV exposure are shown in Figure 1. A large, broad feature, over 500 G in width, develops with exposure time and is attributed to overlapping and varying distributions of defects and will be discussed further in the discussion section. Figure 2 shows the ESR spectra

of ZAP glasses with low (~2.5 mol%) alumina contents and different O/P ratios before (black) and after (blue) 24-96 hours of UV radiation. Two main doublets are present in the spectra, one near 3388 G with g-value of ~ 2.002 and A_{iso} ~40 G, and the second has an average g-value of 2.072 and A_{iso} ~ 850 G. These features have been associated with phosphorus oxygen hole centers (POHCs) and electron centers on a PO_3 unit, respectively (Table 2). A small feature near 3700 G can be attributed to oxygen hole centers (OHC). As the O/P ratio increases, the dominant defect becomes the POHC at a magnetic field of 3375 G, seen in Figure 2b. At O/P ratio = 3.56, there is no evidence of the PO_3 feature with a small signature for the POHC, or possibly defects associated with Zn^{2+} [21]. With the loss of the PO_3 feature there is also a loss of the OHC.

The induced optical absorbance for the low-alumina glasses and are shown in Figure 3. The glass with an O/P ratio of 3.44 had the most significant absorption in the lower visible region, near 300 nm which is indicative of POHC formation. No systematic trends with changes in absorption peaks were observed.

The strongest features in the ESR spectra of the UV-irradiated glasses with similar O/P ratios (3.06±0.04) and increasing alumina contents are the doublets associated with PO_3 defects near 2870 G and 3745 G (Figure 4).

The UV/Vis spectra for ZAP_3.06 are shown in Figure 5. The induced absorbance plots for glasses with varying O/P ratios, determined from the optical absorption spectra, are shown in Figure 3. The main absorption occurs in the 200-300 nm region, where bands for PO_3 and POHC are located (Table 2). Assignments can be seen in Table 2. No clear trend emerges for the effects of O/P ratio on the concentration of defects present.

ESR spectra for ZAP glasses with similar O/P ratios (3.06 ±0.04) and increasing alumina contents are shown in Figure 4. These spectra show evidence for mainly PO_3 and POHC defects. An asymmetry in the POHC feature develops that depends on the alumina content (Figure 4b). No additional defects were detected in the glasses with increasing alumina contents. The induced absorbance spectra for the ZAP glasses with similar O/P ratios (3.06±0.04) show an absorption band between 200-300 nm, which increases in intensity with increasing alumina content (Figure 6).

4.3.2 X-Ray Exposure. Figure 7a shows the ESR spectra for low-alumina ZAP glasses with different O/P ratios after 4 hrs. of x-ray irradiation. The features are dominated by the large signature for the POHC defect near 3360 G, at an average g-value of ~2.003 with A_{iso} = 39 G. There is a secondary doublet with two features indicative of the PO_3 defect, with g = ~2.064 and A_{iso} = 868 G. The features seen here are similar to the spectrum reported by Ebeling et al. for a zinc metaphosphate glass after 4 hrs of x-ray exposure [28]. The larger PO_3 feature in this work as compared to the zinc metaphosphate prepared by Ebeling et al. can be attributed to the presence of alumina from crucible contamination.

The types of defects, and the symmetry of the POHC signature (Figure 7b), that form change with O/P ratio. As the O/P ratio increases (Figure 7a), there is a loss of the PO_3 features (2870 G and 3745 G) and the concomitant development of the PO_2 doublet (3318 G and 3445 G). A broad feature develops in the spectra from glasses with higher O/P ratios, similar to the spectra seen at longer times of UV exposure (Figure 2).

The effect of alumina on the inducement of electronic defects by x-rays in the ZAP glasses with similar O/P ratios (3.06±0.04) can be seen in the ESR spectra in Figure

8. The PO_4 doublet (2625 G and 3880 G) becomes more prominent in the spectra from glasses with greater alumina contents (Figure 8a), although there is no change in the symmetry of the POHC feature centered around 3390 G (Figure 8b).

The UV/Vis spectra for the ZAP_3.06 glass, before and after exposure to x-rays for four hours is shown in Figure 9. The induced absorbance spectra for the ZAP glasses with constant alumina (2.5 mol%) and different O/P ratios (Figure 10a) and with similar O/P ratios (3.06±0.04) and different alumina contents (Figure 10b) reveal new absorption bands near 250 nm, 300 nm and between 500-600 nm for all spectra, although there is no systematic trends in the intensities of any peaks.

4.4 DISCUSSION

4.4.1 UV Exposure. UV radiation at wavelengths near 260 nm produces POHCs and PO_3 electronic defects. Ebeling et al. explains that only the most stable, or favorable, defects form under UV irradiation [28]. As the O/P ratio increases, the PO_3 defects become less stable and only the POHC persists (Figure 2). With the addition of ZnO, the O/P ratio increases and nonbridging oxygens (P-O-Zn) replace bridging oxygens (P-O-P) in the glass network. The concentration of P_2O_5 also decreases which would decrease the sites possible for POHC formation which leads to a decrease in the intensity of the POHC signature, relative to the other defects. It is expected that actual POHC concentration will trend directly with changing P_2O_5 concentrations [21]. Peak deconvolution of UV exposed induced absorbance plots (Figure 3) is difficult due to the negative induced absorbance seen at higher O/P values. Negative values similar to those seen in Figure 3 for induced absorbance have been seen in magnesium metaphosphates

glasses after UV exposure and this has been attributed to the reduction of UV-absorbing impurities as a result of the UV exposure [32].

The induced absorption spectra in Figure 6 indicate that the addition of alumina favors an increase in the number of PO_3 and PO_4 defects created by UV exposure. To maintain a constant O/P ratio in this series, when ZnO is replaced by Al_2O_3, there must also be an increase in the P_2O_5 content, which increases the number of phosphate sites that can act as hosts for defects [33].

4.4.2 X-Ray Exposure. The effects of x-ray irradiation on the ESR spectra of glasses with similar Al_2O_3 conetnts and increasing O/P ratio are shown in Figure 7. Figure 8 shows the effects of x-rays on the ESR spectra of glasses with similar O/P ratios and increasing alumina contents. With increasing O/P ratio there is a decrease in the relative intensity of the PO_3 defect (at 2870 G and 3745 G) and the development of PO_2 defects at 3318 G and 3445 G. Griscom describes POHCs as coulomb traps with a hole in between two non-bridging oxygens [23]. That hole can become localized on one of the oxygens to become the PO_2 defect, and Griscom noted that this tendency increase in glasses with greater non-bridging oxygen concentrations, consistent with the spectral trends in Figure 7 [23].

The presence of defects defects associated with zinc or aluminum sites remains questionable. The dominant isotopic nuclei of aluminum and zinc are spin 5/2 and so the hyperfine splitting of these defects would create 5 or 6 peaks [34]. The change in symmetry of the POHC feature, seen in Figure 7b, may be due to the development of an oxygen hole center related to the Zn^{2+} ion. This asymmetry becomes more pronounced with increasing ZnO content.

As alumina is added to the ZAP glass, the ESR spectra begin to resemble the ESR spectrum from x-ray irradiated aluminum metaphosphate reported by Ebeling et al. [28]. The presence of the PO_4 peak at higher alumina contents is confirmed in the induced absorbance deconvolution shown in Figure 11.

4.4.3 Broad Spectral Feature. The broad feature in the ESR spectra of samples after greater UV exposure times and larger O/P ratios, as seen for certain compositions in Figures 1, 2 and 7, is most likely due to overlapping defect sites. A broad OHC singlet has been reported previously in low-alkali borate glasses [15] but this broad feature spanned only ~50-100 G whereas the broad feature shown here [Figure 12] is over 500 G in width. "Broad" ESR peaks have been related to the clustering of electrons on metal ions in glasses [35]. This is supported by the decrease in electronic defect signatures while the POHC feature persists. Electronic neutrality is still maintained in the glass, but is unresolvable due to the lack of well-defined doublets. Spectra with this broad feature, after UV or x-ray exposure, have not previously been seen in the literature on phosphate glasses, to the knowledge of the authors.

4.5 CONCLUSIONS

It was shown that the response of zinc phosphate glass to UV and x-ray radiation is dependent on the composition. UV irradiation causes the formation of PO_3 and POHC defects. As the O/P ratio increases there is a loss of the PO_3 defect. X-ray exposure excited the entire network and induced the development of PO_3 defects and a large concentration of phosphorus oxygen hole centers. As the O/P ratio increases there is a development of the PO_2 defect and a loss of the PO_3 featureAfter x-ray irradiation, at low enough glass former contents, over-lapping defects can be noted due to electron

clustering on metal ions. The refractive index showed an overall increase for glasses after x-ray irradiation, while no significant change resulted after UV exposure.

4.6 ACKNOWLEDGEMENTS

The authors acknowledge the Department of Education for the Graduate Assistance in Areas of National Need (GAANN) fellowship and the National Science Foundation (DMR 1207520) for funding this work. The contributions of Dr. Jen-Hsien Hsu for the EDS compositional analysis are also greatly appreciated.

Tables

Table 1: Compositions analyzed by EDS and calculated O/P ratios of ZAP glasses

Sample ID	Analyzed Values [mol%]			
ZAP_O/P	ZnO (±4%)	Al_2O_3 (±0.6%)	P_2O_5 (±3%)	O/P ratio
ZAP_3.06	48.5	2.1	49.4	3.05
ZAP-2_3.06	38.2	7.1	54.7	3.04
ZAP-3_3.06	33.2	11.1	55.7	3.10
ZAP_3.23	54.6	2.6	42.8	3.23
ZAP_3.44	60.5	2.8	36.7	3.44
ZAP_3.56	63.5	2.7	33.8	3.56

Table 2: ESR constants and optical absorption assignments for radiation induced defects in phosphates

				ESR parameters			Optical Absorption	
Ref	Defect	Type*	Structure	W [G]	Aiso [G]	g-value (error)	Energy (ev)	Λ (nm)
[21, 26, 27]	POHC	HC	Phosphorus-related non-bridging oxygen hole center	10	40 (3)	2.006 (3)	2.30 (2)	540
							2.89 (4)	430
							3.82 (4)	330
[21, 26, 27]	PO_3	EC	Unpaired electron trapped on the two-coordinated P	100	~800 (40)	2.064 (5)	5.90 (6)	210
[21, 27]	PO_4	EC	Electron-trapped centers on the three-coordinated P	90	1230 (30)	2.142 (8)	5.12 (6)	240
[21, 23, 26, 27]	PO_2	EC?/ HC?	Unpaired electron trapped on the two-coordinated P	70	270 (20)	2.006 (3)	4.68 (8)	240-270
[21, 28]	OHC	HC	Oxygen-related hole centers	70	(singlet)	2.004-2.014 (1)	4.28 (6)	290
[21]	Zn^{2+}	HC	Zinc-related oxygen hole centers	15	(singlet)	1.999	4.28	290

*HC = hole center; EC = electron center

Figures

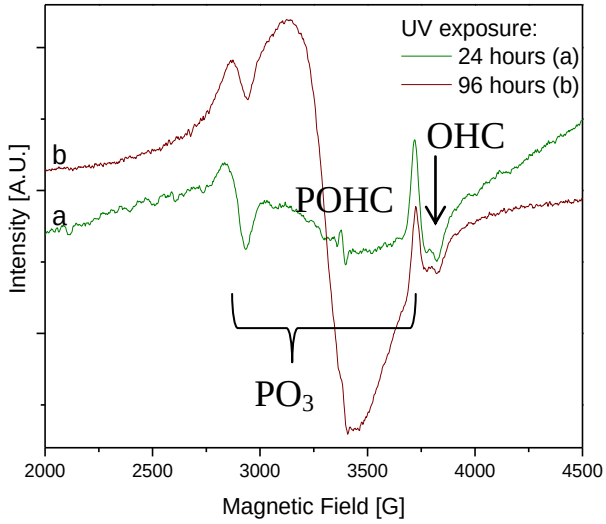

Figure 1: ESR spectra for ZAP_3.06 after UV exposure for 24 hrs. (green) and 96 hrs. (brown).

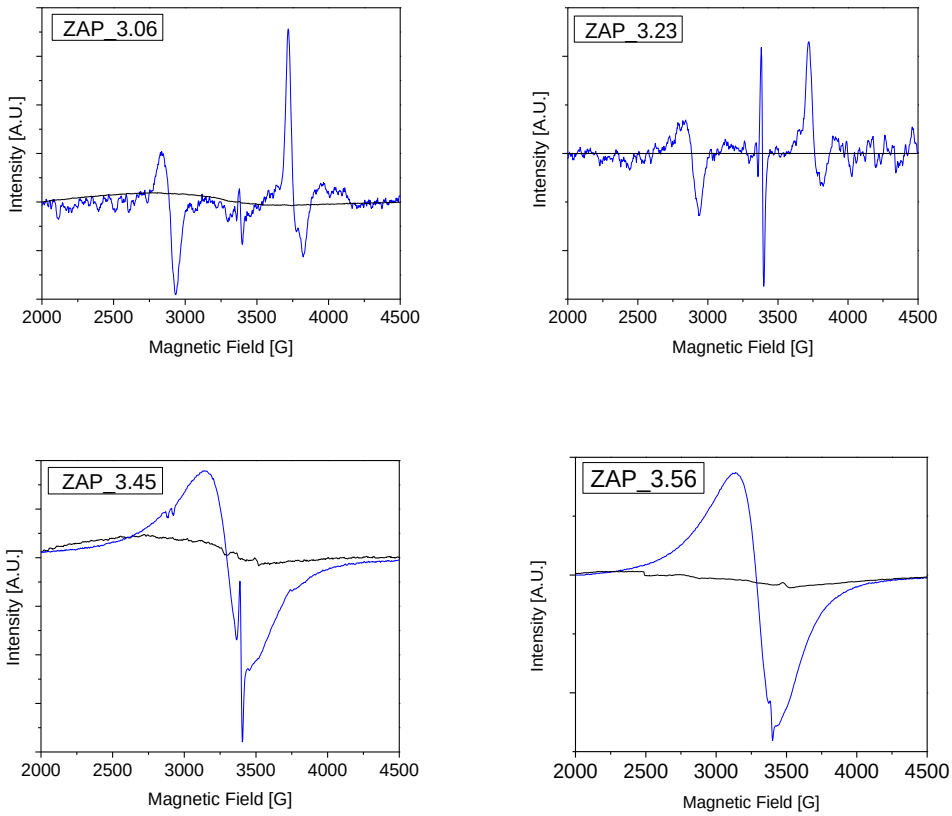

Figure 2: ESR spectra, after UV exposure, for compositions with varying O/P ratios. (2a and 2b after 24 hrs., 2c and 2d after 96 hrs.; Black-pre UV exposure, Blue-post UV exposure)

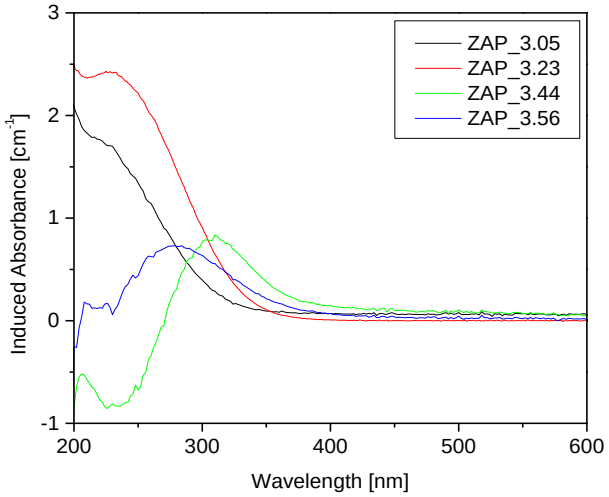

Figure 3: Induced absorbance for ZAP glasses with alumina contents equal to ~ 2.5 mol% and varying O/P ratios

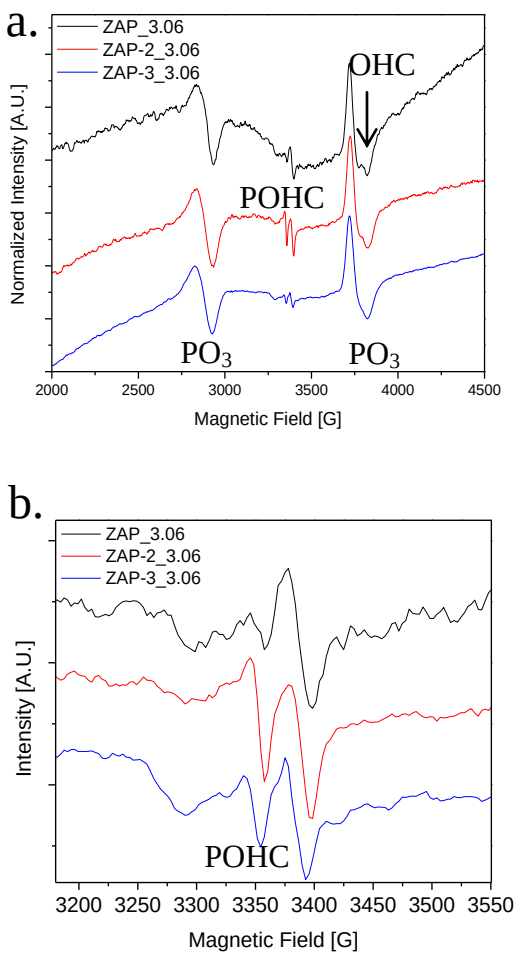

Figure 4: ESR spectra for metaphosphate ZAP glasses with constant O/P ratio (~ 3.06) and increasing alumina contents, after UV exposure for 24 hrs, from a. 2000-4500 G and b. ~3200-3550 G

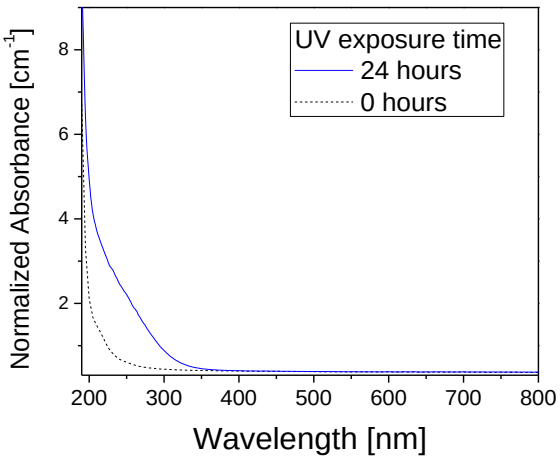

Figure 5: UV/Vis spectra of ZAP_3.06 before [black dash line] and after 24 hr UV exposure [blue solid line]

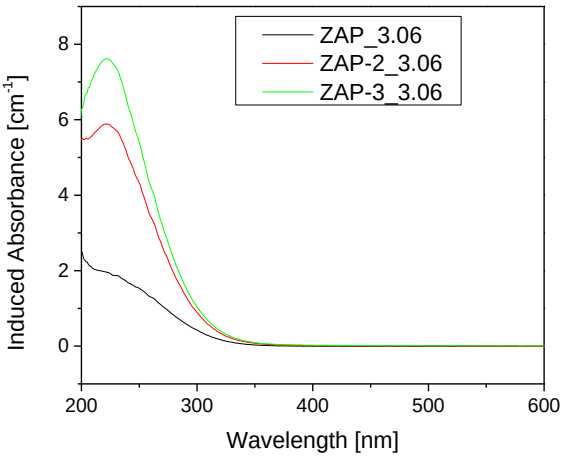

Figure 6: Induced absorbance for metaphosphate ZAP glasses with constant O/P ratio (~ 3.06) and increasing alumina contents

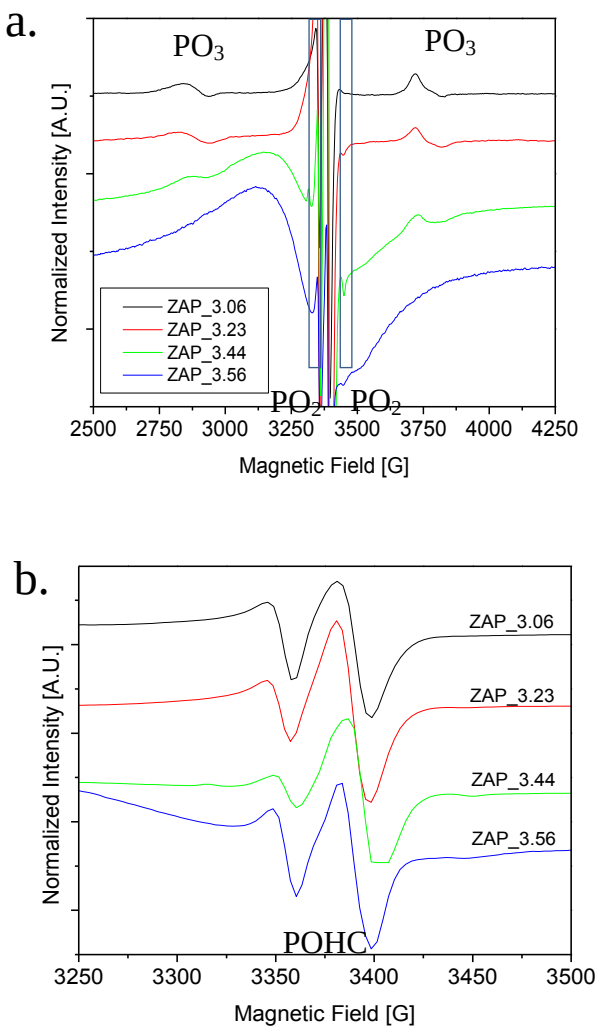

Figure 7: ESR spectra of ZAP glasses with ~2.5 mol% Al_2O_3 with varying O/P ratios from 3.03 to 3.56 plotted from a. 2500-4250 G and b. 3250-3500 G.

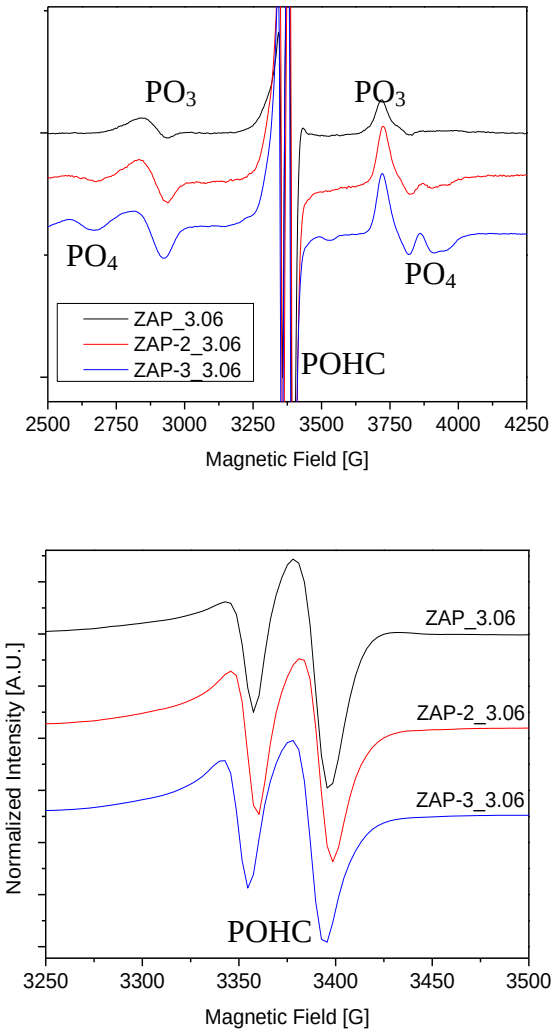

Figure 8: ESR spectra of ZAP glasses with an average O/P ratio of 3.06 (+/- 0.03) with increasing alumina content plotted from a. 2500-4250 G and b. 3250-3500 G.

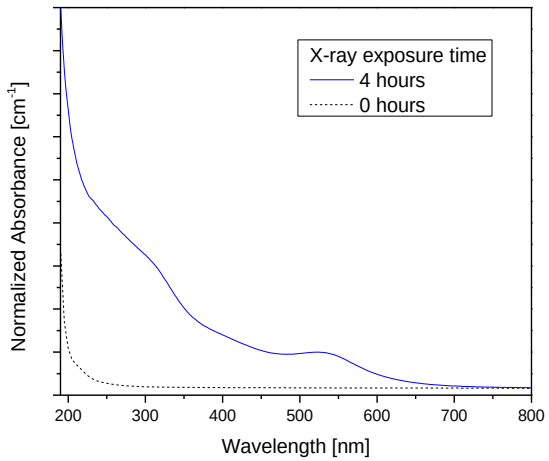

Figure 9: UV/Vis spectra of ZAP_3.06 before [black-dash line] and after 4 hrs x-ray exposure[blue solid line].

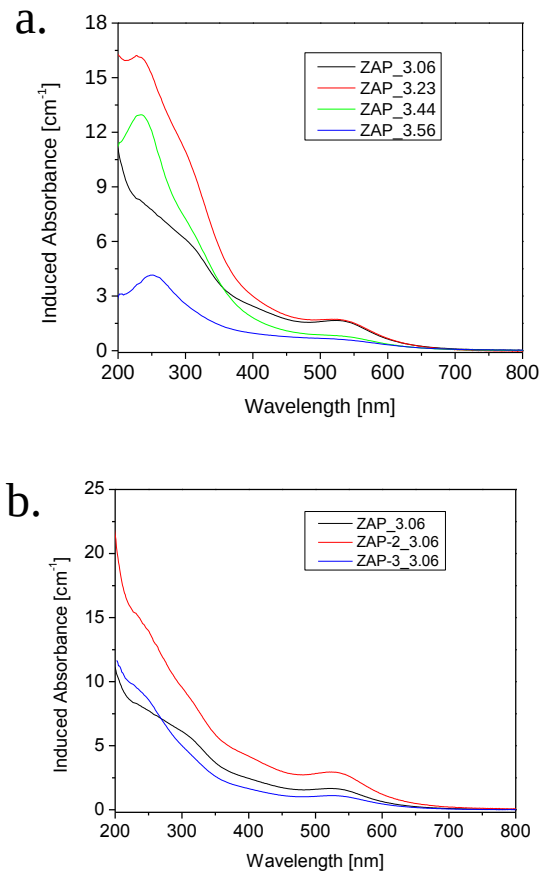

Figure 10: Induced absorbance for ZAP glasses, after x-ray exposure, with a. varying O/P ratios and constant alumina contents (~2.5 mol%) and b. constant O/P ratios with increasing alumina.

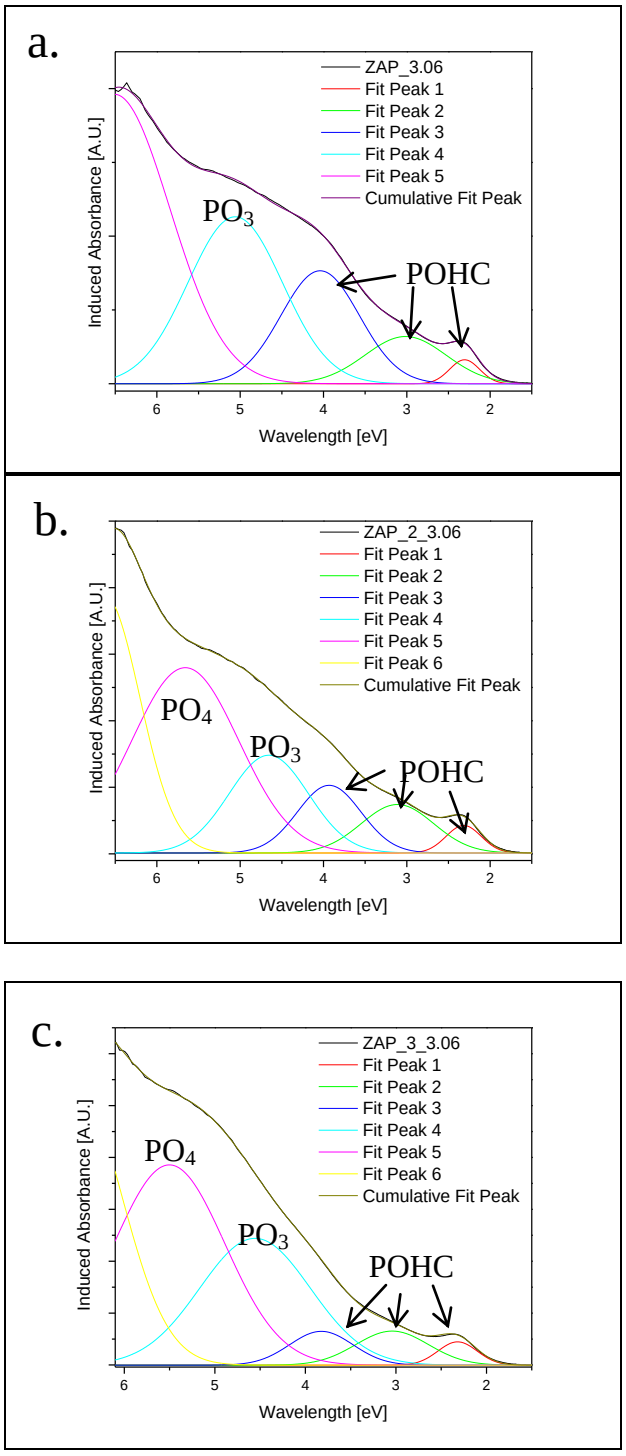

Figure 11: Deconvolution of induced absorbance spectra for a. ZAP_ 3.06, b. ZAP_2_3.06, and c. ZAP_3_3.06 glasses

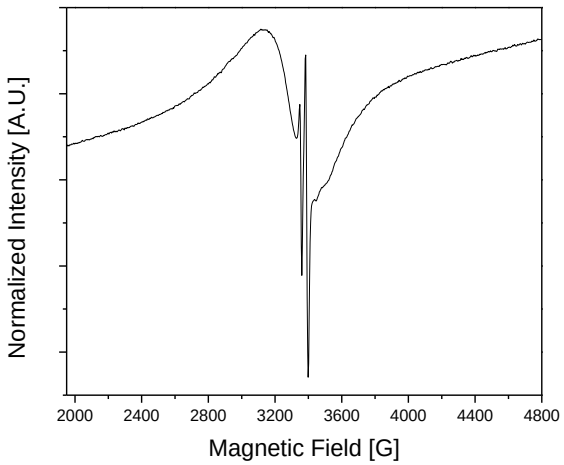

Figure 12: ESR spectrum of ZAP_3.56 after x-ray exposure

REFERENCES

1. Eriah, A. and S.G. Bhat, *Optical properties of samarium doped zinc-phosphate glasses.* Journal of Physics and Chemistry of Solids, 2007. 68: p. 5.

2. Khor, S.F., et al., *Optical properties of ultraphosphate glasses containing mixed divalent zinc and magnesium ions.* Optical Materials, 2013. 35: p. 5.

3. Khor, S.F., Z.A. Talib, and W.M. Mat Yunus, *Optical properties of ternary zinc magnesium phosphate glasses.* Ceramics International, 2012. 38: p. 6.

4. Fletcher, L.B., et al., *Direct femtosecond laser waveguide writing inside zinc phosphate glass.* Optics Express, 2011. 19: p. 7929-7936.

5. Fletcher, L.B., et al., *Femtosecond laser writing of waveguides in zinc phosphate glasses.* Optical Materials Express, 2011. 1: p. 845-855.

6. Ebeling, P. and D. Ehrt, *Influence of modifier cations on the radiation-induced effects of metaphosphate glasses.* Glass Science and Technology, 2003. 2: p. 6.

7. Smith, C.E., et al., *The structure and properties of zinc aluminophosphate glasses.* Journal of Non-Crystalline Solids, 2014.

8. Troy, N., *Materials and Techniques for the Femtosecond Laser Fabrication of Optical Devices in Glass*, in *Applied Science*2012, University of California, Davis: Davis. p. 67.

9. Griscom, D.L., et al., *Fundamental defect centers in glass: Electron spin resonance and optical absorption studies of irradiated phosphorus-doped silica glass and optical fibers.* Journal of Applied Physics, 1983. 54(7): p. 21.

10. Brow, R.K., et al., *The short-range structure of zinc polyphosphate glass.* Journal of Non-Crystalline Solids, 1995. 191: p. 45-55.

11. Sales, B.C., et al., *Structure of zinc polyphosphate glasses.* Journal of Non-Crystalline Solids, 1998. 226: p. 287-293.

12. Suzuya, K., et al., *The structure of binary zinc phosphate glasses.* Journal of Non-Crystalline Solids, 2004. 345&346: p. 80-87.

13. Walter, G., et al., *The structure of zinc polyphosphate glass studied by diffraction methods and ^{31}P NMR.* Journal of Non-Crystalline Solids, 2004. 333: p. 11.

14. Dekker, P., et al., *Annealing dynamics of waveguide Bragg gratings: evidence of femtosecond laser induced colour centres.* Optics Express, 2010. 18(4): p. 10.

15. Bishay, A., *Radiation induced color centers in multicomponent glasses.* Journal of Non-Crystalline Solids, 1970. 3: p. 61.

16. Griscom, D.L., *Electron Spin Resonance in Glasses.* Journal of Non-Crystalline Solids, 1980. 40: p. 62.

17. Griscom, D.L., *Defects in Amorphous Insulators.* Journal of Non-Crystalline Solids, 1978. 31: p. 26.

18. Nuttall, R.H.D. and J.A. Weil, *Double-hole Aluminum Center in alpha-Quartz.* Solid State Communications, 1976. 19: p. 2.

19. Pan, Y., et al., *Single-crystal EPR study of three radiation-induced defects (Al-O_2^{3-}, Ti^{3+} and W^{5+}) in stishovite.* Phys Chem Minerals, 2012. 39: p. 11.

20. Kripal, R., et al., *Electron paramagnetic resonance and optical study of VO^{2+}-doped zinc ammonium phosphate hexahydrate single crystals.* Physica Scripta, 2012. 86: p. 9.

21. Moncke, D., et al., *Irradiation-induced defects in ionic sulfophosphate glasses.* Journal of Non-Crystalline Solids, 2013.

22. Moncke, D. and D. Ehrt, *Irradiation induced defects in glasses resulting in the photoionization of polyvalent dopants.* Optical Materials, 2004. 25: p. 13.

23. Griscom, D.L., et al., *Fundamental defect centers in glass: Electron spin resonance and optical absorption studies of irradiated phosphorus doped silica glass and optical fibers.* Journal of Applied Physics, 1983. 54: p. 21.

24. Origlio, G., et al., *Spectroscopic studies of the origin of radiation-induced degradation in phosphorus-doped optical fibers and preforms.* Journal of Applied Physics, 2010. 108: p. 7.

25. Natura, U., T. Feurer, and D. Ehrt, *Kinetics of UV laser radiation defects in high performance glasses.* Nuclear Instruments and Methods in Physics Research B, 2000. 166-167: p. 6.

26. Ehrt, D., P. Ebeling, and U. Natura, *UV Transmission and radiation-induced defects in phosphate and fluoride-phosphate glasses.* Journal of Non-Crystalline Solids, 2000. 263&264: p. 11.

27. Ebeling, P., D. Ehrt, and M. Friedrich, *X-ray induced effects in phosphate glasses.* Optical Materials, 2002. 20: p. 11.

28. Ebeling, P., D. Ehrt, and M. Friedrich, *Influence of modifier cations on the radiation-induced effects of metaphosphate glasses.* Glass Science and Tehnology, 2003. 76(2): p. 6.

29. Moncke, D. and D. Ehrt, *Photoionization of polyvalent ions*, in *Materials Science Research Horizons*, H.P. Glick, Editor 2007, Nova Science Publishers, Inc. p. 56.

30. Ehrt, D., *Radiation effects in glasses.* Nuclear instruments & methods in physics research. SectionB, Beam interactions with materials and atoms, 1992. 65(1-4): p. 9.

31. Warren, W.L., et al., *Electron and Hole Trapping in Doped Oxides.* IEEE Transactions on Nuclear Science, 1995. 42(6): p. 9.

32. Takebe, H., Y. Baba, and M. Kuwabara, *Dissolution behavior of ZnO-P_2O_5 glasses in water.* Journal of Non-Crystalline Solids, 2006. 352: p. 3088-3094.

33. Weeks, R.A. and P.J. Bray, *Electron Spin Resonance Spectra of Gamma-Ray-Irradiated Phosphate Glasses and Compounds: Oxygen Vacancies.* Journal of Chemical Physics, 1968. 48(1): p. 9.

34. Kittel, C., *Introduction to Solid State Physics*. 7 ed1995: Wiley.

35. Griscom, D.L., *ESR and optical studies of alkali-associated trapped-electron centers in alkali borate glasses irradiated at 77 K.* Journal of Non-Crystalline Solids, 1971. 6: p. 8.

SECTION

3. AFTERWORD

This section summarizes the conclusions found from this PhD research. Following the summary will be a description of problems related to this dissertation that were not solved and suggestions for future work.

Studies were conducted to understand the effects of systematic changes in glass compositions on the structure and properties of glasses in ternary zinc phosphate systems. Previous studies, show that maintaining a constant oxygen to phosphorus (O/P) ratio (3.25), allows for the development of embedded waveguides through femto-second laser irradiation [1-3]. Thus, for the structure and property investigations in zinc phosphate systems, the focus is to conducte systematic studies as a function of the addition of a third metal oxide (Al_2O_3, MgO, or CaO) while maintaining a constant O/P ratio. Irradiation studies were also conducted on binary glasses with varying zinc phosphate compositions as well as ternary zinc aluminophosphate compositions.

1. The ternary zinc aluminophosphate system was studied extensively, and the first comprehensive investigation of structure and properties was completed. It was confirmed that the addition of Al_2O_3 will increase the resistance to dissolution in water of zinc phosphate glasses. The 3-4 orders of magnitude decreases in dissolution rates, with increasing alumina contents, were also accompanied by >300 ˚C increases in glass transition temperatures and with an increase in density of ~15%. The addition of alumina to zinc phosphate glasses results in shorter P-O-Me bonds, as determined by Raman spectroscopy, and processing temperatures were found to increase for greater Al_2O_3 concentrations. A structural model,

previously only applied to binary systems, was used to relate aluminum coordination numbers (CN) to systematic changes in composition. The aluminum CN was found to be dependent on the number of terminal oxygens available and the model was in good agreement with measured CN data obtained from ^{27}Al nuclear magnetic resonance (NMR) spectroscopy.

2. The first phase stability diagram for the zinc aluminophosphate system, was reported. There were no new binary compounds identified, nor were any ternary compounds discovered. The equilibrium study was connected to glass forming tendencies in the system. The limit of glass formation in the aluminophosphate binary was found to correspond to the eutectic point between aluminum metaphosphate and aluminum orthophosphate. Near the glass-forming limit in the zinc phosphate system, phase separation and crystallization was found for the composition that forms zinc pyrophosphate. This shows a driving force for crystallization which indicates that faster quenching rates are needed, as compared to surrounding compositions, in order for glass formation to occur.
3. The property trends in the zinc magnesium phosphate system were explored while keeping a constant P_2O_5 concentration and substituting ZnO for MgO. It was found that the addition of MgO to the glass resulted in a >100˚C increase in the glass transition temperature and dilatometric softening temperature for both O/P ratios investigated. The changes in thermal properties were not accompanied by significant structural organization, as evidenced by minimal changes in the molar volume and Raman spectroscopy measurements. The changes in properties due to increasing MgO contents, such as the large decrease in refractive index, were

attributed to the dissimilar electron configurations of Mg^{2+} (noble-gas ion) and Zn^{2+} (transition metal ion with d-electrons). The lower polarizability of the non-bridging oxygens associated with the magnesium ions resulted in less reactive sites for attack by water molecules, as shown with the decreasing dissolution rates with increasing magnesium content. This argument is another approach for the explanation of property changes for instances where the typical field strength argument is not applicable due to similarities in size and charge, as seen in this work.

4. Zinc aluminophosphate glasses were exposed to ultraviolet (UV) and x-ray radiation and characterized by electron spin resonance and ultraviolet/visible spectroscopy. UV exposure resulted in the formation of defects mainly active in the UV region of the electromagnetic spectrum, whereas x-ray exposure produced defects that absorbed in the visible and UV regions. The phosphorus-oxygen hole center (POHC) defect was shown to be present in all samples exposed to x-rays, and most samples that were exposed to UV light, although to a lesser degree. It is noted that x-rays tend to excite the entire structure, producing all defects that are most likely to occur and the larger concentration of POHCs as compared to UV exposure. This shows that with higher intensities of irradiation, POHC formation is favored. There was no relation found between the study of electronic defect trends that occurred due to changes in compositions and the compositional effects seen by fs laser irradiation in previous studies.

Although many contributions to phosphate-based studies were completed during the course of this work, there are more studies that should be completed in the future.

1. The addition of alumina was shown to improve dissolution rates but many structural changes occurred. Phosphate glasses are of interest for many reasons as optical materials, one of which is the high solubility for rare-earth (RE) doping as compared to silica or silicate glasses. Work should be done to explore the effects of alumina content on the solubility of rare-earths ions, such as erbium and ytterbium, which are frequently used in laser glasses and optically active materials. Pure silica glass experiences rare-earth clustering in its structure when doped with the large ions (~1 Å), which is why doping is typically limited to concentrations of ~ 100 ppm [4]. It has been noted that additions of alumina to the silicate network allow for easier, and more homogeneous, introduction of larger concentrations of RE ions [5, 6]. Multi-component phosphate glasses are known for open, chain-like structures that are more accommodating for higher RE contents before devitrification (> $3x10^5$ ppm) [4]. The additions of alumina to phosphate glasses may increase the RE solubility, as seen in silicate glasses. It was noted, in this work, that the addition of alumina increases molar volume and decreases density. This relates to a more open structure which should be able to accommodate more RE ions.

2. The work initiated on the glasses in the zinc calcium phosphate (ZCP) system should be completed. There is currently no systematic study of the structure, properties and dissolution behavior of glasses in this system. These glasses are of interest as bioglasses that allow the formation of hydroxyapatite [7] and are possibly another option for optical materials that allow for embedded waveguide formation while having a higher resistance to aqueous attack, as compared to binary zinc phosphate glasses.

3. Work should be done on aluminum metaphosphate glasses for fs laser exposure. The notion that the zinc phosphate system would allow for the development of viable waveguides under fs laser writing was thanks to structural similarities with vitreous silica [8]. Both have tetrahedrally connected structures and, it has been shown that certain zinc phosphates would allow the formation of wave-guiding structures. It has been shown that crystalline aluminum metaphosphate has a structure of AlO_6 polyhedra and phosphate tetrahedra connected in chains similar to the rings that form the pure silica network [9]. As a result of the comparable structural organization, it is of interest to determine if an O/P = 3.0 glass can produce a similar response as silica and as zinc phosphates with an O/P ratio = 3.25.

APPENDIX A

EFFECTS OF THE DIRECT SUBSTITUTION OF CAO FOR ZNO IN ZINC PHOSPHATE GLASSES

Charmayne E. Smith, Ryan P. Jones, Richard K. Brow
Missouri University of Science and Technology
Rolla, MO 65409

Introduction

Phosphate glasses are of interest for many reasons including their high solubility for rare-earth doping, low processing temperatures and low glass transition temperatures (T_g). Recently it has been found that certain compositions of the zinc phosphate system show promise as bulk substrates for femtosecond (fs) laser processing used for the formation of wave guiding structures [10, 11].

Although zinc phosphate glasses are useful due to their large glass forming regions and favorable response to fs laser writing, they lack chemical durability, which may hinder their usage. It has been shown that the addition of a third oxide, such as Al_2O_3 and Nb_2O_5, to the binary zinc phosphate system may lead to a decrease in the aqueous dissolution rates, which indicates an improvement in the chemical durability.

Phosphate anionic structures can be described using the Q^n-terminology, where 'n' represents the number of bridging oxygens on a phosphate tetrahedron [12]. For example, changes in the types of phosphate tetrahedra with the addition of ZnO can be represented by the reaction:

$$2Q^n + ZnO \rightarrow 2Q^{n-1}$$

Here, the oxygen ions accompanying the ZnO added to phosphate glasses replace bridging oxygens (P-O-P) with nonbridging oxygens (P-O-Zn) on the phosphate tetrahedra. This reaction holds true for any divalent oxide added to the phosphate network. Through use of the oxygen to phosphorus (O/P) ratio, the number of phosphate

tetrahedra per chain is fixed by the composition. Many studies have been conducted to investigation how the structures and properties change with varying O/P ratios.

Matsubara et al. found that the zinc coordination for compositions near the metaphosphate (O/P = 3.0) regime is approximately 4 while calcium has a higher coordination of about 5 [13]. There has been some work in the ternary zinc calcium phosphate system due to interest in the biocompatibility of calcium phosphate glasses which have been shown to have the ability of crystallizing to form hydroxyapatite [7].

This paper investigates the effects of CaO addition on the zinc phosphate system, while maintaining constant average chain lengths in the phosphate network. To the authors' knowledge there has been no work completed, to date, on the glass forming diagram and the systematic investigation of the effects of direct substitution of CaO for ZnO on glass properties in the ZnO-CaO-P_2O_5 system.

Experimental Procedure

Zinc calcium phosphate (ZCP) glasses were prepared by batching appropriate mixtures of $NH_4H_2PO_4$ (ACS, 98.0% - Alfa Aesar), ZnO (reagent grade, ≥ 99.0% - Sigma Aldrich), and $CaCO_3$ (Alfa Aesar, 98%) to produce 15-25 grams of glass. The batches were thoroughly mixed, calcined in high purity alumina crucibles (AdValue Technology, 99.9%) for 15-18 hours at 500 °C to evolve water and NH_3, then melted at temperatures between 1000-1300 °C for 1-3 hours, depending on the composition. Melts were quenched by pouring into cylindrical steel molds (10 mm in diameter and 25 mm tall) when possible, or by quenching between two copper plates. Samples were annealed near their glass transition temperatures (T_g) for two hours.

Annealed samples, 10 mm in diameter and ~1 mm thick, were polished to a 1200 grit (~5 μm) finish for optical measurements. Refractive index at 632.8 nm was measured using a prism coupler (Metricon model 2010/M); the uncertainty of these measurements is ±0.0004.

The density of annealed glass samples was measured by Archimedes' method using distilled water as the immersion liquid (error = ±0.009 g/cm^3). Three samples of each glass were measured and the standard deviation was recorded. The molar volume was calculated by dividing the density of each glass by the molecular mass which was calculated from the analyzed glass compositions of polished samples, as determined by a Helios NanoLab 600 FIB/FESEM equipped with an energy dispersive spectrometer (EDS). Three different pieces of three, or more, samples were analyzed in a similar manner, and from these analyses, the overall estimated relative uncertainty of the reported compositions is ±2.5 %. All glasses that were measured with EDS had ≤ 3.2 mol% Al_2O_3 contamination in the composition.

Glass transition temperatures (T_g) were determined by differential thermal analysis (DTA, Perkin-Elmer DTA-7) by heating 35-45 mg of glass powders (< 75 μm) at 10 °C/min in high purity, open alumina crucibles under nitrogen flow. The onset method was used to determine T_g and the estimated uncertainty is ±5 °C.

Weight loss measurements were made on bulk glasses to determine relative aqueous durability in deionized (DI) water at room temperature (~20 ˚C) for up to 170 hours. Polished samples (~5 μm) were rinsed with acetone and dried before testing. A constant sample surface area (SA) to solution volume ratio of 0.035 cm^{-1} was used for each experiment. Samples were removed from the water periodically, dried and weighed,

and then returned to the solution. Three samples were tested for each condition and the dissolution rates, determined by the average weight loss, are reported.

Results and Discussion

Glass Forming Region

A ternary diagram of the ZCP glasses attempted thus far is shown in Figure 1. The compositions and properties measured for these glasses can be seen in Table 1. The glass forming limits of the ZnO-P_2O_5 (~71 mol% ZnO) and CaO-P_2O_5 (~60 mol% CaO) binaries are in agreement with the literature [14, 15]. It was shown that if roller quenching techniques were used to increase the glass forming limit, then ZnO concentrations could reach up to ~80 mol% in the binary system before glass formation was not possible, excluding phase separation at ~ 75 mol% ZnO [16]. As CaO is added, the non-glass forming region increases. This may be due to the numerous CaO crystalline compounds that form in the calcium phosphate binary. The driving force for crystallization is increased and larger melting temperatures, or faster quenching rates, may be required to increase the glass forming limit of the CaO-P_2O_5 binary than those used in the current body of work. The increased tendency of forming crystalline compounds can be noted in the free energy of formation for the orthophosphates of each of the binary systems. Ca has a heat of formation of 55 kJ/mol, while zinc is 27 kJ/mol [17, 18] which is relatable to the easier glass formation tendency of zinc phosphates over calcium phosphates. The lower the value of free energy indicates a smaller free energy of formation which suggests that the composition will more easily form a glass.

Glass Properties

To understand the effects of CaO on the properties of zinc phosphate glasses with constant O/P ratio, the ZnO was replaced by CaO and data for the metaphosphate glass compositions will be discussed in this work. All properties measured to date can be found in Table 1.

It was found that as CaO replaced ZnO in the composition, there was a decrease in dissolution rates by ~ 5 orders of magnitude Figure 2. This is a large decrease and may have to do with the ions electronic configurations.

The density and molar volume of glasses with O/P ratio of 3.0 are shown in Figure 3. As CaO is added there is a decrease in both the density and the molar volume. This is interesting as they are typically inversely related. Calcium has a smaller mass than zinc which explains the decrease in density with the addition of CaO. Although zinc is larger in mass, it has a smaller coordination number. Higher packing densities are attributed to greater coordination numbers so the molar volume decreases with increasing CaO content due to calcium having a higher coordination number.

The glass transition temperatures (Figure 4) and the refractive indices (Figure 5) both increase with increasing CaO content. Zinc has a greater electronegativity than calcium; therefore calcium will have a lower affinity for the bonding electrons. The lower electron affinity of calcium means the electrons are more available to interact with light which produces an increase in refractive index. This is also evidenced by the higher ionic refractivity of Ca^{2+} (1.2) as compared to Zn^{2+} (0.7) [19].

Conclusions

The glass forming diagram was introduced and systematic changes in properties with the direct substitution of CaO for ZnO was discussed. With the addition of CaO there was a decrease in the glass forming region which can be connected with the respective heats of formation for CaO and ZnO. The dissolution rates decreased by ~ 5 orders of magnitude as the compositions changed from zinc phosphates to calcium phosphates. There was a density and molar volume decrease, the former controlled by the relative ionic masses while the latter is most likely determined by the coordination numbers of the ions. The glass transition temperature and the refractive indices both increased with increasing CaO content, which can be attributed to differences in electron configuration, but was not discussed in the current work.

Acknowledgements

The authors acknowledge the Department of Education for the Graduate Assistance in Areas of National Need (GAANN) fellowship and the National Science Foundation (DMR 1207520) for funding this work. The contributions of Dr. Jen Hsien Hsu for the compositional analysis by EDS of the ZCP glasses are greatly appreciated.

Tables

Table 1: Compositions and properties of prepared zinc calcium phosphate glasses

mol% ZnO	mol% CaO	mol% P_2O_5	O/P	Density (g/cm^3)	Molar Volume (cm^3/mol)	Tg (°C)	Refractive index
49.5	0.0	50.5	3.05	2.899	38.88	450	1.5268
25.1	25.4	49.5	3.01	2.795	37.54	473	1.5441
0.0	48.9	51.1	2.98	2.656	37.64	545	1.5483
56.6	0.0	43.4	3.23	3.032	35.51	438	nm
23.7	33.0	43.3	3.15	3.066	32.38	nm	nm
21.0	36.9	42.1	3.19	3.016	32.33	nm	nm
17.3	45.1	37.7	3.33	3.019	30.73	nm	nm
62.6	0.0	37.4	3.44	3.321	31.33	441	1.5729
36.5	28.9	34.6	3.44	3.236	29.37	514	1.606
68.0	0.0	32.0	3.56	3.552	28.37	453	1.6115
66.4	0.0	33.6	3.63	3.418	29.77	nm	nm
61.4	8.8	29.8	3.68	3.651	26.62	464	1.631
50.7	18.5	30.8	3.62	3.459	27.58	nm	nm
23.8	46.2	30.1	3.66	3.181	27.63	nm	1.615

Figures

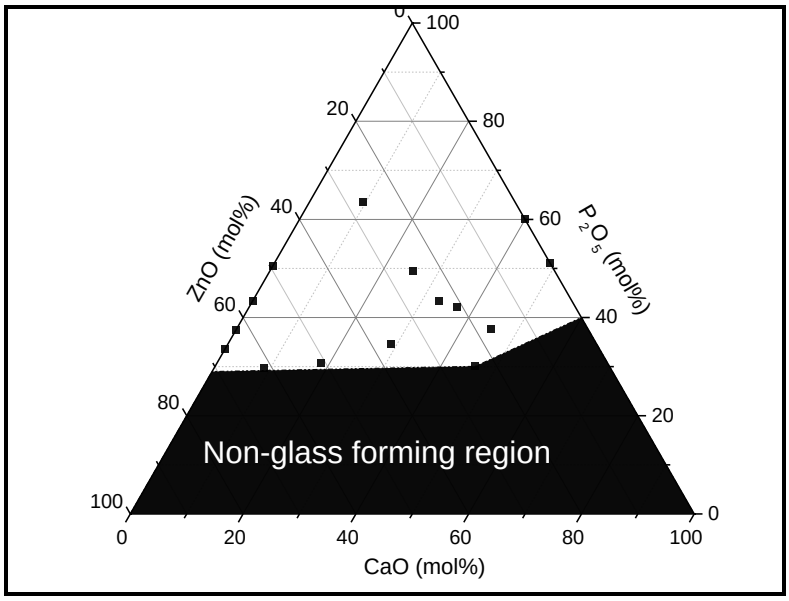

Figure 1: Measured glass forming diagram for the ZCP glass system.

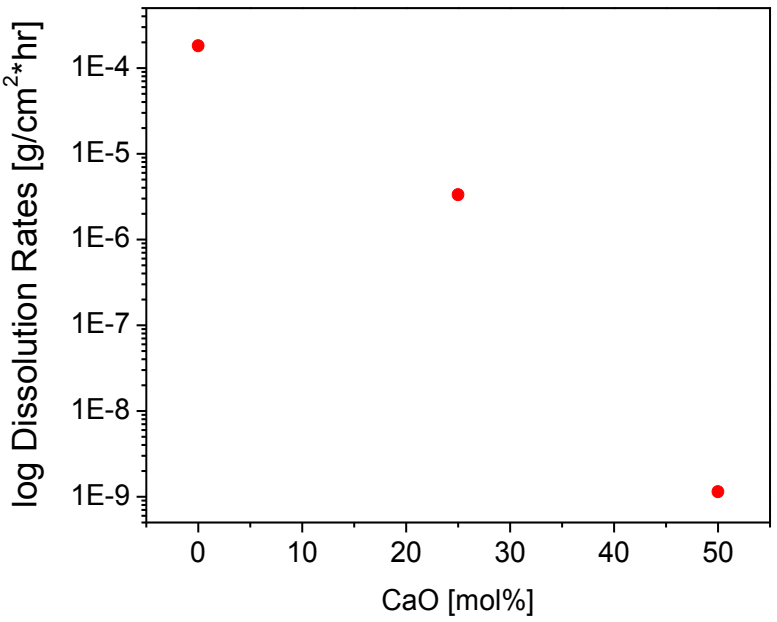

Figure 2: Log dissolution rates for ZCP metaphosphate glasses immersed in water at room temperature

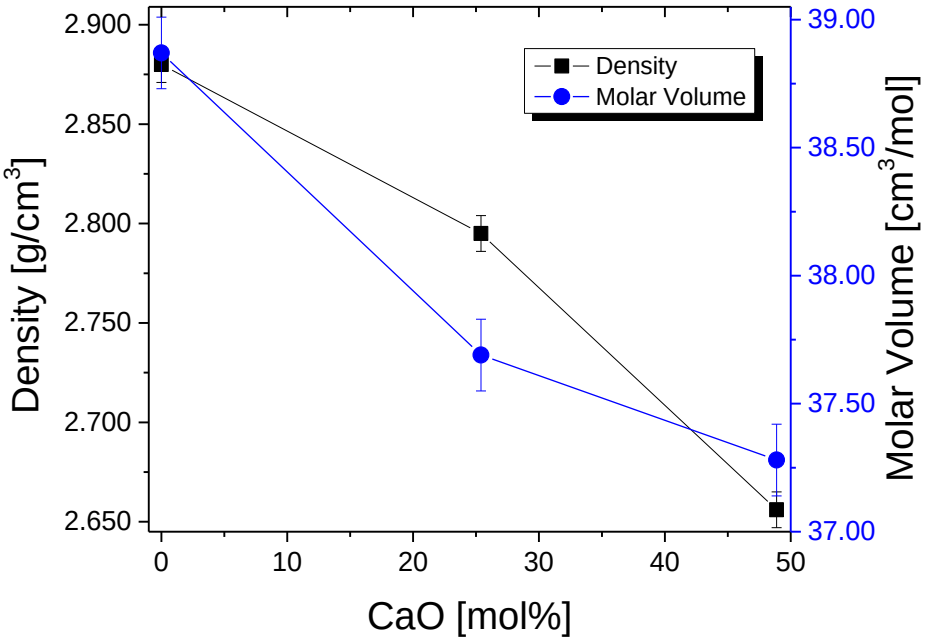

Figure 3: Density (black squares) and molar volume (blue circles) for varying CaO concentrations of metaphosphate glasses.

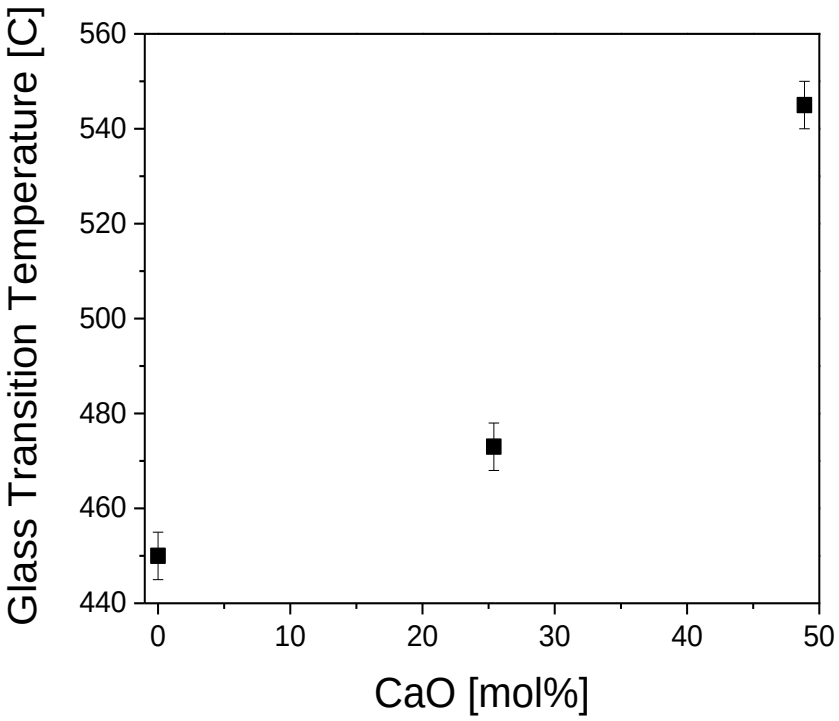

Figure 4: Glass transition temperatures for ZCP metaphosphate glasses

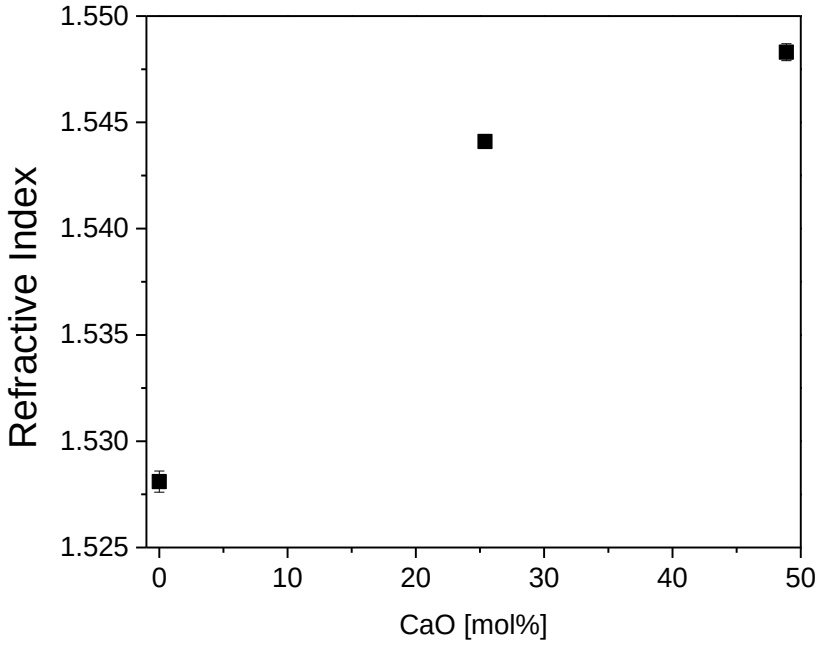

Figure 5: Refractive indices for ZCP metaphosphate glasses

APPENDIX B

EFFEECTS OF THERMAL HISTORY ON DENSITY AND REFRACTIVE INDEX OF A ZINC PHOSPHATE GLASS

Introduction

The femtosecond (fs) laser responses of the zinc phosphate glass with an oxygen to phosphorus (O/P) ratio of 3.25 are similar to the responses to pure silica glass. Irradiation under certain conditions will result in the densification of the focal volume and, as a result, produces a wave-guiding structure with a refractive index higher than that in the bulk.

The reasons behind this response are unknown in the silica glass. One speculation is that the increase in the refractive index, and density, with increasing fictive temperature, results in a densified volume as a result of laser irradiation [20]. The effects of thermal history on density and refractive index for the O/P ratio = 3.25 zinc phosphate glass were investigated.

Experimental Procedure

The zinc phosphate glass was prepared by batching appropriate mixtures of $NH_4H_2PO_4$ (ACS, 98.0% - Alfa Aesar), ZnO (reagent grade, ≥ 99.0% - Sigma Aldrich), and $CaCO_3$ (Alfa Aesar, 98%) to produce 15-25 grams of glass. The batch was thoroughly mixed, calcined in a high purity alumina crucible (AdValue Technology, 99.9%) for 15-18 hours at 500 °C to evolve water and NH_3, and then melted at ~1050 °C for ~2 hours. The melt was quenched by pouring into a cylindrical steel mold (10 mm in diameter and 25 mm tall). The glass was annealed at 500 °C for two hours.

Once annealed, the sample was cut into discs and polished to a 1200 grit (~5 μm) finish for optical measurements and heat treatments. Three polished pieces were used for

each temperature of interest (375 °C, 455 °C and 480 °C) and three polished pieces were left untreated (representing 500 °C due to annealing).

Refractive index at 632.8 nm was measured using a prism coupler (Metricon model 2010/M); the uncertainty of these measurements is ±0.0004.

The density of annealed glass samples was measured by Archimedes' method using distilled water as the immersion liquid (error = ±0.009 g/cm^3). Three glass samples were measured for each temperature and the standard deviation was recorded.

Results and Discussion

The density and refractive index both decrease with increasing fictive temperature, as can be seen in Figure 1a and Figure 1b, respectively. If the thermal history behavior resembled that of pure silica then the refractive indices and density values would increase with increasing fictive temperature. This shows that the thermal history may not have an impact on the formation of viable waveguides, as no conclusions can be drawn from the comparison of the trends seen with silica versus the zinc phosphate glass with an O/P ratio = 3.25.

Conclusions

Further work should be done to understand what characteristics and properties of the glasses will impact the formation of viable waveguides. This work showed that the thermal history may not be indicative of the tendencies for densification under femtosecond laser irradiation, as the trend is contrary to what would be expected, when comparing to the behavior of pure silica.

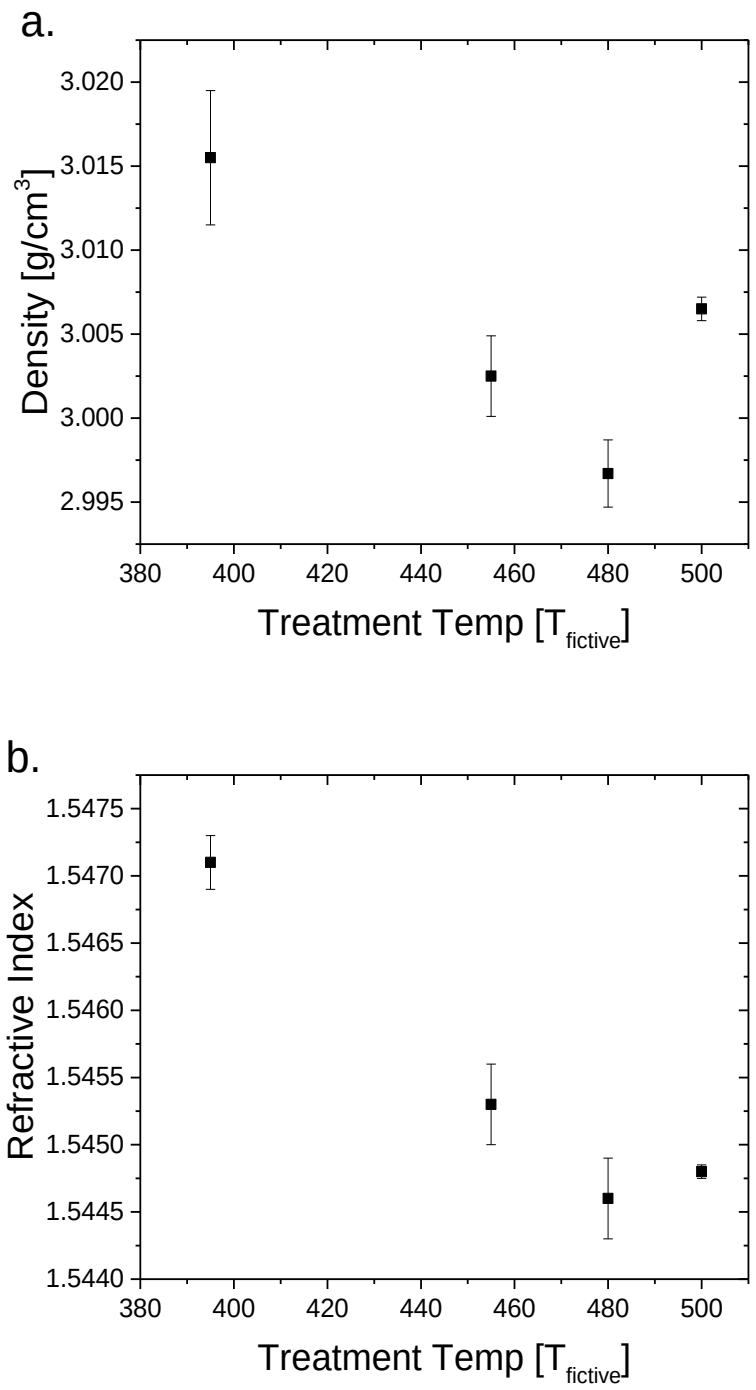

Figure 1: The a) density and b) refractive index as a function of fictive temperatures.

REFERENCES

1. Fletcher, L.B., et al., *Direct femtosecond laser waveguide writing inside zinc phosphate glass.* Optics Express, 2011. 19(9): p. 7.

2. Fletcher, L.B., et al., *Femtosecond laser writing of waveguides in zinc phosphate glasses.* Optical Materials Express, 2011. 1: p. 11.

3. Troy, N., *Materials and Techniques for the Femtosecond Laser Fabrication of Optical Devices in Glass*, in *Applied Science*2012, University of California, Davis: Davis. p. 67.

4. Auzel, F. and P. Goldner, *Towards rare-earth clustering control in doped glasses.* Optical Materials, 2001. 16: p. 11.

5. Quimby, R.S., W.J. Miniscalco, and B. Thompson, *Clustering in erbium-doped silica glass fibers analyzed using 980-nm excited-state absorption.* Journal of Applied Physics, 1994. 76: p. 7.

6. Ainslie, B.J., *A review of the fabrication and properties of erbium-doped fibers for optical amplifiers.* Journal of Lightwave Technology, 1991. 9: p. 8.

7. Lucacel, R.C., O. Ponta, and V. Simon, *Short-range structure and in vitro behavior of ZnO-CaO-P_2O_5 bioglasses.* Journal of Non-Crystalline Solids, 2012. 358: p. 7.

8. Hoppe, U., et al., Z. Naturforsch, 1995. a50: p. 11.

9. Walter, G., G. Goerigk, and C. Russel, *The structure of phosphate glasse evidenced by small angle x-ray scattering.* Journal of Non-Crystalline Solids, 2006. 352: p. 11.

10. Fletcher, L.B., et al., *Direct femtosecond laser waveguide writing inside zinc phosphate glass.* Optics Express, 2011. 19(9).

11. Fletcher, L.B., et al., *Femtosecond laser writing of waveguides in zinc phosphate glasses.* Optical Materials Express, 2011. 1: p. 845-855.

12. Brow, R.K., *Review: the structure of simple phosphate glasses.* Journal of Non-Crystalline Solids, 2000. 263&264: p. 28.

13. Matsubara, E., et al., *Structural study of binary phosphate glasses with MgO, ZnO, and CaO by X-ray diffraction.* Journal of Non-Crystalline Solids, 1988. 103: p. 8.

14. Brow, R.K., et al., *The short-range structure of zinc polyphosphate glass.* Journal of Non-Crystalline Solids, 1995. 191: p. 45-55.

15. Kishioka, A., M. Hayashi, and M. Kinoshita, *Glass formation and crystallization in ternary phosphate systems containing Al_2O_3.* Bulletin of the Chemical Society of Japan, 1976. 49.

16. Tischendorf, B., et al., *A study of short and intermediate range order in zinc phosphate glasses.* Journal of Non-Crystalline Solids, 2001. 282: p. 147-158.

17. Sales, B.C., L.A. Boatner, and J.O. Ramey, *Chromatographic studies of the structures of amorphous phosphates: a review.* Journal of Non-Crystalline Solids, 2000. 263&264: p. 12.

18. Van Wazer, J.R., *Phosphorus and its Compounds Volume I: Chemistry*. Vol. 1. 1958, New York: Interscience Publishers, Inc. 954.

19. Fanderlik, I., *Optical Properties of Glass*. Glass Science and Technology. Vol. 5. 1983, New York: Elsevier.

20. Haken, U., et al. *Refractive index of silica glass: influence of fictive temperature*. Journal of Non-Crystallin Solids, 2000. 265: p. 10

VITA

Charmayne Smith was born on in 1987 to George and Yvonnette Smith in Chesapeake, Virginia. Charmayne attended school in various places due to her military family. In her senior year at Hanahan High School in South Carolina (2005) she won female athlete of the year and student of the year. She also participated in extracurricular activities including volleyball, basketball, soccer, and student council.

Her undergraduate career was completed at Clemson University and she received a bachelor's degree in Ceramic and Materials Engineering from the Materials Science and Engineering department. At Clemson Charmayne was part of the honor's college and received grants and fellowships due to her achievements in high school. She was recruited by Prof. Kathleen Richardson to work in her glass processing and characterization lab, under the guidance of Prof. Laeticia Petit, which brought her to a subject matter she recognized she could happily devote her life to. Charmayne realized that she wanted to continue to explore the world of glass science. Through Profs Richardson and Petit's support, she began to pursue a graduate student position which was made easier by the great experiences that she received as a part of the glass research group, including: an REU in Bordeaux, France, presenting at various conferences and receiving awards, and becoming first or co-author on at least two publications.

Charmayne met Prof. Richard Brow in Montepellier, France at a short glass school which was a huge turning point. Later, she applied for a GAANN fellowship and PhD position at Missouri S&T to work in Prof. Brow's glass lab. She was awarded the fellowship by a committee including Profs. Huebner, Hilmas, O'Keefe, and Brow. Four years later she received her doctorate in Materials Science and Engineering in May 2014.